UNIVERSITÀ DEGLI STUDI DI MILANO

Scuola di Dottorato in Fisica, Astrofisica e Fisica Applicata
Dipartimento di Fisica

Corso di Dottorato in Fisica, Astrofisica e Fisica Applicata
Ciclo XXVIII

Development of an innovative LIBS system for on-line quantitative analysis of raw coal

Settore Scientifico Disciplinare FIS/01, FIS/03

Tesi di Dottorato di:
Daniele Andrea REDOGLIO

Supervisore:	Dr. Marco A. C. POTENZA
Co-Supervisore:	Ing. Umberto PERINI
	Dr. Sergio MUSAZZI
Coordinatore:	Prof. Marco BERSANELLI

Anno Accademico 2015/2016

Abstract

Every day in the world 64'125 GWh of electricity are produced and consumed: to satisfy this huge demand, many different power sources are employed, and in the last years the renewable energies share has kept on increasing. However, coal is still the main energy source and, thanks to the huge growth of China energy production, the amount of electrical energy produced this way is increasing: every day 12.1 million tons of coal are burned to fulfill 40% of the global electrical energy demand. In Italy, even if only 16.7% of the total power generation is obtained with coal combustion, coal is still the third power source, after natural gas and hydroelectric, and we have to import it in the amount of 17.5 million tons every year.

Coal has an extremely variable composition, and heat power, pollutants generation and, consequently, cost, strongly depends on that composition; for these reasons whoever deals in coal is always on the look for instruments that allow to perform faster and more accurate analysis of coal composition.

Devices able to perform on-line quantitative analysis of coal chemical composition are already commercially available; however, they are extremely expensive and must undergo strict regulations, due to the fact they employ either x-rays, gamma rays or neutrons. On the other hand, laser induced breakdown spectroscopy, or LIBS, has proven itself as a cost effective solution and has found many applications in other fields.

In my Ph.D. thesis I have developed a working prototype for on-line quantitative analysis of coal based on LIBS, following every step of its realization. The main task has been the design and realization of an innovative collection optic that allows to perform measures on raw coal, at a distance of 1 meter from a conveyor belt; the innovative part consists in the fact that it doesn't resort to the use of moving parts, decreasing its cost and increasing its reliability. My tasks also included the development of the software for data collection and analysis, the test of the instrument and its calibration . I have been deeply involved also into the choice of the components and the design of an instrument for the test in a real power plant.

Contents

Chapter 1

Introduction

The goal of my work was the development of a working prototype for a system able to perform on-line quantitative analysis of raw coal using laser induced breakdown spectroscopy; the reason why such an instrument is of great interest to coal dealers and power plants, and why LIBS is a suitable method to perform such analysis will be addressed in the next chapters, so I will give a complete description of the goals of my thesis after that, in section 2.6.

In this section I will provide a context for the research, describing why coal and its analysis are so important, even for "developed economies", and how coal analysis can be carried out.

1.1 Coal in energy production

Since the beginning of the industrial revolution, coal has always been the main source of primary energy, to be used for heating purposes and for power generation as well.[1–5] Coal is cheap, widespread all over the globe and coal-fired power plants don't require advanced technology. For all these reasons, among available fuels, coal does represent the first choice for power generation in emergent economies: for example 75.5% of Chinese electrical energy is produced by burning coal.

Because of their good efficiency, (up to 50% electrical efficiency, 94% overall efficiency with thermal cogeneration) along with their really high capacity factor (about 7900 hours per year, up to a maximum of 8700 hours per year) coal fired power plants are considered a good choice, even in the

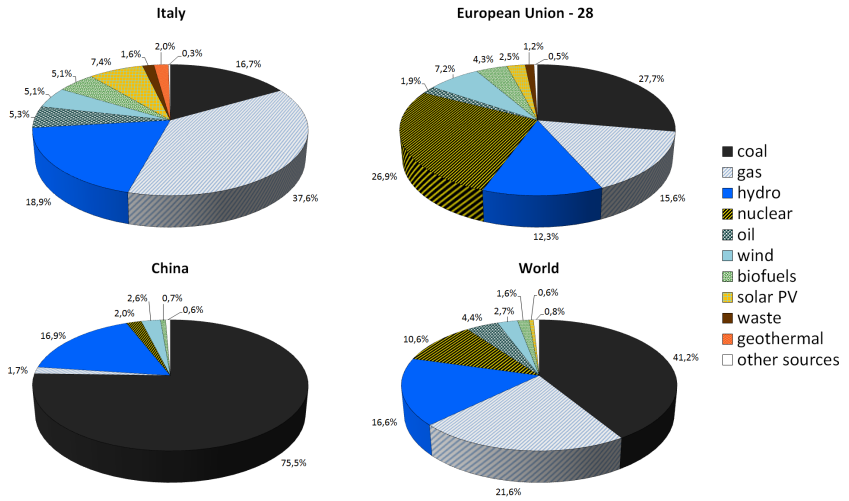

Figure 1.1 – Energy production by source for Italy, China, EU-28 and World. [5]

most advanced economies: for example 45.6% of German electric energy is produced by coal power plants. In Italy, due to the lack of coal mines and for environmental concerns, the main electrical energy source is natural gas, mainly coming from Russia and northern Africa; however, with an 16.7% share, coal is the third choice and it has to be imported in the amount of 17.5 million tons every year.[5, 6]

The main drawback in using coal as an energy source is represented by the production of dangerous pollutants as a results of its combustion, like e.g. sulfur dioxide, nitrogen oxides, PM_{10} and $PM_{2.5}$.[7–9] In addition, coal combustion produces a high amount of CO_2. While CO_2 production is unavoidable, the other pollutants emission can be controlled by proper abatement processes. These pollutants emissions are particularly relevant in old power plants (lacking in abatement systems) or when burning low quality coal.

Every day in the European union 1.2 million tons of coal are burned in order to provide electricity, with the production of 6.5 thousand tons of nitrogen oxides, 30 thousand tons of sulfur dioxide and 61.6 thousand tons of PM_{10}.[4, 9, 10] In order to prevent health hazards and environmental pollution, all these undesired byproducts have to be captured and properly treated, which means an additional cost to the energy production.

Figure 1.2 – Coal inside the sealed storage dome at Enel SpA's Torrevaldaliga Nord thermoelectric coal-fired power station. This image was originally posted to Flickr by EnelSharing at http://flickr.com/photos/36090952@N06/16733812328. It is licensed under the terms of the cc-by-2.0.

Another problem that coal fired power plants have to deal with is represented by the production of ashes: it has been estimated that 827 million tons of ashes were produced worldwide in 2012 as byproducts of coal combustion for power generation.[10, 11] In the past, flying ashes coming from coal combustion were usually dispersed in the atmosphere along with the flue gases with great hazard for human health. It should be noticed, in fact, that while most of the ashes can be assimilated to inert material, sometimes they can contain toxic elements, like arsenic and heavy metals, or even radioactive elements.[8, 12] The concentration of these elements is usually low, around $20 ppm$, nevertheless capture and disposal of ashes is now mandatory and strictly regulated.[10]

Worldwide, most of the ashes are disposed of in landfills or ash ponds, but in the last years an increasing fraction, roughly 40% of their amount, is recycled: most of them are used in the concrete industry, as well for soil stabilization and rehabilitation of opencast mine sites, in the production of bricks, expanded clay, clinker and other geopolymers.[10, 11, 13]

Fly ash production is also problematic due to a phenomenon called slagging: the problem arises when burning coal with high concentration of low melting elements, such as sodium and potassium.[14, 15] In this case ash particles may fuse and stick onto the high temperature surfaces of the boiler and the furnace. The formation of fused ash deposits can corrode metal surfaces, decrease heat transfer efficiency and even trigger a positive feedback loop, in which the decrease of heat transfer will increase the furnace temperature and the subsequent ash deposition rate.

Last, but not least, coal is a very heterogeneous material and every load has a different elemental composition, leading to a different calorific value: in order to keep the combustion process efficient, the fuel flow rate and the combustion parameters have to be tuned accordingly to the coal composition.

For all these reasons, it is important to have an accurate knowledge of the coal elemental composition, in order to schedule maintenance and keep combustion operational parameters, like temperature and airflow, inside the optimal values. Extensive dissertations on the existing methods for coal analysis have already been performed[16, 17], and it is beyond the topic of this thesis, so I will give only a brief sum up.

1.2 Standard analysis

All aspects of the coal analysis are strictly regulated: there are about 160 different standards, between ISO and ASTM, ranging from sample preparation and handling to single element analysis.

Due to coal high inhomogeneity, even its sampling must adhere to standards, which specify even the size and shape of the shovel used to collect the samples[18, 19]. Usually, for every lot of about 1000 tons, 35 samples of $2 - 5\ kg$ are taken; they are then crushed, mixed together and divided into subsamples. The number of samples and subsamples may vary, and depending on the variability of the coal and the desired precision of the results.[20]

The analysis of coal is usually divided in four parts: proximate analysis, calorific value analysis, ultimate analysis and ash analysis. The proximate analysis provides an evaluation of the moisture, volatile and ash content of the coal; it is the first and simplest test performed on coal, and it is usually used to estimate the economic value of a load. The calorific value analysis provides the calorific values of the coal, meaning the amount of

heat the coal can produce when burned. The ultimate analysis provides the concentrations of carbon, hydrogen, nitrogen, sulfur and oxygen and its results are used together with the calorific value to perform combustion calculations, in order to determinate parameters like the coal feed rate or the sulfur emission. Ash analysis provides, as the name states, the concentration of all the elements that are present in the ashes, both majors and traces.

Proximate analysis is usually performed using thermogravimetric methods [21, 22]: about $1\,g$ of sample is weighed and placed inside an oven, then it is heated up to 110 ℃ while fluxing nitrogen and weighed periodically until the weight is constant. The humidity fraction is calculated as the ratio between the mass loss and the original mass. The temperature is then increased up to 950 ℃ and held constant for 7 minutes, then the sample is weighed again: the mass loss will give the volatile content. The temperature is then lowered down to 750 ℃ and pure oxygen is fluxed inside the oven until the weight is constant. The weight of the remains will give the ash fraction, while the so called "fixed carbon" is obtained by difference.

These tests are empirical, because of the lack of comparison with known samples to evaluate the bias. In fact, variations in grain size and weight of the sample, as well as the size, weight and material of the crucible, the rate of the temperature rise, the final temperature and the duration of heating can significantly affect the test results.[23] In addition, during the last part of the test, the amount of oxygen introduced into the burning chamber is not measured, and part of it is used for the oxidation of the elements that form ashes; for this reason the ash weight is actually greater than the sum of the weights of the incombustible elements. As a consequence, the fixed carbon fraction, measured as what is missing to reach 100%, is smaller than the actual fraction of carbon contained in coal.

The calorific value is obtained by burning a fixed amount of coal inside a combustion bomb and by measuring the temperature increase with a calorimeter.[24]

Due to the great number of different ways to perform this analysis, the standard method for the measurement of carbon, hydrogen, nitrogen and sulfur does not provide neither a particular procedure nor the instruments specification, but requires the fulfillment of requirements about calibration, precision, repeatability and reproducibility of the results.[25–28] In the most common method a small sample of coal, ranging between 2 and 500 mg, is burned in a controlled atmosphere, then the combustion fumes are analyzed.

The major elements in ashes - silicon, aluminum, iron, calcium, magnesium, sodium, potassium and titanium - are usually measured using the

absorption spectroscopy technique: a solution ash and water is prepared with the remains of the proximate analysis, then its absorption spectrum is compared with the absorption spectra obtained from other solutions of known composition.[29, 30]

Trace elements analysis can be performed in different ways, and, as for ultimate analysis, the standard procedure doesn't require particular methods or apparatuses; the most common methods so far employed are the atomic emission, the atomic absorption and the mass spectrometry, alone or in combination.[31, 32]

1.3 Alternative analysis

All the aforementioned methods require a lot of time to properly collect the coal and prepare the test samples: the proximate analysis, for example, requires few hours to be completed. Usually a couple of days may pass from when the samples are collected to when the results come in, if the tests are performed by external laboratories. For this reason, coal producers and buyers are always looking for faster and cheaper methods to test the coal quality; this is particularly true for power plants, where a real time analysis of the coal fed to the burners is an important asset to optimize the combustion efficiency.

Laboratory analysis

In the last years several new techniques have been developed to perform on line coal analysis.

X-ray based techniques, such as X-ray diffraction[33, 34], X-ray fluorescence[35], X-ray absorption spectroscopy [36] and X-ray scattering are well established and widely used methods. These methods rely on the interaction between X-rays of known energy and the inner shell electrons, in order to retrieve information on coal composition and internal structure. They have a good limit of detection, about 0.2%, but they perform best in the analysis of heavier elements, while the major components of coal have low atomic number. In addition, the results of their analysis may be affected by the size and shape of the samples. Their major drawbacks are represented by the use of X-ray sources, which have to undergo a strict regulation, and the need of vacuum chambers to be operated. All this makes these instruments costly, heavy and cumbersome.

Atomic spectroscopy techniques rely on the absorption and emission of light at given wavelengths in order to retrieve the presence and abundance of an element in the high temperatures atomic vapours. Different heating sources, like flames, plasma discharges and graphite furnaces, and the use of both emission and absorption techniques, lead to a great number of different methods, each one with its strengths and weaknesses. The most used and effective one for coal analysis is the Inductively Coupled Plasma Atomic Emission Spectroscopy, or ICP-AES.[37] In this method, an argon plasma, generated by means of an induction coil, is used to dissociate the sample into its atoms and ions constituents. The emitted light is collected and analyzed by means of a spectrometer.

Due to its low limit of detection, that can be as low as 100 parts per trillion for some elements, the high reproducibility of its results and the fact that the measure can be easily automated, ICP-AES is one of the most used technique for coal analysis and it is included in some international standards for major and trace elements analysis. Its main drawback is that it needs an accurate sample preparation and that the best results are obtained when the coal is predigested using different acid solutions[38]: in this way the elements used for the preparation, like hydrogen, oxygen and halogens, can not be measured.

It is possible to use fine ground coal nebulized in argon[39], but the precision and reproducibility of the results are generally not as good as the ones obtained with acid digestion. Lastly, this method does not provide information on the internal structure of the coal, for example it doesn't distinguish between the hydrogen contained in moisture and the one bound in hydrocarbon chains.

Mass spectrometry methods work by ionising the atoms of the sample and measuring their mass-to-charge ratio; there are many different ways to perform the ionization of the atoms, but the one that gives the best results is, as for atomic emission spectroscopy, the use of an inductively coupled argon plasma.[40, 41] Inductively Coupled Plasma Mass Spectroscopy, or ICP-MS, offers the same advantages of ICP-AES, with a slightly better limit of detection; however it suffers from the same drawbacks. In addition, for volatile elements, like Hg, ICP-MS shows a pronounced memory effect, due to the retention of these elements in multiple location of the instrument.[42]

The use of laser ablation of coal pellets has been tested as an alternative source of particulate to feed to the plasma, with the advantage of avoiding water and acid contamination of the samples; although this method has a relatively high cost, it doesn't need radiation sources.

Neutron Activation Analysis employs a neutron reactor or a radioactive source to bombard the sample with neutrons, forming radioactive isotopes: the gamma ray emission is then recorded at different times, in order to reconstruct the different radioactive decay path and recover the composition of the sample. While the best results could be obtained by measuring the gamma ray emission at many different times, with delays that range from minutes to months, depending on the elements, due to the need of a fast analysis the most used technique is the Prompt Gamma Neutron Activation Analysis, or PGNAA.[43] In this method only the shortest lived radioactivity is recorded (around one minute) and a radioactive source, usually californium-252, is used instead of a neutron reactor.

PGNAA can measure the concentration of most of the ash constituents, as well as the hydrogen and sulfur[44] content, but has a relatively low precision in the detection of carbon, nitrogen and oxygen. Prompt Fast Thermal Neutron Analysis, or PFTNA, can overcome this limitation using short bursts of high energy neutrons and recording the gamma emission both during the burst and while no neutrons are emitted.[45] The drawbacks are the high amount of radiation emitted and the short life span of the neutron generator employed.

A lot of other methods, as Raman Spectroscopy[46], Nuclear Magnetic Resonance[47], Microwave Absorption[48] or Infrared Spectroscopy[49], are used to recover additional information, like the moisture content or the fraction of carbon bound in hydrocarbon chains.

On-line analysis

In order to provide real time data on the processed coal, different on-line analysis methods have been developed and are actually employed both in mines and power plants; these systems can provide different information, like moisture content, ash concentration, calorific value or ash composition. The results of these tests are used in coal mines and preparation plants for sorting and blending different coals, as well to ensure that the quality meets the requirements; in power plants those results are essential to adjust the feed rate so to meet the boiler requirements and comply with the emission regulations.

All the instruments already described are suitable to work in power plants and provide real time measurements, once coupled with an automated system that collects the coal and prepares the samples; only some of them, however, are suitable to be installed directly on conveyor belts for

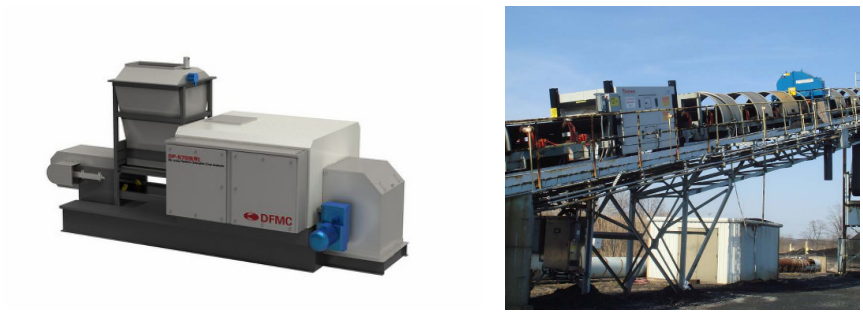

Figure 1.3 – Pictures of two online PGNAA element analyzers. Courtesy of DFMC Ltd. and Thermo Fisher Scientific Inc.

the coal transport. The first solution provides more accurate results, while the second one has a lower cost, lower size and a lower complexity.

Moisture meters provide information on the moisture content of the coal, and their presence is essential because the moisture content can not be inferred from other on-line analysis. The most common system is based on a microwave emitter and receiver installed across the conveyor belt in such a way that the microwaves cross the coal under test; the water molecules absorb the radiation and the measured attenuation provides information on the moisture content. While being simple and cheap, this method provides information only on the free moisture, because the moisture fixed inside the coal structure can not vibrate and absorb the microwaves. Magnetic resonance tuned on the hydrogen in water can be employed to measure the whole moisture content, but instruments based on this principle are large, sophisticated and expensive.

Ash meters usually employ gamma ray absorption and emission to measure the ash fraction of a coal sample. The most common method is the DUal-Energy gamma-ray Transmission, or DUET: two sources of gamma rays at different energies are installed under the conveyor belt, while a detector over the conveyor belt measures the attenuation of the two beams. The attenuation of the high energy gamma ray is roughly proportional to the mass of the material on the conveyor belt, while the energy of the second source is chosen so that the beam is attenuated mostly by ash components and not by carbon, hydrogen, nitrogen and oxygen. Measuring both the attenuations it is possible to evaluate the fraction of ashes inside the coal.

Commercially available element analyzers are mostly based on neutron analysis: the most reliable and widely diffused ones are based on PGNAA.

As their laboratory counterparts, these devices have good accuracy and low limit of detection, but they can not measure accurately the content of carbon, nitrogen and oxygen. PFTNA based instruments, on the other hand, can provide a complete and accurate analysis of all the elements in the coal, but the use of a high energy radioactive source entails the use of greater shieldings. Moreover, the nuclear sources for PFTNA are more expensive and have a shorter life. X-ray Fluorescence spectroscopy, or XRF, are a cheaper alternative to neutron analysis; without the presence of a radioactive source the shielding can be smaller and lighter. On the other hand, the system can test only the surface of the coal and can't detect elements with atomic number lower than 10, namely carbon, hydrogen, oxygen and nitrogen; that makes it suitable to check ash composition, but it doesn't provide information on the coal heating power.

Last, but not least, surging as a potential competitor for online coal elemental analyser, there is the technology investigated in this work, LIBS. I will describe it in details in the next chapter.

Chapter 2

Laser Induced Breakdown Spectroscopy

In this section I will discuss LIBS: I will address briefly its history[50, 51], its applications and how it works. I will weigh its pros and cons and address the full goal of this research.

2.1 History and applications

Laser Induced Breakdown Spectroscopy (LIBS), also known as Laser Induced Plasma Spectroscopy (LIPS), is a powerful technique for quantitative analysis of chemical composition. At its core, this technique relies on a powerful laser shot to ionize a small portion of the sample, then the spectrum of the light emitted by the plasma is analyzed in order to retrieve information on the sample's composition. The first analytical application of laser-induced plasma for spectrochemical analysis of surfaces was presented in 1963, shortly after the invention of the laser. Since then, several different realizations and applications of the LIBS have been studied, but it was only in the last 20 years that the interest in this technique has been reawakened; this was mostly due to the advent of smaller and cheaper digital spectrometers, along with faster and powerful computers, which allowed faster, accurate and automated measures.

Thanks to its flexibility and portability, LIBS systems are now widely spread in many fields[52]: LIBS analyzers can be easily employed in material sorting, being them ferrous[53–55], glass[56] or plastic[57]; they are

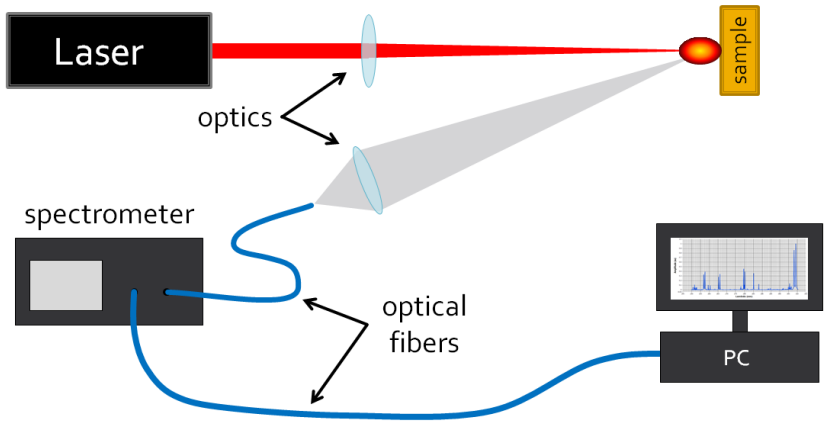

Figure 2.1 – schematic representation of a LIBS system.

employed in smelting facilities to check products quality[58, 59]; they found application in garbage recycling plants for sorting different wastes[60]; they are employed in heritage cultural preservation for dating and authenticity check[61–65]; they are used for explosive[66, 67] and nuclear[68–70] material search; they are used in mining facilities[71–73]; they are employed in biomedical application for biopsy[74] and bacteria sorting[75, 76]; they are used by environmental researchers for plant[77, 78] and soil[79, 80] analysis; they have forensic application for gunpowder[81], paint[82], glass[82] and bone[83] recognition; they are employed in nuclear industry and radioactive waste disposal[84]. They can work nearly in any atmospheric condition, except for explosive one[85–87]; they can perform measurements on liquid, solid, aerosol and gaseous materials; they can work both underwater[64] and in space[85]; both handheld and standoff devices exist and are widely employed. The Mars rover Curiosity is equipped with a LIBS instrument (ChemCam)[88] for remote rock analysis, and its performance has paved the way for the use of other laser-induced spectroscopy instruments in future missions.

2.2 Plasma dynamics

LIBS devices employ an high energy laser, usually with an extremely short pulse duration, for the generation of the plasma. Notwithstanding the great number of researches published on the topic[89–92], the interaction between

the laser and the sample, and the subsequent plasma generation and heating, are not completely understood. Different plasma generation dynamics are involved, depending on the laser pulse duration, energy and wavelength: some accurate studies and reviews on this topic can be found[93–97], so I will describe only the most common case, in which a near infrared laser of moderate irradiance ($\sim 10^9$ W/cm^2) with a short pulse duration (FWHM $\sim 5\,ns$) ablates a solid sample.

In the first hundreds of picoseconds of interaction with the laser, a portion of the sample is heated to the point that the material begin to boil and evaporate: a small fraction of the laser light is absorbed by the generated gas plume, while most of the power keep going into heating and ablation of the sample.

After a couple of nanoseconds from the beginning of the phenomenon (1-5 ns depending on the laser power) the energy deposited by the laser in the gas plume is enough to ionize only a fraction of the atoms, generating a small volume of plasma; this plasma is opaque to the laser radiation and absorbs all the incoming energy in a process known as inverse bremsstrahlung, in which an electron, inside the electric field of an atom, absorbs a photon. The laser radiation no longer reaches the sample and instead keeps heating the plasma plume, releasing more electrons and increasing the efficiency at which the plasma absorbs the radiation; this phenomenon is known as "plasma shielding". Each electron will lose energy to other atoms through inelastic collisions, freeing other electrons and establishing an avalanche reaction known as plasma breakdown. While the plasma plume expands at supersonic speed and its temperature increases, it can blast off some other material from the sample.

Once the laser pulse has ended, the plasma begins to cool down and eventually its expansion will come to a halt, then it will begin to shrink; during the cooling phase the atoms begin to combine and form molecules, then clusters and particulate. When LIBS is performed in high density media, like in liquids, the cooling and sudden pressure drop can lead to cavitation phenomena, with a subsequent reheating and secondary light emission[98, 99].

During the plasma generation and cooldown the light is emitted in different ways: the main emission during the heating phase is a continuous spectrum due to the bremsstrahlung radiation. When the plasma begins to cool down, the light emitted by recombination of electrons and ions is added to the continuous spectrum, while the lines emitted by transitions between electronic levels will start at different times, depending on the temperature

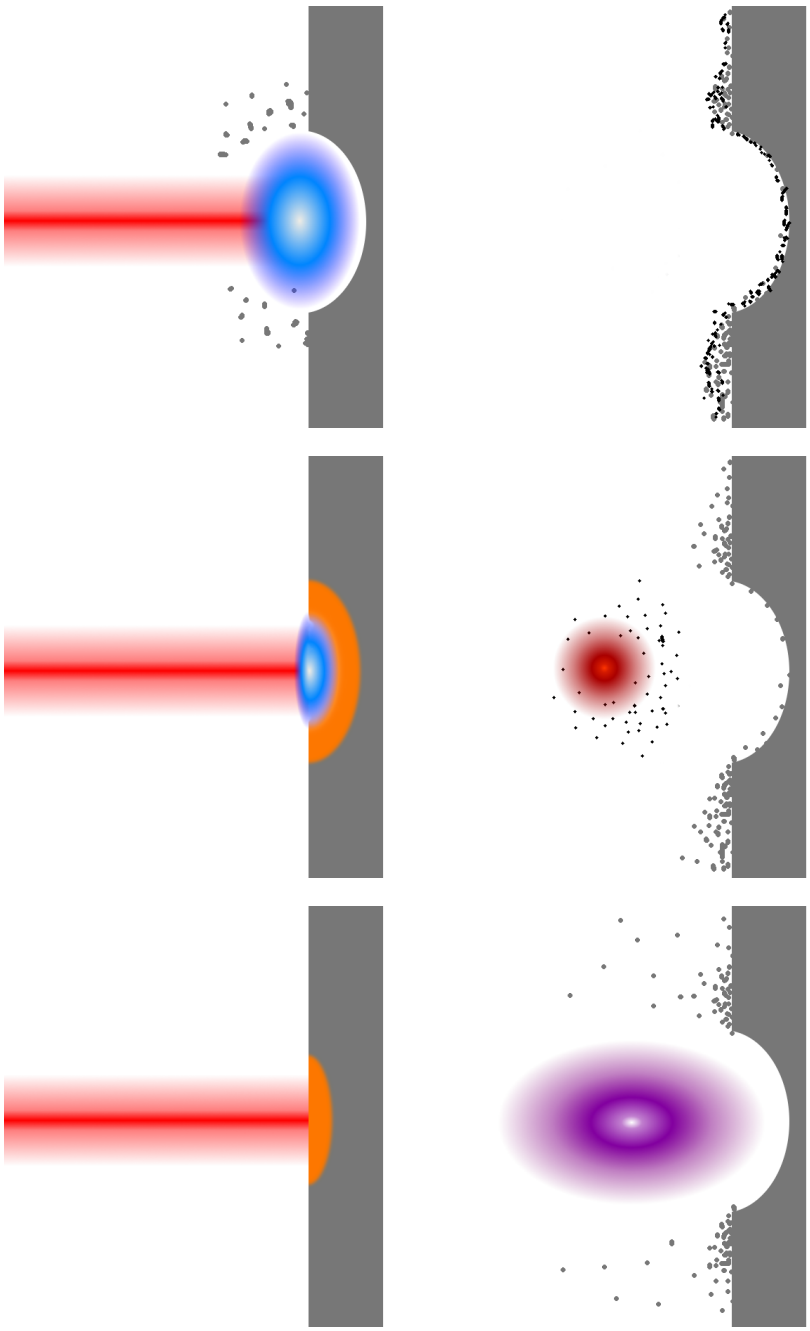

Figure 2.2 – Schematic representation of the plasma evolution: heating, plasma formation, plasma heating, plasma expansion and plasma cooling.

and electronic density of the plasma. At an earlier stage the continuous contribution to the spectrum will be dominant, while later it becomes negligible compared to the atomic emission. In proper conditions of plasma temperature, density and composition it is possible to observe light due to molecular emission, even from vibrational and rotational transitions.

The emitted light is collected with an adequate optics and delivered to a spectrometer. Intensity and broadening of the different lines can provide information on the plasma composition, along with temperature and electron density.

2.3 Configurations

There are several different possible configurations for a LIBS set-up, depending on the number of laser pulses per measure, the angle of incidence on target, the kind of collection optics used and the angle from which the light is collected.

The most important discriminant is whether the system employs a single pulse laser or a double pulse one: in the double pulse configuration, a first laser pulse ablates the material from the sample, while a second delayed pulse reheats the plasma. A double pulse laser can be obtained in different ways: by synchronizing two different lasers, by opening the Q-switch of the laser cavity two times during the same pumping cycle or by splitting the beam and making the two beams travel along different paths. When they reach the sample, the two pulses can be collinear or orthogonal: an orthogonal configuration is sometimes preferred when performing experiments on the behaviour of the plasma, because it avoids a secondary ablation of the sample.

On the other hand, a system employing an orthogonal configuration is more complex, because it needs a fine tuning of both the delay and position of the second laser pulse, thus making it suitable only for laboratory instrumentation and with an accurately prepared sample. Instead, it is more common to use a collinear configuration when performing analytical measurements of the sample composition, because the secondary ablation increases the intensity of the emitted light, thus increasing the precision of the measure; moreover, this configuration is easier to build and can work even when the distance between the laser and the sample changes.

Other differences in LIBS systems can be found in whether the system employs a focalization optics for the laser or not. Focalization of the laser

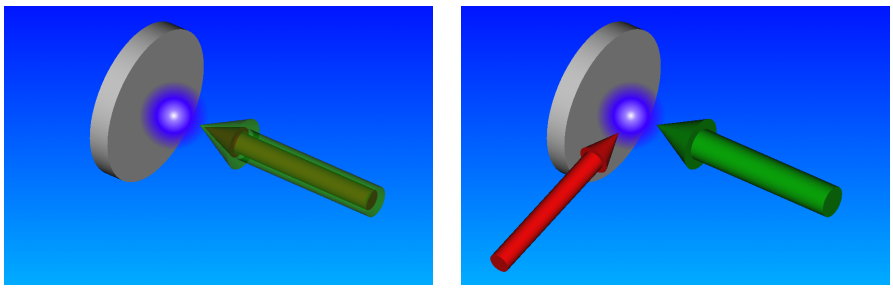

Figure 2.3 – collinear and orthogonal configuration.

can provide a higher fluence, thus increasing the temperature of the resulting plasma; while this can allow to see spectral lines related to higher energy transitions, the introduction of focusing optics forces the system to work at a fixed distance, unless some sort of auto-focusing is employed. In fact, a change in the distance between the focusing elements and the sample will result in a change of the fluence of the laser, and if the focus is above the sample surface it is possible that the spark will be triggered in air, thus greatly decreasing the ablation of the sample and the reproducibility of the measure. Moreover, given the already high energy of the laser employed, the focalization system requires the use of particular elements that can endure the stress induced by the repeated laser shots; usually a lowering of the repetition rate is also needed. A system that makes use of a laser working without focalization, on the other hand, is simpler, and more suitable for analysis on samples that can not be moved or prepared (like in the case of analysis of artworks.

Another aspect of the LIBS system is the collection of the plasma radiation: the systems can be divided in three categories, depending on whether they use a collection optics or not and whether they use an optical fiber to deliver the light to the spectrometer or not. A system in which neither an optical fiber nor a collection optics is employed is both impractical and dangerous for the well being of the spectrometer: in fact it is difficult to position the spectrometer in such a way that the slit is right in front of the plasma, and during the ablation there are great chances that the plasma byproducts will either ruin the slit or enter the spectrometer.

The simplest method uses a large multimode optical fiber (usually with a core diameter of 200-600 μs) to collect the light from the plasma and deliver it to the spectrometer; this system is cheap, simple and, due to the typical numerical aperture of the fibers, doesn't require an accurate

alignment. It has, nevertheless, a very low efficiency, due to the small size of the fiber, and the debris from the plasma emission tend to be sputtered on the surface of the fiber. Additional care should be used when choosing the suitable optical fiber, because typical silica fibers don't transmit light in the UV region, and the ones that can (known as "High OH fibers") usually lose this capability after exposition to deep UV light (a phenomenon known as "solarization"); solarization resistant fibers do exist, but they usually have a greater attenuation and don't transmit light at wavelengths greater than 1200 nm.

The most common configuration involves the use of one or more lenses that focus the light onto the face of an optical fiber, that then deliver the light to the spectrometer. This system has a greater collection efficiency due to the fact that the system collects the light from a greater surface; depending on the geometry of the system, the collection efficiency can be limited by the diameter of the lens, the diameter of the core and the numerical aperture of the fiber, usually leading to the curve of the efficiency, as a function of the light source distance, showing one or more peaks. A major drawback of this system is the fact that most optical glasses are opaque to wavelengths shorter than 350 nm and that the chromatic aberration increases exponentially as the wavelengths shorten: for example a fused silica lens with an effective focal length of 50 mm at 587 nm shows a shift in the position of the focal point of 9.1 mm as the wavelength changes from 200 nm to 900 nm, 18% of the effective focal length; this shift slightly increases as the distance between the lens and the light source increases. Typical achromatic and apochromatic lenses don't work, because the optical glue used is photoactivated and thus completely opaque to wavelength shorter than 340 nm; the only solution that works from UV to NIR is an air spaced triplet, usually composed of two aspheric positive silica lenses and one negative CaF_2 lens. These objects, however, have a small aperture and are expensive (thousands of euros); moreover the CaF_2 lens is brittle and highly hygroscopic, making the whole item unsuitable for outdoor use.

The system that provides the best results in terms of efficiency employs a mirror based optic that couples the plasma with the entrance slit of a spectrometer; in this way there are no chromatic aberrations, as instead happens when using a lens system, nor attenuation problems, like for optical fibers. Moreover, with the use of appropriately shaped mirrors, it is possible to create an optical copy of the light source directly in front of the entrance slit of the spectrometer, greatly increasing the collection efficiency of the system and allowing to perform spatially resolved spectroscopy. On the

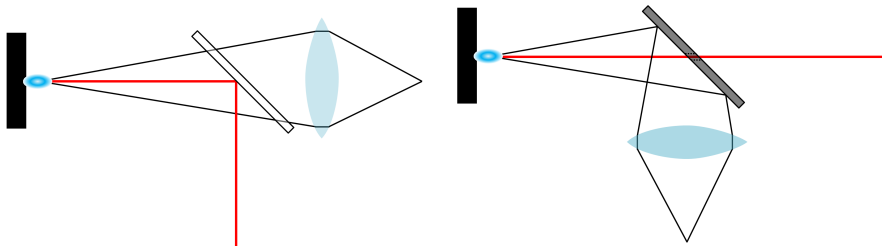

Figure 2.4 – Schematic representation of on-axis configuration, using either a dichroic mirror or a broadband mirror with a hole in the middle.

other hand, this configuration needs a really accurate alignment and doesn't handle well vibrations; moreover the system can't perform measures when the plasma is even slightly out of focus. In conclusion this configuration is perfect for laboratory instruments, but can not be employed for portable or "outdoor" devices.

A third parameter that must be evaluated is the direction from which the light is collected: on the same axis of the laser, orthogonal to the laser or slightly off axis. Orthogonal collection is the preferred configuration in laboratory set-ups, especially when coupled with the mirror-only collection optics, because it allows the recovery of information about plasma shape and plasma evolution; on the other hand, it can't be employed when the position of the sample is not fixed, because if the position of the plasma changes the system no longer delivers the light to the spectrometer.

On-axis configurations are the most commonly used for stand-off LIBS system, because a change in the distance between the sample and the system does not jeopardize the measure, except for a change in the collection efficiency; these systems usually employ a holed mirror or a narrowband dielectric mirror to separate the optical path of the laser from the path of the plasma light. Stand-off applications that employ focusable optics usually employ the same optics to both focus the laser beam and recover the plasma light: in this way it is ensured that the light is collected from the same region in which the plasma has been ignited.

A slightly off axis configuration is usually preferred for small and simple system where the distance between the probe and the sample vary in a range of a couple of millimeters; for this reason it is widely employed for handhold and portable devices.

2.4 Strengths and weaknesses

The LIBS has many advantages that, as shown previously, make it a very flexible technique. First of all, in most cases LIBS doesn't require sample preparation: the measure can be performed directly on the item to be tested, greatly decreasing the duration of the measure and avoiding all the sample preparation work. This is especially true when the object under analysis is a hard solid, for example in the case of metal alloy, when the test requires that the sample is transparent, like for absorption spectroscopy, or when the sample preparation has critical impact on the results, like for scanning electron microscopy.

Another advantage is the fact that every laser shot can provide enough information to perform the measure; in this way the results can be provided in a matter of seconds, and the measure can be performed on different places in little time: a fast device can perform as much as 20 measures per second.

LIBS measures are nearly non-destructive: due to the fact that each shot ablates only a few tens of picograms of material, the sample under test is left almost unaffected.

LIBS can reveal any element with a good detection limit; the actual limit, however, strongly depends on the set-up. For example, some elements, like carbon and silicon, show spectral lines only in the UV region: in order to observe these wavelengths proper spectrometers and collection optics are needed.

LIBS components can be easily miniaturized, so it is possible to realize portable and even handhold devices; thanks to the great advances in the field of laser diodes and ccd spectrometers, many different small LIBS analyzers have been developed in the last years.

LIBS doesn't require a specific atmosphere to work, and instead can be performed in nearly any ambient condition; many studies have been carried out on the behaviour of laser induced plasma in different gases, like air, nitrogen, argon[87] or helium[100], and liquids, like water[64, 98, 99] and any kind of oils[101]. It has been tested also in a wide range of pressures, from ultra high vacuum in space up to 280 bar in water to simulate deep ocean condition. Extra care should be used when working in flammable or explosive atmosphere, but sometimes laser induced plasmas have been used to start the combustion needed to perform other measures, like flame atomic absorption spectroscopy.

LIBS measures can be performed remotely; by using optical fibers or telescopes to deliver the laser on the sample and collect the plasma light, it

Figure 2.5 – Pictures of a standoff and an underwater LIBS systems. Courtesy of professor Javier Laserna, University of Malaga. [63, 64]

is possible to perform measures from distances that can range from a few centimeters up to several meters[63, 66, 102]. This is particularly convenient when testing for dangerous substances, like explosive[66] or radioactive[68] materials, when the object under analysis is out of reach or when it can not be moved.

LIBS devices don't use radioactive sources, like PGNAA and XRF do: in this way no cumbersome shielding is required and the security compliances are by far less strict. The resulting devices are a lot less expensive, small, easy to maintain and operate.

Notwithstanding all these strength points, LIBS has drawbacks too, and the same feature may be favorable or not, depending on the application. For example, LIBS measures involve only a small volume of material on the surface of the sample: this means that in the case of inhomogeneous materials the sample must be ground to a fine powder and then pressed into a pellet, or the measure has to be repeated on different places all over the sample. On the other hand that means also that the techniques has a good spatial resolution: it is possible, for example, to map the concentration of the components all over the sample surface and at different depths[103, 104].

Other problems involve the so called "matrix effect": many different parameters affect the intensity of a single spectral line, like plasma temperature, electron density, plasma optical density, or the presence of other atoms and molecules. Those parameters, in turn, depend on other quantities that are not always possible to control, like sample composition, sample's surface colour and roughness, atmospheric pressure, temperature and composition, laser pulse duration, energy and wavelength, and so on.

All these problems can be overcome with additional measurements performed on the plasma, for example using internal reference, recording brightness and shape of the plasma plume for every shot, performing spatially resolved measurements of the plasma emission or working in controlled atmosphere, but in this way the system loses most of its advantages in terms of flexibility and portability. Each different system has to be tailored on the specific requirements of the measure.

2.5 LIBS for coal analysis

Because of its promising features, LIBS has been identified as a viable method for the on-line analysis of coal in substitution of the existing techniques. LIBS systems, in fact, are compact, do not require sample preparation, can be operated on-line also in the presence of hostile environments and the results of the analysis can be obtained in a short time.

A great number of studies have been carried out so far to check the validity of this technique for the characterization of coal samples (see for example references [105–120]); most of them, however, refer to measurements performed under almost ideal conditions. That is, coal samples are crushed prior the analysis and pressed to pellets to produce a flat rigid surface; furthermore, samples are kept at a fixed distance from the focusing lens. In this way irradiance of the impinging laser beam can be controlled and the collecting optics can easily be conjugated to the fixed position where the plasma plume is generated, thus optimizing the collection efficiency.

Really few works have presented, as of today, a system to perform on-line measures on coal, and nearly all of them involved the collection of samples of coal, either before[121] or after[122, 123] it is crushed in mills, and the production of pellets for the analysis. Some of them didn't require the production of pellets, but they still needed a device for the collection of the coal from the conveyor belt.

To our knowledge, only two LIBS measuring systems have been utilized so far for on-line characterization of raw coal samples in real field conditions. In one case[124] the system has been installed in a coal mine in South Africa and, since the instrument working distance was limited to $\pm 2\,cm$, an ultrasonic sensor was used to enable a moving optics to maintain a fixed distance from the sample with changes in coal height of the order of $\pm 12.5\,cm$. In the other case[125] the LIBS system did not include an automatic control of the focusing mechanism (i.e. the focusing/collection

optics is fixed), but it has been installed in a peculiar position, not usually available in other plants, where the height variation of the coal stream would not exceed its working distance (about 5 cm). In both cases no further studies have been published.

2.6 Goals

This project was carried out in the frame of a cooperation agreement between ENEL Ingegneria e Ricerca (Pisa) and RSE (Ricerca sul sistema Energetico) and was sponsored by an RdS project(Ricerca di Sistema, a fund to support the Research in the field of the Electric and Energetic System). The work was performed in the RSE laboratory; the research team was led by Umberto Perini, and also included Sergio Musazzi, Elena Golinelli and Franco Barberis.

The topic and goal of the research was to study the feasibility of a LIBS device that could measure the chemical composition of coal on the conveyor belt of a coal fired power plant. The request involved the study and characterization of the components needed for this system, the realization of a prototype and a test on known coal samples. The software for data analysis was to be provided by a third party and later implemented into the instrument.

The instrument had to be able to measure the intensity of the spectral lines of carbon, hydrogen, nitrogen, oxygen, sulfur and the major ash components; it had to work on a conveyor belt and it had to not alter the flow of the coal in any way, due to security issues. When the third party didn't comply, the requirements later changed to include the software to perform the spectral data analysis.

Chapter 3

Components choice

In this section I will describe the main components of the instrument, explaining the reasons of the choices. I will begin with a description of the synthetic spectra generator, because it has been a fundamental asset for the choice of the other components of the system, as well as during the data analysis. In the same section I will also asses the theory needed for the development of the software. In the other sections I will discuss the main components of the system: the laser source, the spectrometer, the optical fibers, the trigger generation system and the sample holder.

The collection optics will be discussed in a dedicated chapter 4.

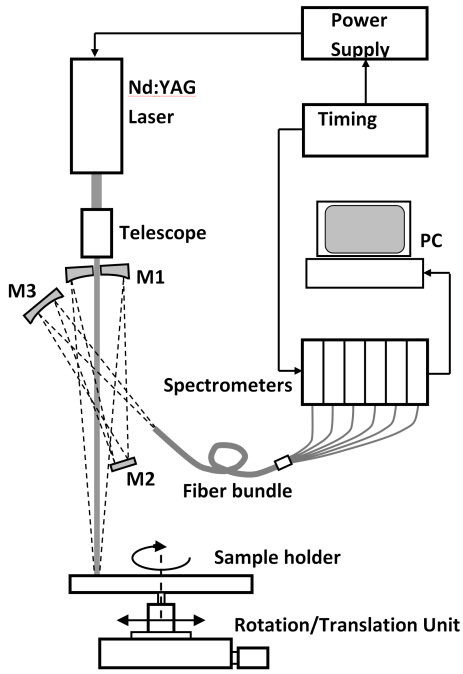

Figure 3.1 – Schematic representation of the LIBS system.

3.1 Synthetic spectra generator

To be able to define the specifications of the main components of our system, in addition to referring to the existing literature, it was decided to develop an algorithm that provides simulated LIBS spectra. This was mandatory, in order to have an idea of the strength of the spectral lines that could be seen in a plasma from coal samples. For the development of this algorithm an homogeneous, isotropic, optically thin plasma in Local Thermal Equilibrium was assumed: none of those condition are actually fulfilled in real plasma[91, 126–128], as I will discuss in chapter 5, but the model provides nevertheless information about the order of magnitude of the spectral lines and possible overlapping between them.

Under the aforementioned conditions, the probability distribution of an electron between the levels of a given ionization state is given by the Boltzmann law

$$P_j(T) = g_j U(T) \exp\left(\frac{-E_j}{K_B T}\right) \tag{3.1}$$

where j is an electronic level with associated energy E_j of an atom with given ionization, g_j is the degeneracy of that state, $P_j(T)$ is the probability of that level being occupied at temperature T, $U(T)$ is the partition function for the atomic species at the given ionization state, K_B is the Boltzmann constant.

The distribution of the atoms of a single element between its ionization states can be obtained using the Saha[129] equation

$$n_{r+1}(n_e, T) = 2\frac{n_r(T)}{n_e}\frac{U_{r+1}(T)}{U_r(T)}\left(\frac{2\pi m_e K_B T}{h^2}\right)^{\frac{3}{2}} \exp\left(-\frac{\chi_{r+1}}{K_B T}\right) \tag{3.2}$$

where n_i is the number of atoms in the ionization state i (being I the neutral state, II the singly ionized state and so on), n_e is the electron number density, m_e is the electron mass, h is the Planck constant and χ_{r+1} is the energy needed to ionize once the atom from the state r to the state $r+1$.

The equation can be changed in order to express N_{r+1} as a function of n_1

$$n_{r+1}(n_e, T) = n_1 \frac{U_{r+1}(T)}{U_1(T)}\left(\frac{2}{n_e}\right)^r \left(\frac{2m_e K_B T}{h^2}\right)^{\frac{3r}{2}} \exp\left(-\frac{X_{r+1}}{K_B T}\right) \tag{3.3}$$

where X_{r+1} is the energy needed to ionize the neutral atom r times. If the total number of atoms is unknown, it is still possible to retrieve the relative concentration of the different ionization states.

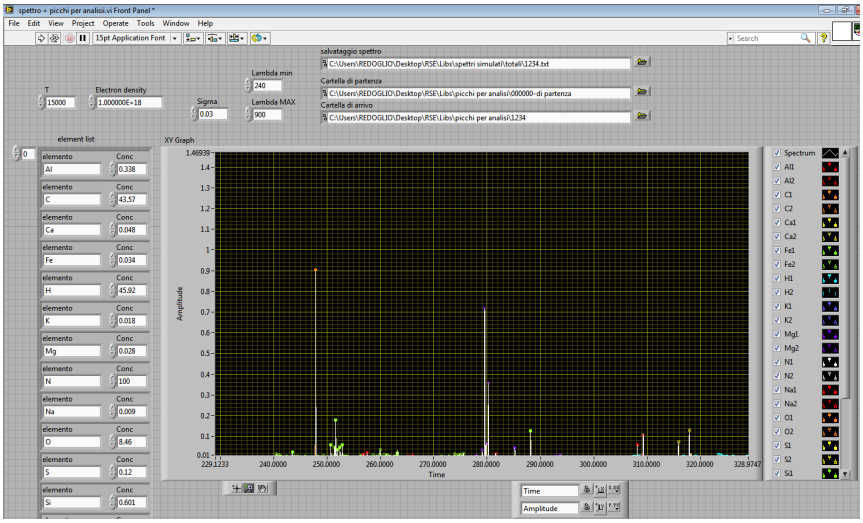

Figure 3.2 – User interface of the synthetic spectra generator software, with a sample spectrum.

The power emitted at the wavelength associated with the transition from level j to level i of a given ionization state, with $E_j > E_i$, is obtained from the Einstein equation

$$W_{j,i} = \frac{cn_j}{\lambda} A_{j,i} \tag{3.4}$$

where c is the speed of light, n_j is the number of atoms in the energy level j and $A_{j,i}$ is the Einstein emission coefficient for the transition. The absorption and stimulated emission contributions are being neglected due to the optically thin plasma hypothesis.

Combining the equations (3.1), (3.2) and (3.4)it is possible to obtain the power of the spectral line for a given transition

$$I_{j,i}(n_e, T) = \frac{C}{\lambda} n_r(n_e, T) \frac{g_j A_{j,i}}{U_r(T)} \exp\left(-\frac{X_{r+1}}{K_B T}\right) \tag{3.5}$$

where C is a constant depending only on the experimental configuration.

The developed algorithm receives as inputs the values for temperature, electron number density and instrumental broadening, as well as the relative concentrations of the involved elements and provides a synthetic spectrum based on the reported equations.

The Einstein coefficient, wavelength and degeneracy of transitions, as well as ionization and level energies, were obtained from the NIST atomic

spectra database; as a reference for temperature and electron number density we used the values obtained by Dong et al.[130] and Rebolledo et al.[131]

In order to make the software work, a lot of approximations have to be made, starting from the partition function. The partition function is defined as

$$U(T) = \sum_j g_j \cdot e^{-\beta E_j} \tag{3.6}$$

where $\beta = \frac{1}{K_B T}$. Due to the fact that the number of energy levels is infinite, it is not possible to calculate the exact value of the partition function. However, in the majority of cases the contribution of higher energy levels is negligible, so a good approximation can be achieved by setting a cutoff to the energy of the levels; on the other hand, a different cutoff can lead to different results if the temperature changes dramatically and it is a really difficult task to predict how a cutoff will influence the outcomes. For our models we decided to use all the energy levels available on the NIST database.

Another approximation was the limitation to the number of ionization states. We found that, in the ranges of temperature and electron densities usually explored in coal LIBS experiments, the fraction of atoms ionized more than three times is negligible; for this reason, only the data for the firsts four ionization states were used in the Saha equation, and the spectra contributions were calculated using only the transitions of the neutral and singly ionized state.

In addition, only the lines relative to transitions for which the Einstein coefficient is known can contribute to the simulated spectrum; the Einstein coefficient is known for all the strongest transitions, but not for all the less strong ones, especially for those elements that have thousands of low intensity transitions, like iron and titanium.

The last major approximations that were made were the optically thin plasma approximation and the LTE approximation; the most problematic aspect of this simplification is that reabsorption[132, 133] of the light by the outer, colder layers of the plasma is not taken into account, but for typical coal compositions this phenomenon is negligible in most instances.

3.2 Laser

The laser is the core element of any LIBS set-up. When it comes to possible sources for a LIBS experiment, there are many choices available: different

Figure 3.3 – Picture of the laser employed in the prototype.

groups in the world, performing LIBS experiments, have successfully employed lasers with wavelengths ranging from UV to IR, with pulse durations from milliseconds to femtoseconds. Some references can be found in [93, 94, 97].

It has been proven that UV lasers have a better radiation-matter coupling, providing a better ablation efficiency (the amount of ablated material per energy unit); moreover, in the case of metallic surfaces, the reflective index decreases with the wavelength, thus increasing the amount of energy delivered to the sample.

On the other hand, IR lasers need to reach a lower fluence in order to obtain plasma production; in addition to that, UV lasers usually require a 3rd or 4th harmonic generation stage, greatly decreasing the energy output (usually around 30% of the original power) and increasing both size and cost of the system.

The pulse duration greatly affects the ablation dynamic: at the present date there is no complete model that accurately describes the whole process of ablation and ionization, so I will give a only qualitative description of the phenomenon. I have already described in section 2.2 how the ablation process evolves when the pulse lasts for a couple of nanoseconds: when the pulse lasts longer (microseconds and milliseconds ranges), due to the

plasma shielding only a smaller fraction of light can actually reach the target, resulting in a lower ablation efficiency. On the other hand, a greater fraction of light interacts with the ablated material, thus creating a hotter, longer-lasting plasma. The increased life and temperature of the plasma lead to an increase in the chance of the plasma blasting off some material from the sample: this decreases the precision of the ablation, both in terms of quantity and position.

When using pulses with a duration of few picoseconds, all the radiation is being absorbed by the sample before the gas plume begins to expand: in this way the interaction between the laser and the gas is minimized, resulting in a greater ablation efficiency, at the cost of a colder plasma. In this way the risk of interaction between the sample and the expanding plume is also reduced, resulting in a cleaner hole and a more accurate ablation.

When using femtoseconds laser, the ablation and ionization dynamics seem to change completely, although the physical mechanisms behind ionization and material removal in fs-laser ablation are still debated and not well understood. One of the most widely accepted hypothesis states that, due to the fact that the energy deposition time is much smaller than relaxation and heat diffusion time, the material under the laser beam spot is heated quasi adiabatically and begins to ionize before it can leave the surface.[134] Other theories on the interaction between the laser and the sample do exist in which more exotic ionization processes (like multiphoton ionization and tunnel ionization) are involved. As a tangible outcome, femtosecond ablation results in extremely clean holes, usually with no heat transfer to the surrounding area; fs-ablations usually results in smaller, hotter plasmas than ps-ablation, due to the fact that only the matter that directly interacts with the laser is involved in the plasma formation.

In our measure we needed a high temperature plasma, because some of the main components of coal, like carbon and hydrogen, have spectral lines that have maximum intensity when the plasma temperature is higher than 15000 K; in addition to that, our system had to face a great variability in shape and composition of the sample. For these reasons, we chose a Nd:YAG Q-Switched laser (Quantel Brio), operating at a wavelength of 1064 nm; the laser delivered 100 mJ of energy per pulse, with a pulse duration of 3.7 ns, a beam diameter of 4.5 mm and a repetition rate of 20 Hz. We coupled it with an inverted galilean telescope, in order to reduce the size of the beam retaining, at the same time, the depth of field of the system; the obtained beam had a waist diameter of 500 μs, a Rayleigh range of 18 cm, a fluence of 51 J/cm^2 and a power density of 13.8 GW/cm^2.

3.3 Spectrometer

The spectrometer is the other core element of any LIBS set-up.

In order to record the lines emitted by every element, a LIBS spectrometer usually needs to cover a wide spectral range; in addition, some elements like iron and titanium have a lot of lines with very close wavelengths, so a spectrometer with a good spectral resolution is needed in order to be able to separate the different lines. For example, our instrument had to be able to see the $247.9\,nm$ emission line of carbon, the $422.7\,nm$ line of calcium and the $656.3\,nm$ line of hydrogen. The most prominent lines of nitrogen, oxygen and sulfur can be found in the infrared, between $750\,nm$ and $1100\,nm$, along with other secondary lines of carbon, while most of the other interesting elements, like aluminum, silicon and magnesium, have emission lines in the ultraviolet band. In addition, as said, both iron and titanium have thousands of lines spread all over the spectrum: for this reason a good resolution is needed to distinguish the different lines one from another.

Ideally, the best solution money can buy consists in Echelle spectrographs: these devices have two different dispersing elements placed orthogonally to each other, so that the light is dispersed into a two dimensional spectrum with wavelengths across and along a series of lines. In this way it is possible to achieve a spectral resolution and a spectral range much greater than those in traditional spectrometers, because the number of pixels available is hundreds, if not thousands, times greater.

Echelle spectrometers usually employ cooled intensified CCDs as recording devices: that provides a good signal to noise ratio even for low intensity signals. Moreover, the use of intensifiers allows integration times that can be as short as $200\,ps$: this can be extremely useful when studying really fast phenomena like the ones involved in LIBS experiment.

On the downside, Echelle spectrometers are really expensive: the body alone, without the camera, has prices that start from fifty thousands euro for the smaller models and quickly reach and pass the hundreds of thousands euro when longer focals and more advanced features, like aberration corrections or built-in calibration sources, are involved. Intensified cameras themselves have prices that range from fifteen thousands of euro for the older models up to over fifty thousands of euro for the most advanced cameras.

Moreover, Echelle spectrometers are somewhat fragile and affected by temperature variations, usually resulting in a loss of one or both the wavelength and intensity calibration; the use of cooled cameras solves some of

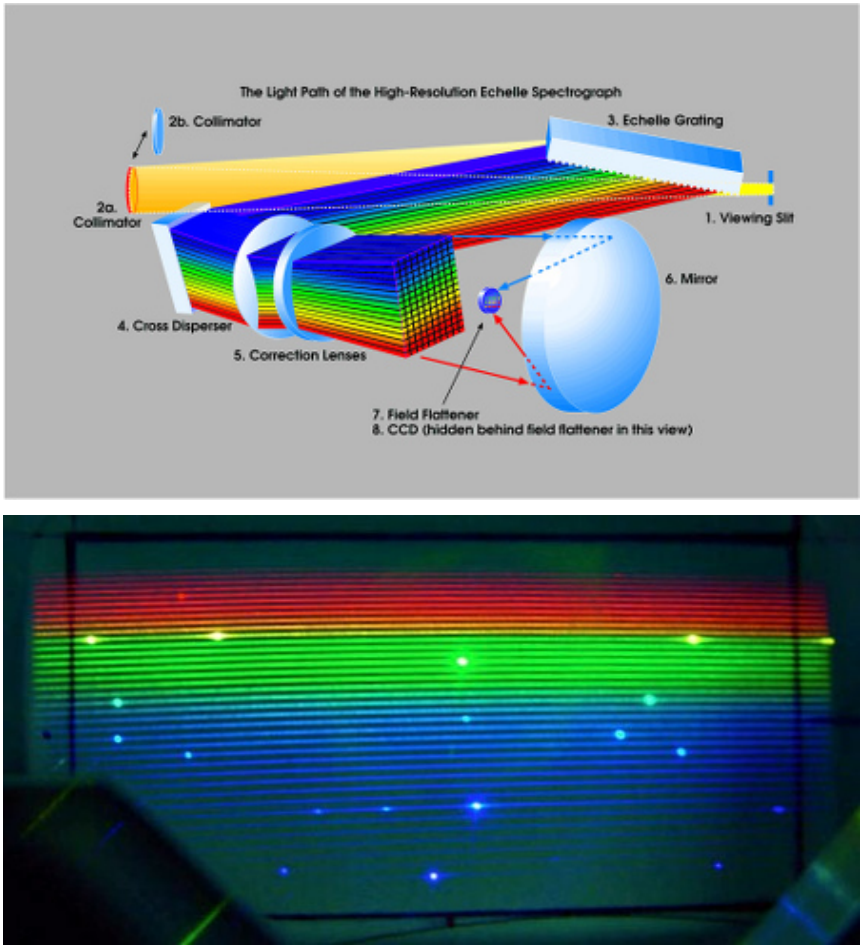

Figure 3.4 – On the top, schematics of an Echelle spectrograph (Keck Telescope HIRES, courtesy of Dr. Steven S. Vogt). On the bottom, A color image of the echelle spectrum projected onto a translucent screen in the SOPHIE échelle spectrograph, Observatoire de Haute-Provence.

the problems, but not all of them. For all those reasons, we didn't deem Echelle spectrometers suitable for our application, although we still think they are the best solution for anyone that doesn't work outside a laboratory (and that can afford their cost).

A cheaper alternative involves the use of an array of CCD coupled compact Czerny-Turner spectrometers: the overall cost is greatly decreased (around 20k€) but the quality as well. CCDs have a much lower signal to noise ratio, lower sensitivity and a longer integration time: the electronic shutter integrated in most of the spectrometers has a minimum integration time of 1.1 ms, while the typical LIBS plasma lasts for hundreds of nanoseconds, a few microseconds tops. Moreover it is not possible to have a wide spectral range with high sensitivity and resolution, then the simultaneous use of spectrometers with different spectral ranges (and in some cases different kind of sensors) is mandatory. This means that the plasma light collected needs to be split among all the spectrometers, introducing additional losses and decreasing the intensity of the light that each of them receives.

To maintain a reasonable light level for each spectrometer in the array, their number has to be limited, and consequently the number of pixels over which the whole spectrum is sampled is largely smaller than for the Echelle spectrometers. The greatly decreased number of available pixels entails a reduction of resolution or spectral range (or both). The only real advantage that an array of spectrometers has over an Echelle spectrometer is that each spectrometer can be tailored to the spectral range that it has to measure, changing the grating and the sensor in order to maximize the efficiency.

For example, coal spectra show multiple lines in UV and deep UV region, so we used four spectrometers with 3600 and 2400 lines/mm gratings to cover the region between $180-500nm$, while we used only two spectrometers with lower resolution between 500 nm and 900 nm, where the lines were more spaced out. In addition, a CCD or a grating that is optimized for UV wavelengths won't work well (or at all) in the NIR region; Echelle spectrometers suffer from the same problem, and the most advanced employ two different cameras to record different regions of the spectrum.

Following the advice of other researchers working on LIBS applications, we decided to acquire seven AvaSpec-ULS2048 spectrometers from Avantes, alongside the hardware and software needed to make them work together. We considered the possibility of employing Ocean optics spectrometers, but at that time their equivalent model, the HR2000, suffered badly of trigger

Figure 3.5 – A picture of the spectrometers with the optical fibers.

jitter and in the end they could not be used for triggered LIBS measurements. The spectrometers were equipped with a 10 μs slit (according to sensor pixel dimension and spectrometers internal optics), in order to maximize the resolution, and different gratings to cover the spectral range of interest, according to the table 3.1.

Later measures showed that the last spectrometer doesn't provide useful information because all the atomic emission lines are covered by strong molecular emission bands; for this reason, we decided to employ only the first six spectrometers, in order to increase the fraction of light delivered to each one of them.

After a thorough characterization of the spectrometers, we found several problems, both in the control software and in the hardware. The main

range (nm)	grating	detector coating	psf FWHM (nm)
177.3 - 251	UV 3600 lns/mm	UV	0.03
245.9 - 312.3	UV 2400 lns/mm	UV	0.05
304.6 - 416	UV 2400 lns/mm	UV	0.05
401.4 - 496.9	UV 2400 lns/mm	—	0.07
482.1 - 721.5	VIS 1200 lns/mm	—	0.13
697.2 - 902.8	VIS 1200 lns/mm	—	0.15
883.5 - 1057.5	NIR 1200 lns/mm	—	0.20

Table 3.1 – Wavelength range, grating type, optional detector coating and point spread function FWHM for each spectrometer.

problem was that the sensor is extremely noisy: we were told by the manufacturer that the signal to noise ratio was 200:1, however, what they actually meant was that at the lowest possible integration time the dark current noise distribution FWHM is 1/200th of the maximum value that the sensor can measure. In our functional tests of the spectrometers, in addition, we found out that with integration times greater than 5 seconds, the dark current alone saturates the output; luckily, we always could work at the lowest integration time, but due to the low intensity of the recorded signal it was necessary nevertheless to perform an average of a great number of acquisitions (at least 250, usually between 1000 and 4000).

The second greatest problem we faced was the fact that the software provided by the manufacturer to control the spectrometers acquisition was not stable at all, jammed and crashed any odd time and was ridden of major and minor bug. After a lot of testing, a lot of complaining, a couple of meeting with the programmers and seven re-release of the software, at last, we were able to make the spectrometers system work most of the times.

Another great problem we had to overcome is that when the acquisition had to end before the beginning of the LIBS signal, the spectrometers measure the same spectra they measure with "normal" timing, but shifted in wavelengths. We don't know what actually causes this behaviour, because Avantes always denied the problem, but we believe that this is due to the fact that the employed CCD linear array does have neither a mechanical shutter nor an effective electronic shutter (as it really should) that prevents charge collection during the readout - charge transfer - phase; we believe that the charges are directly transferred to the readout amplifier

stage without an intermediate step into a protected buffer. In this way the light reaching the sensor during the readout can still be recorded as if it reached a different portion of the sensor during the integration time (fig. 3.6). We discovered this behaviour when we tried to measure the spectrum emitted only during the early stage of plasma evolution and we intended to use the shutter, that should stop charge acquisition at the end of the acquisition period, as a gate, but the aforementioned problem clearly forbids that kind of measure.

We encountered a lot of other inconvenience during the use of the software: for example, the software automatically saves the acquired spectra only into a proprietary binary file that can be opened only with the acquisition software. It is possible to convert those files into a standard ASCII format, but it is not possible to automate the procedure, so each file had to be loaded and then re-saved in order to be further analyzed. Avantes never provided the file structure, so we had to perform a bit-per-bit analysis of the files in order to recover at least the wavelengths and spectral information; we were never able to recover headers and metadata, though. Last, but not least, many features supported by the spectrometers were not implemented into the software.

In the end we decided to use the LabVIEW dll provided with the software to build our own control software, even though it took a great deal of time; a relevant part of the code, in fact, was not documented and the provided examples were either badly coded or plainly broken. On the bright side, all the effort put in the building of a functioning control software provided us with a better knowledge on what the spectrometers could or could not actually do. For example, we discovered, although we were assured of the contrary, that it is not possible to control two different arrays of spectrometers using two different external triggers: on the other hand, we discovered that, thanks to a hidden feature, it is possible to set for each spectrometer a different delay between the time it receives the internal trigger and the time it starts the acquisition. A more detailed description of the software features can be found in the appendix A.3.

In order to get the correct values for amplitude and wavelengths, the spectrometers had to be calibrated.

First of all, each time we performed a measure session we had to acquire a dark frame reference, in order to be able to remove the average value of the dark current. The standard procedure we used consisted in taking 10'000 single "dark" spectra, using the same integration time we intended to use

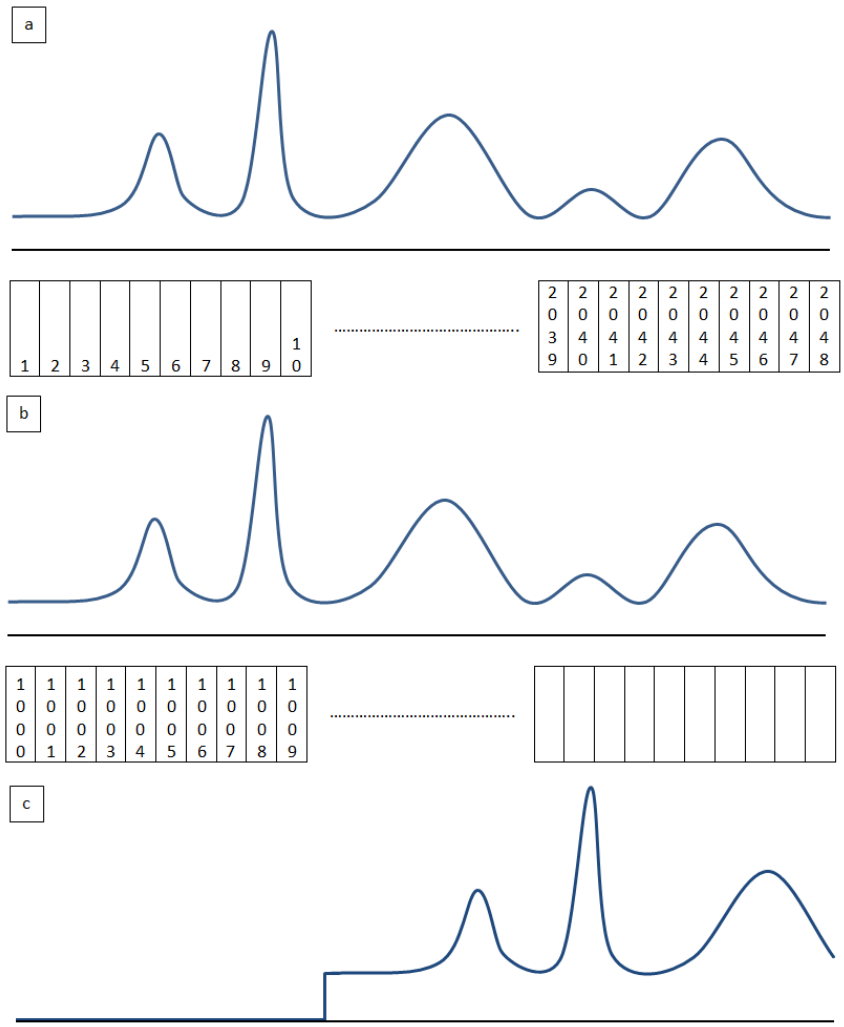

Figure 3.6 – When the light pulse comes during integration time (a) the pixels are charged, then the charges are sequentially transferred to the readout stage; when the light pulse reaches the sensor during the readout time(b), part of the pixels have been already read: the now charged pixels are then read as if they were coming from a different portion of the sensor. The recorded spectrum (c) is a truncated and shifted replica of the original one.

for the measure, while keeping the slits covered; those spectra were then averaged in order to obtain the dark reference. Every time we then performed a measure, that reference was subtracted from the acquired spectra.

The second correction done was the wavelengths correction: a wavelength calibration was already provided with the spectrometers, but when we tried to merge the spectra coming from different spectrometer we found that they didn't overlap. When we measured the wavelength of some well known lines, we found that the provided calibration was sometimes off of more than $0.5\,nm$. We used both an Ar-Hg calibration lamp and the lines from the LIBS spectrum of Anticorodal aluminum alloy to perform the calibration.

The third correction was the intensity calibration: we used the Ocean Optics DH-2000-CAL radiometric calibration source to measure the efficiency of the system and apply the appropriate corrections.

3.4 Optical fiber

In order to deliver the light to the six spectrometers, we had to develop a way to shine the light coming from a single optical fiber into six different slits; the usual way to do so is the use of an optical fiber coupler/splitter. This device consists in two optical fibers joined in such a way that the two cores are melted together; the length of the section along which the cores are joined determines the fraction of light that is passed from one fiber to the other.

While this approach works well enough when only two spectrometers are involved, our situation was quite different. First of all, each junction had a loss, and the need of 5 junctions made those losses problematic, due to the already low signal; another problem came with the fact that the fraction of light exchanged across the junction depends on the wavelength. The only way to reduce the dependency from the wavelength is to use a large core multimode fiber, but the coupling of these fibers with our narrow slits leads to unbearable losses (coupling a $600\,\mu s$ fiber with our $10\,\mu s$ slit lead to a loss of 97.9% of the incoming light).

We developed an alternative method to increase the efficiency of the light splitting procedure: we designed a bundle of 78 small fibers ($50\,\mu s$ core, $65\,\mu s$ external diameter) that is split into six tails. Each tail ends with a connector in which 13 fibers are stacked into a linear array, to better match the entrance slit of the spectrometers. In order to ensure that each

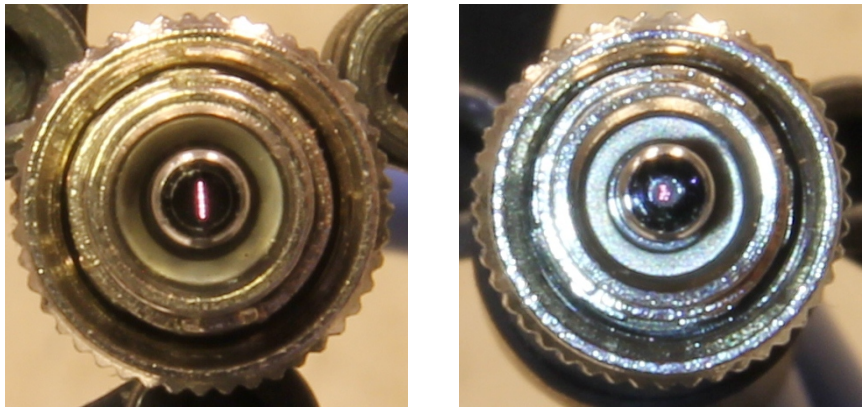

Figure 3.7 – Close-up pictures of the two ends of the fiber bundle: on the left, one of the six tails connected to the spectrometers, on the right, the connector with all the 78 fibers bundled together.

fiber received the same amount of light, we added a $5\,m$ long $600\,\mu s$ core multimode fiber before the bundle: when we use a fiber with a core so large, the output intensity profile no longer depends on the spatial intensity distribution on the input face. In this way the coupling efficiency resulted to be 13.6% (each spectrometer would receive 2.3% of the light collected by the 600um fiber).

Reducing the diameter of the small fibers could allow the increase in efficiency, but there are limits on how small the fibers can be, if we want them to be able to guide all the wavelengths of our spectra. With a $10\,\mu s$ core fiber with $20\,\mu s$ external diameter it is possible to achieve an efficiency of 18.8%, while employing more exotic fiber, with square core and square cladding, it is possible, in theory, to reach efficiency of 25%; however, the limited vertical size of the sensors, coupled with the width of the slits, limits the possible efficiency at 21.2%. In addition, such fibers have to be custom drawn, and their cost far exceeded our budget. On the bright side, the use of larger fibers gives us a small tolerance ($\pm 1.7°$) while coupling the connector with the slits.

3.5 Trigger generator

In order to synchronize the laser shot and the spectrum acquisition, we had to develop an appropriate delay chain: we used an Agilent 3220a waveform

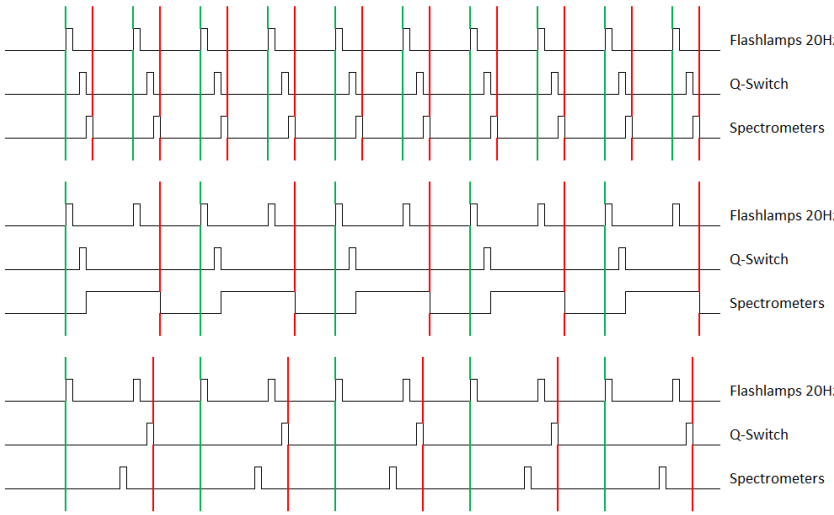

Figure 3.8 – Examples of delay configurations: in green the beginning of a trigger cycle, started by the first available flashlamps trigger, in red the ending. On the top, the typical configuration, with the laser operating at 20 Hz, and the acquisition beginning a little time after the laser pulse. In the middle the triggers configuration used to operate at 10 Hz: by increasing the duration of the spectrometers trigger it is possible to achieve lower frequencies. On the bottom, the delay configuration used to begin the acquisition before the beginning of the lamp flash.

generator and a SRS DG535 delay/pulse generator to provide all the triggers we needed for the system to work. The waveform generator provides a $10us$ long TTL signal at a frequency of $20Hz$ (the flashlamps repetition frequency of the Laser): this signal is used both to synchronize the flashlamps of the laser and to trigger the delay generator; the delay generator then provides trigger signals for the spectrometers and the Q-switch of the laser.

By changing the delay between the flashlamp and the Q-switch it is possible to change the energy and the duration of the pulse: because we had no need to do so in our experiment, we decided to operate in the optimal regime, using the delay provided by the manufacturer.

The system doesn't allow to change the frequency at which the flashlamps operate: in fact flashlamps frequency must be fixed in order to keep constant the heat exchange rate between the Nd:YAG crystal and the surrounding environment. The only way to change the laser pulse rate was then to skip a fixed number of lamp flashes between two consecutive Q-Switch

openings: that was done by sending to the spectrometers a trigger pulse as long as the delay we want to set between the two Q-Switch pulses. In this way the pulse generator has to wait the end of a delay routine before it can start another one, meaning that it waits the end of the spectrometer trigger before sending another laser trigger; the spectrometers are unaffected by the duration of the signal, because they use only the rising edge of the pulse as a trigger. The delay between two laser pulse, however, can only be a multiple of 50 ms, the delay between two lamp pulses.

It is possible to start the spectrometers acquisition before the laser pulse by delaying the Q-Switch trigger long enough that the Q-Switch opens after the second flash, as shown in figure: in this way, however, it is possible to achieve a maximum repetition rate of only 10 Hz.

3.6 Coal circulator

In order to test the system we had to develop a way to reproduce the conveyor belt of a power plant: in this situation the coal is presented in pieces with sizes varying from 1 mm to 10 cm, traveling at speeds up to

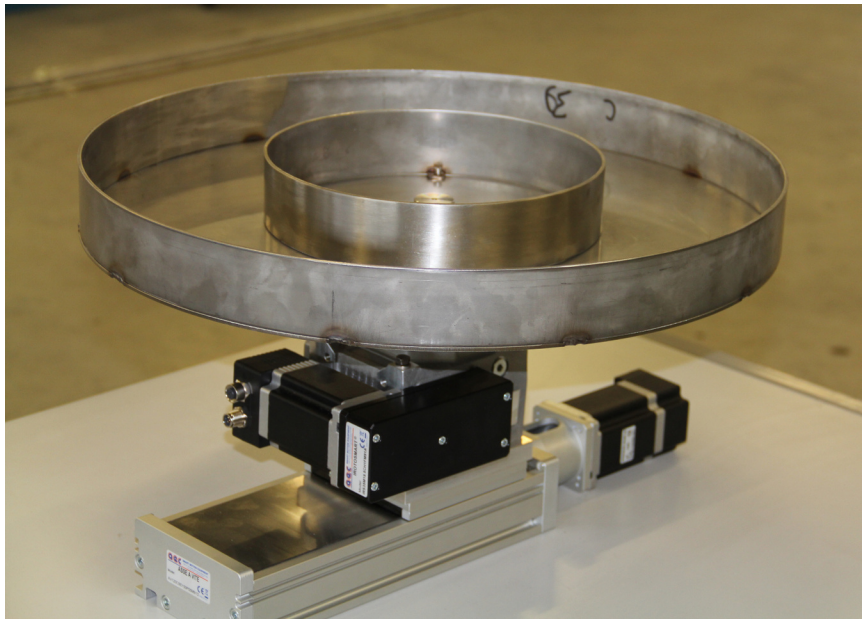

Figure 3.9 – Picture of the coal circulator.

$3\,m/s$ and variations on the height of the coal layer of about $15\,cm$. To simulate these conditions we designed a device, that we called circulator, where a circular tray is kept rotating by a motorized stage, while a second translation stage can move the tray axis along a radial direction. A motor control unit regulates the translation and rotation speed. With the rotation of the tray it is possible to reproduce the moving surface of the coal, while the translation allows to sample different points of the coal samples. The device is enclosed in a case for safety reasons and it is mounted on a cart. The circular tray has an outer diameter of $40\,cm$, an inner diameter of $20\,cm$ and a depth of $10\,cm$; it can rotate at a maximum speed of $200\,rpm$ ($4.2\,m/s$ on the outer edge), but only rotation speeds lower than $60\,rpm$ ($1.3\,m/s$) have been used, because otherwise the centrifugal force would push all the coal against the outer edge, leaving the inside part of the tray empty.

The translation stage can travel for $25cm$ at a maximum speed of $0.2m/s$; the speed was set so that the stage would make a whole trip back and forth in the time that was needed for the measure. For example, for an acquisition of 4000 samples at a rate of $20Hz$ the translation speed was set at $2\,mm/s$.

In order to avoid the dispersion of coal dust in the laboratory, we kept the pressure inside the case lower than the pressure outside using an aspirator; the air flow entering through the opening for the laser also keeps the laser beam path free from dust particles.

Chapter 4

Collection optics

The development of a suitable collection optic was one of the most important parts of my work: during the development of the final prototype, different kinds of optics have been tested and employed. The final prototype had several requirements:

- a depth of field of at least 10 cm, but preferably of 15 cm or more, in order to be able to collect light even when the distance from the sample changes, as is likely to happen to the coal on a conveyor belt;
- a field of view diameter of at least 2 mm, in order to be able to collect the light coming from different areas of the plasma with the same efficiency;
- the ability to collect light with wavelengths ranging from 200 nm to 900 nm;
- a collinear optical geometry (the optical axis of the receiving optics must be the same of the laser).

To compare the different configurations, we defined the collection efficiency of the system as the fraction of light, emitted by a point-like source, that the system is able to couple into a 600 μs 0.22 NA optical fiber. The systems were usually designed to work at a distance of 1m from the sample and the depth of field were defined as the range of distances within which the efficiency is higher than half of its maximum value. In order to design

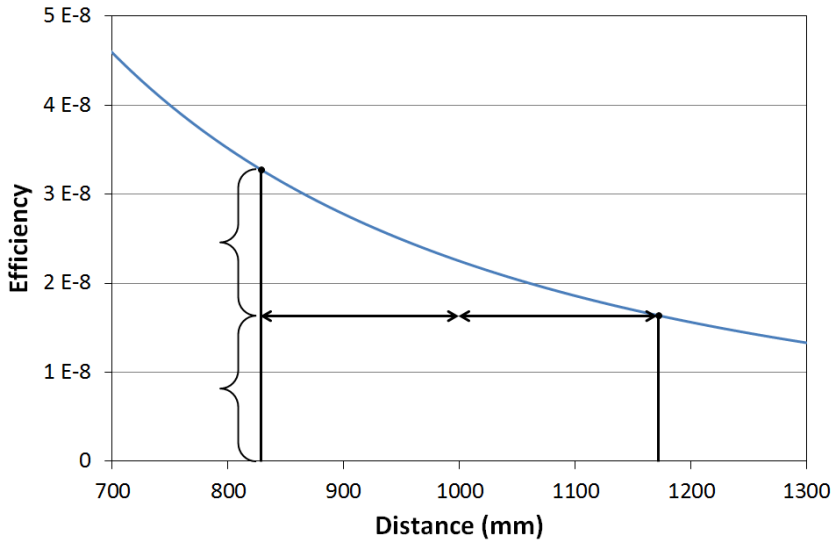

Figure 4.1 – Collection efficiency of a 600 μs core optical fiber; the depth of field of this configuration is estimated as the distance interval, symmetric around 1 m, in which the highest efficiency is twice the lowest one.

and test the optical systems, I used both commercial and proprietary software: I used WinLens3D to develop a basic model of the system, then I used a ray-tracing software I wrote by myself to perform the efficiency analysis. Details on the ray-tracing software can be found in appendix A.2.

4.1 Bare fiber

A bare fiber placed in front of the sample is the simplest and cheapest collection system. It collects light from a broad angle, making the alignment really easy, and it works at any wavelength (limited by the transmission efficiency of the fiber as any other system). Its efficiency is limited only by the diameter of the fiber's core and for this reason it has the best efficiency among systems with the same aperture.

Its main drawback is that the diameter of the fiber can't be increased, so its overall efficiency is really low, especially at great distances, while when positioned near to the sample, it risks suffering damage from the impact of debris produced during the ablation.

At the distance of 1 m, using the reference fiber, the efficiency of this

system is $9 \cdot 10^{-8}$, while its depth of field is of 34 cm in the range between 83 and 117 cm.

4.2 Diffractive optics

The easiest way to increase the efficiency of the collecting system is to use a lens: in this way it is possible to collect the plasma light from a greater area; however, the use of lenses brings some problems.

First of all there is the problem of the spherical aberration, but that can be easily solved by using aspherized lenses, commercially available in a large variety of diameters and focal lengths. Then we have the problem of the glass opacity; most of the optical glasses are optimized to work in the visible range of the electromagnetic spectrum, while they are opaque to the UV and IR band. Among the most used materials only two are transparent in the whole range from 200 nm to 1100 nm: the fused silica and the calcium fluoride. While the latter has better optical properties, it is brittle and prone to be damaged by humidity and thermal shocks. Fused silica, instead, is a stable and reliable material, but lenses made with this material have a great chromatic aberration; when using wavelength in the range from 200 nm to 1100 nm a fused silica plano-convex lens has a chromatic aberration of 19%

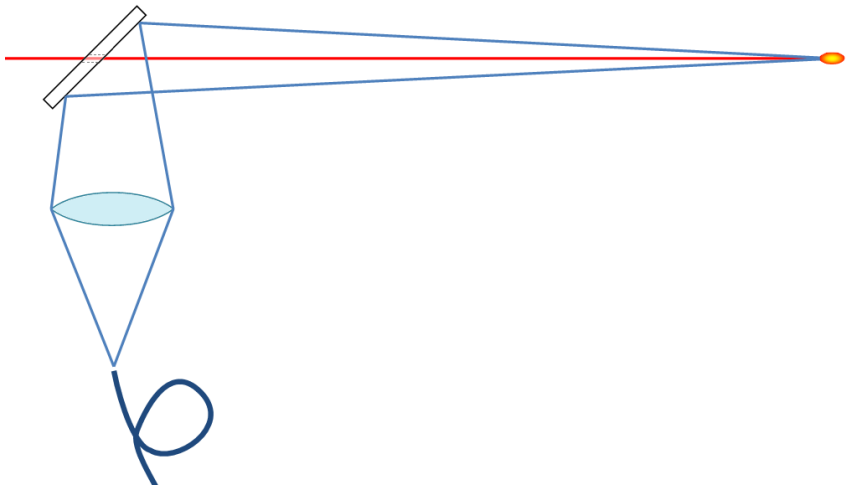

Figure 4.2 – Schematic of a diffractive collection optic; a holed mirror is employed in order to collect the light on the same axis of the laser.

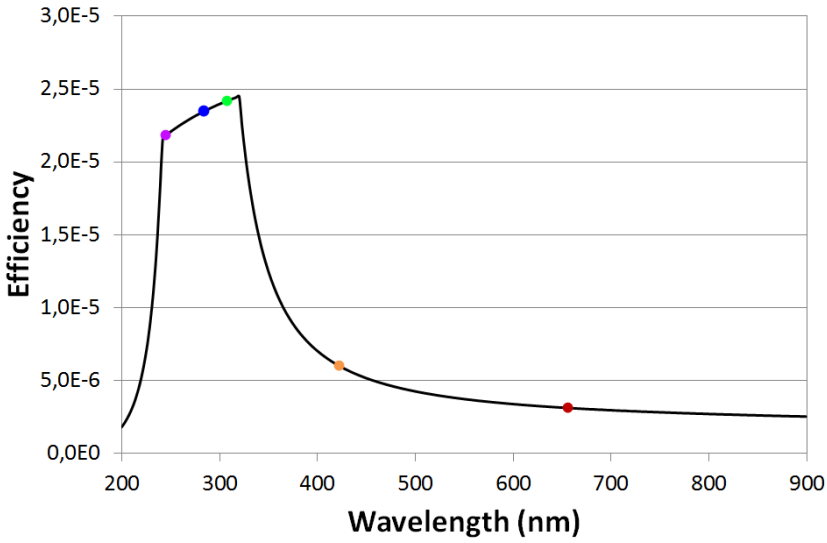

Figure 4.3 – Collection efficiency of a plano-convex fused silica lens as a function of the wavelength; the lens has a diameter of 1" and a focal length of 2". The five coloured dots mark the wavelengths of the spectral line of carbon, silicon, aluminum, calcium and hydrogen.

of its effective focal length at 500 nm. Once the lens and its distance from the optical fiber have been chosen, the efficiency of the collection system depends both on the position and the wavelength (fig. 4.3), and only a small fraction of the spectrum can be collected at the same time.

To overcome this problem, the typical approach involves the use of achromatic lenses: a focusing lens is coupled with one or more defocusing lenses made with a different glass, and the focal lengths are designed so that the different dispersing powers of the lenses compensate each other, greatly decreasing the chromatic aberration.

Most of the achromatic lenses, however, are built by gluing the elements together using UV-cured optical adhesive, therefore they are completely opaque to wavelengths under 320 nm. For our application we needed an air-spaced corrected triplet, an apochromatic lens in which the components are held together by an external housing.

As the simulation shows (fig. 4.4), this kind of lens has a good depth of field, and a large field of view as well; in addition, there is a big volume, around the working point, inside which the efficiency depends only on the

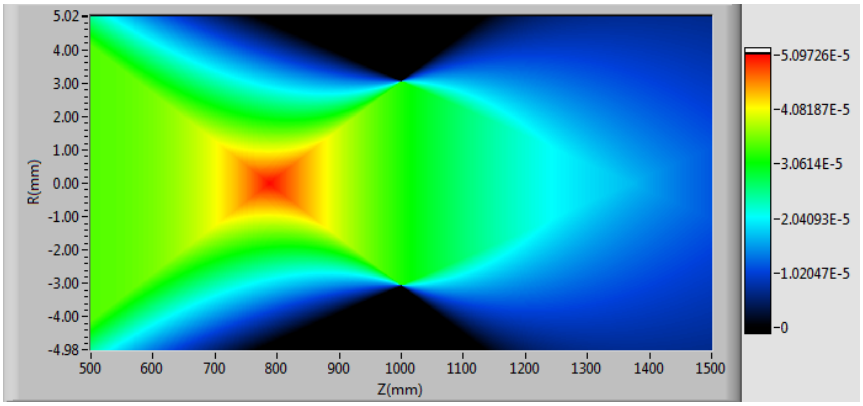

Figure 4.4 – Collection efficiency of an ideal lens, with a diameter of 22.5 mm and 90 mm of effective focal length, coupled with a 600 μs core, 0.22 NA optical fiber.

distance and not on the lateral displacement. However, these lenses have a small aperture, thus limiting their overall efficiency, especially when the working distances are so great. In addition, they employ CaF_2 lenses and, as we have already said, this material is not suitable for application in harsh environments. Last, but not least, they are expensive (2k€ the cheapest ones, while custom-made ones can be far more expensive); for all those reasons, we resolved to not use these lenses, but as a last resort.

4.3 Reflective optics

Using reflective optics is a simple way to avoid all the problems related to chromatic aberration and the use of mirror based collection optics for laboratory set-ups is well documented in literature.

One of the most effective configurations (fig. 4.5) involves the use of two parabolic mirrors to couple the plasma with the entrance slit of the spectrometers. The two mirrors have different focal lengths: the first one is selected and placed in such a way that the plasma is generated in its focal point and has a short focal length, so that it can collect the emitted light from a wider angle. The second mirror, instead, creates an image of the plasma directly onto the spectrometer slit and has a longer focal length, in order to match the small numerical aperture of spectrometers.

This kind of configuration is perfect for laboratory set-ups, where the

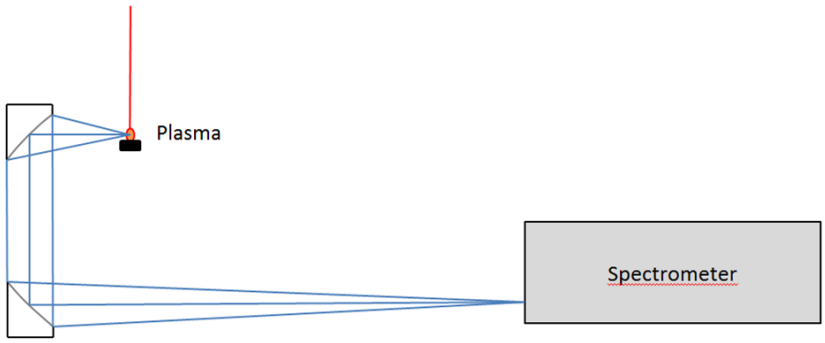

Figure 4.5 – Schematic of a reflective collection optic; this particular configuration, made with two parabolic mirrors, recreates an exact replica of the plasma light directly on the entrance slit of the spectrometer.

exact position of the plasma is known, because the wide acceptance angle and the really short depth of field allow to select a precise portion of the plasma to be analyzed; however the same properties that make it great in laboratory, make it unsuitable for on-line application. For these reasons we investigated alternative configurations of mirror based collection optics that could provide the desired characteristics.

Off-axis parabolic mirror

The first configuration we have investigated is composed of a single holed parabolic mirror; instead of placing the plasma in its focal point, we used the mirror backwards, placing the optical fiber in its focal point. If the distance of the plasma from the mirror is adequately larger than the focal length, then the light is collected as if it came from a source at infinite distance. Using the ray tracing software I have built, we simulated the behavior of different mirrors and studied their efficiency. As it is clearly visible from the figure 4.7, this kind of optics suffer badly of coma aberration.

We tested different combinations of diameters and focal lengths and we found out that as the focal length increases, so does the size of the spot on the face of the optical fiber: this is due to the fact that as the focal length increases, the approximation of infinitely distant source is less accurate, increasing the coma aberration.

On the other hand, mirrors with too short focal length will focus the light from angles greater than the acceptance angle of the fiber, thus reducing

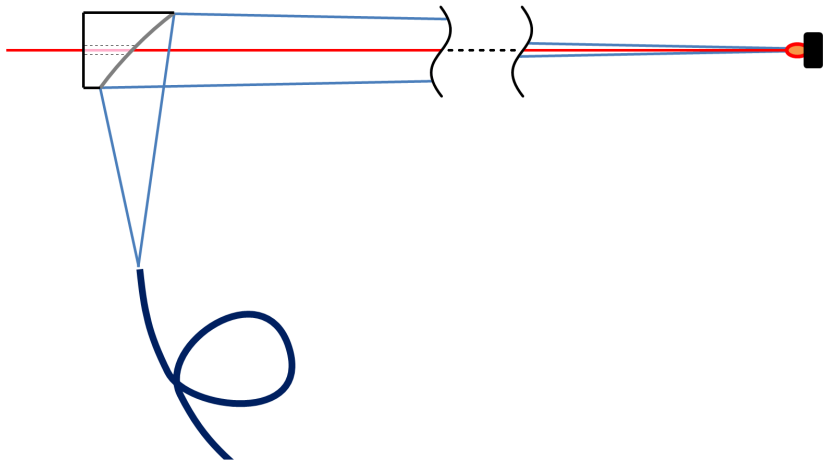

Figure 4.6 – Schematic of a reflective collection optic; this configuration employs a single holed parabolic mirror to focus the plasma light onto the face of the optical fiber.

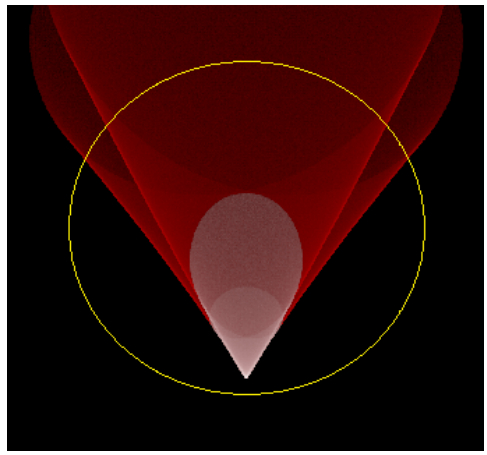

Figure 4.7 – Numerical simulation of the light spot generated on the input face of the fiber by a point-like source; the yellow ring represent the core of the optical fiber, the white area is the light actually collected by the system, while the red area is the light collected by the mirror but not coupled into the fiber due to its limited NA.

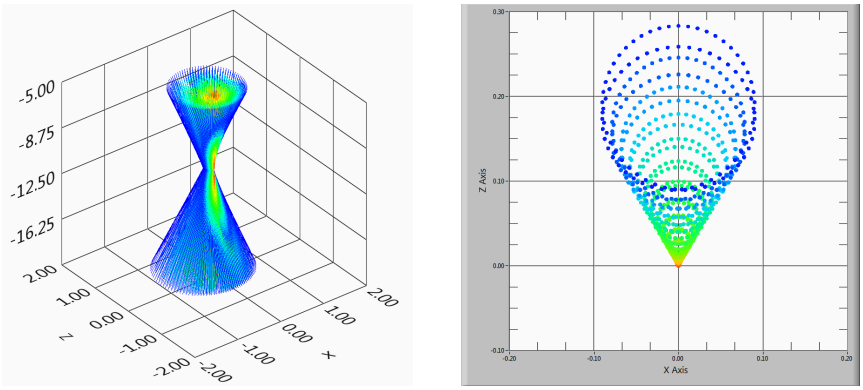

Figure 4.8 – On the left, ray tracing for the parabolic mirror in the proximity of the focal point, where the optical fiber is placed; on the right, the section along the horizontal plane. It can be seen that the rays reflected by the outer rim of the mirror fall further from the center and with a greater angle.

the overall efficiency. The optimal focal length is the one long enough to avoid loss for limited NA, but not so long that the spot is so big that most of the light fall out of the fiber.

Larger mirrors have the advantages of collecting more light, however the diameter of the mirror affects both the angle and the size of the spot: as we can see in figure 4.8, the light reflected by the outer rim of the mirror draws a double looped path on the face of the fiber, and the larger the mirror is, the farther from the tip of the coma the double loop will be. In addition, the light reflected by the outer rim will be the one that will reach the fiber at the greatest angles; for both these reasons, for each focal length there is a value for the diameter beyond which increasing the diameter does not provide a better efficiency.

Once we had found the optimal size and focal length, we evaluated the collection efficiency of this configuration. As we expected, the system doesn't have a cylindrical symmetry, and as the light source is moved from the optimal working position, the spot on the fiber is badly distorted. As a consequence, the volume from which the system collects light, defined as the volume in which the collection efficiency is greater than half of the maximum value, has a peculiar shape, with lobes and protrusions (fig. 4.9). This situation is not desirable, because it means that the light emitted by different parts of the plasma plume would be collected with different efficiency.

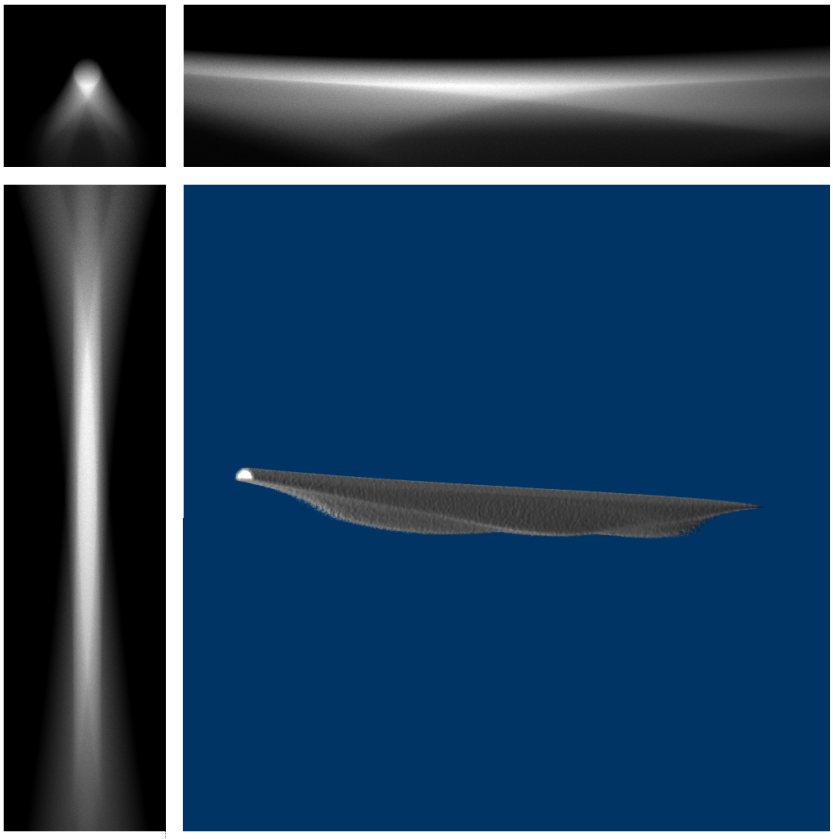

Figure 4.9 – Numerical simulation of the collection efficiency of a single holed parabolic mirror. The main figure reports the volume inside which the collection efficiency is greater than half of the maximum value; the collection efficiency on the three main planes is plotted around that.

There were other reasons that lead us to the decision of not using parabolic mirror: for example, most of those mirrors are built using a replication process that leaves the surface too rough to be used for deep UV application. Another problem comes from their thickness ($\sim 3\,cm$): boring the hole for the laser beam without damaging the mirror would be extremely difficult. For all those reasons we chose to investigate other possible solutions.

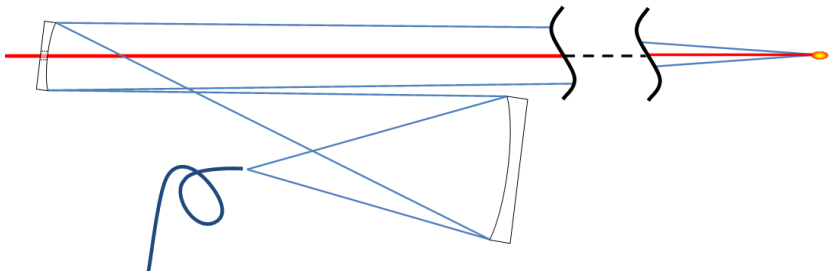

Figure 4.10 – Schematic of a reflective collection optic; this configuration employs two spherical mirrors with the same tilt and curvature radius to remove spherical aberrations.

Spherical mirror

Inspired by the design of Czerny-Turner spectrometers, we devised a set-up in which the use of two spherical mirrors allows us to obtain an image of the plasma devoid of most of the aberrations. Some simulations, carried out with the software WinLens3D, showed that most of the properties of the system depend on the focal length of the first mirror, while the second one works in a 2F-2F configuration and provides only the correction to the spherical aberrations.

As in the parabolic mirror configuration, in order to obtain a long depth of field the focal length of the first mirror should be small compared to the distance from the plasma; however, if the focal length is too small some of the light would be lost due to the NA of the fiber. In addition, a great curvature radius/mirror diameter ratio weakens the aberration correction ability of the system.

On the other hand, a long focal length brings other problems into the system; for example, the longer the focal length, the bigger the whole system would be, and the smaller the distance of the second mirror from the plasma would be. This problem is also doubled by the fact that the best correction power is obtained when both the mirrors have the same curvature radius.

In addition, the system is slightly astigmatic, due to the tilt angle of the two mirrors, and an increase in the focal length would also increase the size of the light spot on the fiber. Last, but not least, during the search for the optimal configuration we had to make sure that the mirrors did not intersect the light beam; we had also to take into account the space needed for mirrors and fiber holders. As for the other configurations, we selected

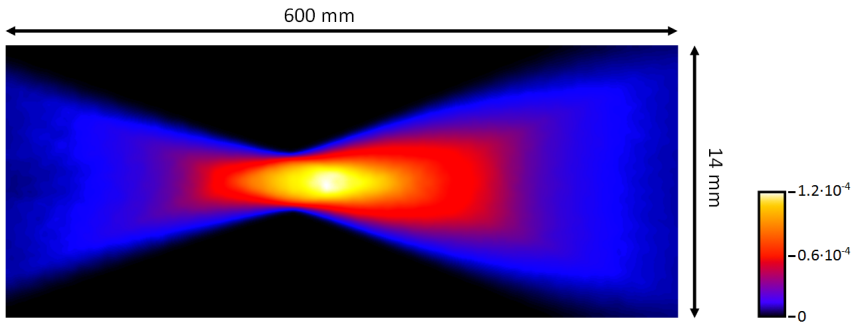

Figure 4.11 – Numerical simulation of the collection efficiency of the system in the vertical plane containing the optical axis; the mirrors are out of the picture on the far left.

the elements from the ones that were commercially available at the time.

We found out that for our needs the best configuration is the one that uses two mirrors with a focal length of 8" (203.2 mm). We ran some simulations using my ray-tracing software and compared the results with the ones obtained for the other configurations: as it can be seen from the graph 4.12, the spherical mirror configuration is, by far, the most efficient, between the investigated configurations, that can be built without resorting to custom made components. This is mainly due to the fact that this configuration allows the use of big elements, and that the surface of the first mirror is four times the surface of the parabolic mirror and five times the surface of the corrected triplet. As an added bonus, the collection volume has a much more regular shape than the parabolic mirror's one, and it is nearly symmetric around the optical axis. It has however a smaller depth of field than the other two systems, but it is still big enough for our requirements.

We built a small scale set-up, based on this configuration but with mirrors of 2" FL, to test the system on a laboratory scale; the details about the tests will be provided in chapter 5. The full scale system, however, would be too big to work, if realized using this design: the second mirror would be only 30 cm away from the coal bed. We chose to use a plane mirror to fold the optical path and reduce the size of the system; this solution cost us an additional 15% decrease in the collection efficiency, due to the low reflectivity of broadband mirrors, but allowed us to build a system that is 35 cm long, leaving 65 cm between the flat mirror and the coal bed. This was estimated to be more than enough to safely operate on a conveyor belt.

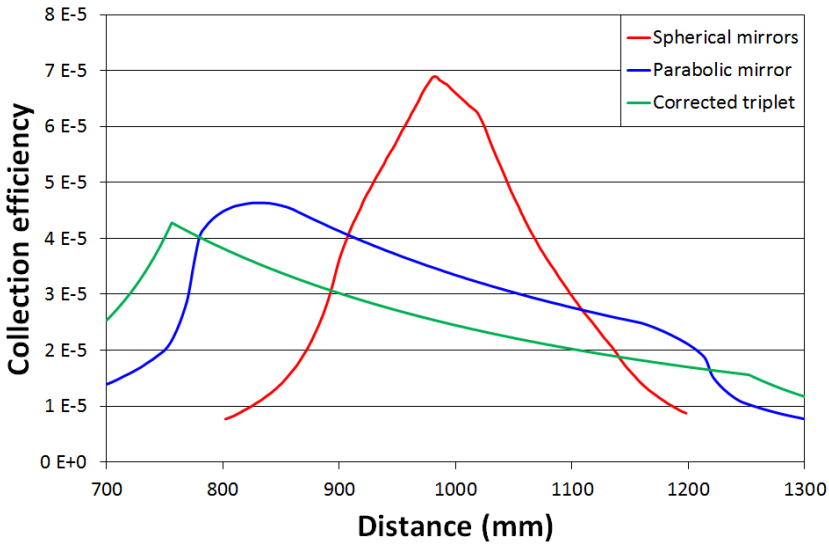

Figure 4.12 – Comparison between the collection efficiency along the optical axis of the three systems.

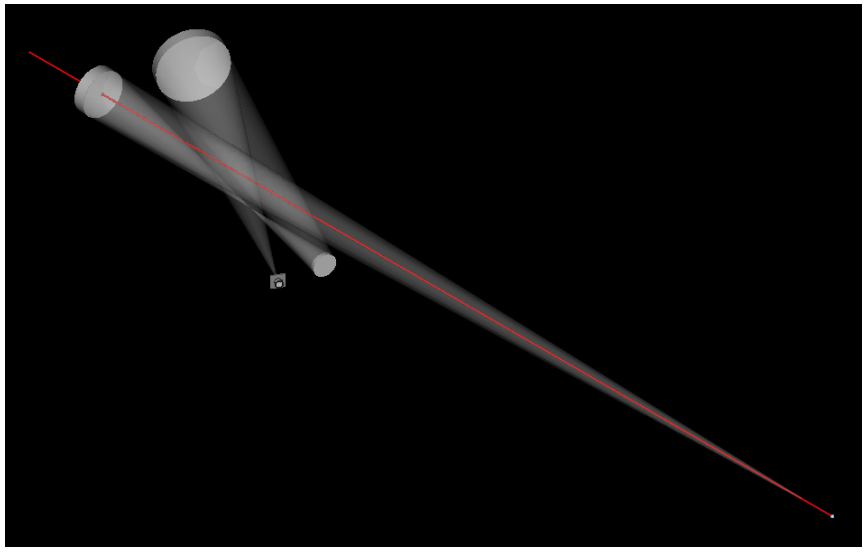

Figure 4.13 – Rendering of the full scale prototype.

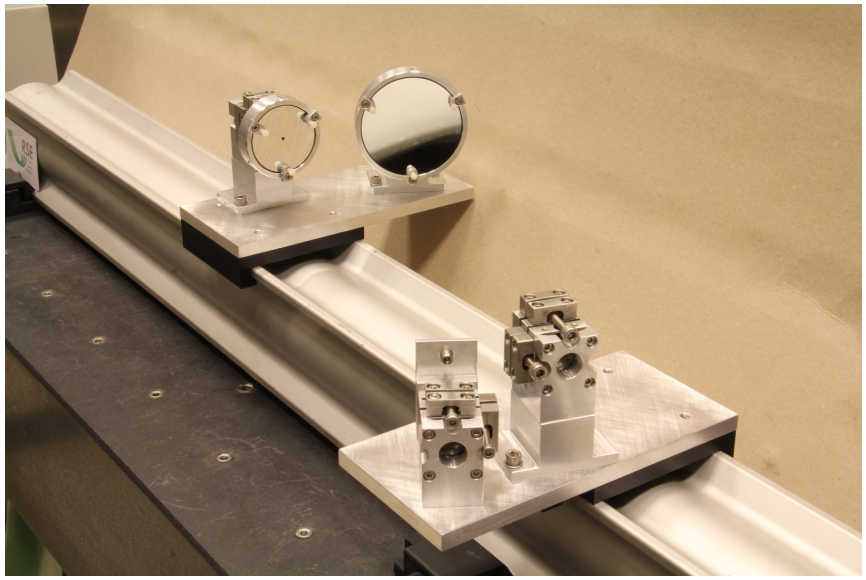

Figure 4.14 – Picture of the full scale prototype.

4.4 Prototypes

We have actually built two prototypes of the collection optic.

The first one was a small scale prototype that we used to perform tests on the rotating stage; all the measures performed on the coal were done using this system. We used two spherical mirrors with 1" diameter and 2" focal length and the system worked at a distance of 30 cm from the plasma; due to the limited size, this system didn't need the flat mirror for the folded configuration. The system has a reduced depth of field (11 cm), and, although the size of the mirrors is reduced, the smaller distance between the plasma and the collection optics allows us to achieve a collection efficiency similar to the one obtained with the full scale system.

For the full scale prototype we used two 8" focal length mirrors, the first one with a 2" diameter while the second had a 3" diameter; we used a 25 mm diameter flat mirror for the folded configuration. All the spherical mirrors are made of aluminized pyrex® 7740 with an UV enhancing dielectric coating and have a surface accuracy of $\lambda/4$; the flat mirror had a fused silica substrate and a surface accuracy of $\lambda/10$. We also designed and realized the mirror mounting, so that we could perform a fine tuning on the pitch and yaw of every mirror during the building phase and then securely lock them

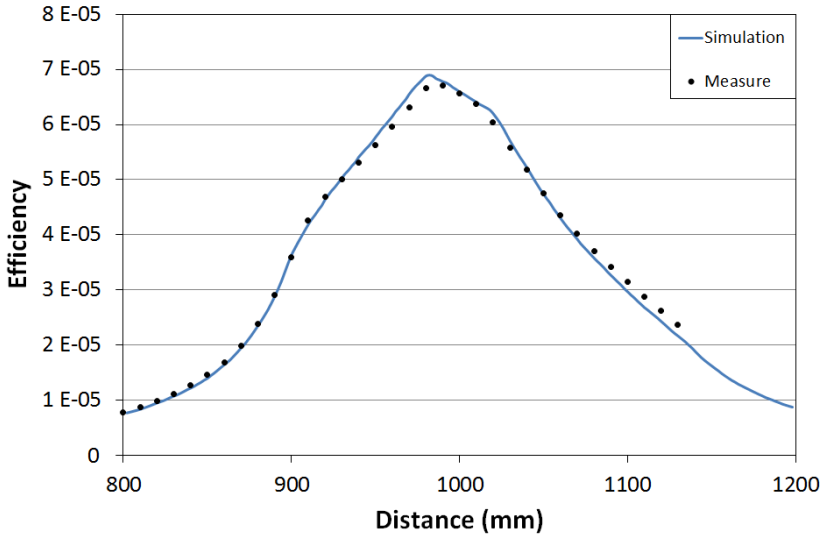

Figure 4.15 – Results of the collection efficiency measure (black dots) compared with the numerical simulation (solid line).

in position.

We tested the efficiency of the system using a 200 μs core optical fiber connected with an halogen lamp as a probe point-like source; we connected the 600μs collecting fiber to a power meter, in order to measure the collected light fraction. In order to obtain the power of our "point-like source", we placed the collecting fiber directly in front of the light source and measured the light collected from different distances; knowing the size of the collecting fiber's core and the distance between the two fibers, we were able to obtain the power of an equivalent point-like source placed on the face of the 200 μs core optical fiber. As it can be seen from the results (fig. 4.15), the actual efficiency of the collecting system agrees really well with the data obtained from the numerical simulations.

Chapter 5

Laboratory test

In this section I will describe the measures that were performed on coal, along with the data analysis. All the measures were performed using the apparatus described in 3, coupled with the small scale prototype for the collection optics described in section 4.4.

Figure 5.1 – Picture of the test system at work.

In our tests we used seven different coals of known composition.

Ideally, it would be possible to analyze each of the collected spectra, obtain the chemical composition of the plasma from each shot and then perform an average of the results obtained from different shots in order to estimate the chemical composition of the whole sample. However, as it can be easily seen from image 5.2, the noise amplitude on the single spectrum is greater than the amplitude of the lines that we want to measure: for this reason, we chose to compute the average of the spectra before the analysis.

In addition, the overall intensity of the spectra can change greatly from shot to shot, due to the coal surface shape, roughness and orientation: however, with a number of averaged spectra great enough, the averaged spectrum no longer changes from measure to measure. An increase in the

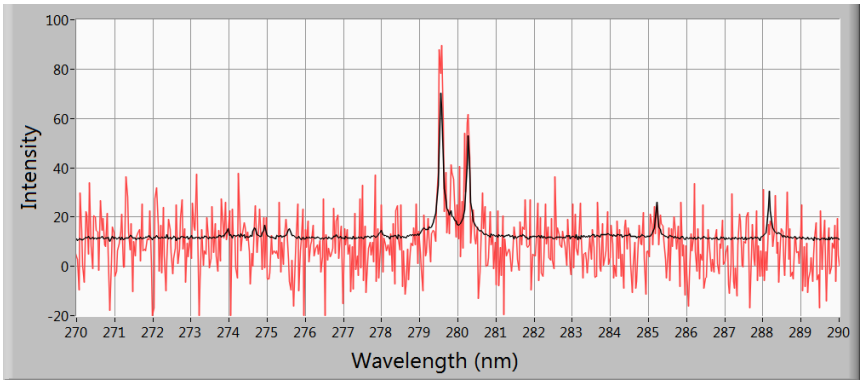

Figure 5.2 – In red, an example of single spectrum, in black, the average of 1000 spectra.

number of averaged spectra will also increase the signal to noise ratio. We found out that, using our set-up, the average of more than 1000 spectra reduces the intensity fluctuations to an acceptable level.

To be on the safe side we decided to acquire 4000 spectra for each measure: while a greater number of averages is still desirable, in order to improve the signal to noise ratio, the time needed to perform such a measure and the memory needed to store it would make it not practical.

5.1 Calibration Free

Once obtained the coal spectra we had to recover the chemical composition from the intensity of the spectral lines: the algorithm we wanted to use is the so-called "calibration free", firstly described by Ciucci, Corsi, Palleschi et al. in [135]. This algorithm is based on the equation (3.5)

$$I_{j,i}(n_e, T) = \frac{C}{\lambda} N_r(n_e, T) \frac{g_j A_{j,i}}{U_r(T)} \exp\left(-\frac{X_{r+1}}{K_B T}\right) \tag{5.1}$$

where n_r is the concentration of the atoms of the given element with ionization r, $U_r(T)$ is the partition function, $A_{j,i}$ is the Einstein coefficient for the transition between j and i, g_j and E_j are respectively the degeneracy and the energy of the level j.

$$\exp\left(-\frac{E_j}{K_B T}\right) = \frac{\lambda I_{j,i}(n_e, T)}{g_j A_{j,i}} \frac{U_r(T)}{C n_r(n_e, T)} \tag{5.2}$$

$$-\frac{E_j}{K_B T} = \ln\left(\frac{\lambda I_{j,i}\left(n_e, T\right)}{g_j A_{j,i}}\right) + \ln\left(\frac{U_r(T)}{C n_r\left(n_e, T\right)}\right) \tag{5.3}$$

$$\ln\left(\frac{\lambda I_{j,i}\left(n_e, T\right)}{g_j A_{j,i}}\right) = -\frac{E_j}{K_B T} + \ln\left(\frac{C n_r\left(n_e, T\right)}{U_r(T)}\right) \tag{5.4}$$

$$y = -\frac{1}{K_B T} x + \ln\left(\frac{C n_r\left(n_e, T\right)}{U_r(T)}\right) \tag{5.5}$$

$$y = mx + q_r \tag{5.6}$$

For each spectral line it is possible to obtain a pair of coordinates that locates a point on the so called Boltzmann plot; those points are grouped together based on the element and ionization state, then a linear fit is performed on each group. In this way it is possible to recover the value of m, ideally the same for every element, and from that the temperature of the plasma. With the temperature of the plasma it is possible to compute the partition function of each elemental species; then, using the q value from two different ionization states of the same element, it is possible to obtain the electron number density of the plasma. From the Saha equation (3.2)

$$n_e = 2\frac{n_r\left(n_e, T\right)}{n_{r+1}\left(n_e, T\right)} \frac{U_{r+1}(T)}{U_r(T)} \left(\frac{2\pi m_e K_B T}{h^2}\right)^{\frac{3}{2}} \exp\left(-\frac{\chi_{r+1}}{K_B T}\right) \tag{5.7}$$

q_r was defined as

$$q_r = \ln\left(\frac{C n_r\left(n_e, T\right)}{U_r(T)}\right) \tag{5.8}$$

then

$$\exp\left(q_r - q_{r+1}\right) = \frac{n_r\left(n_e, T\right)}{n_{r+1}\left(n_e, T\right)} \frac{U_{r+1}(T)}{U_r(T)} \tag{5.9}$$

Combining eq. (5.7) and eq. (5.9) together it is possible to obtain n_e

$$n_e = 2\left(\frac{2\pi m_e K_B T}{h^2}\right)^{\frac{3}{2}} \exp\left(q_r - q_{r+1} - \frac{\chi_{r+1}}{K_B T}\right) \tag{5.10}$$

With the temperature and electron number density it is possible to calculate the Cn_r value for each element and ionization state; usually the first 4 ionization states (neutral, +1, +2 and +3) are enough to cover more than 99.9% of the total number of atoms. Knowing that the sum of all the Cn_r value should give 1, it is possible to find the value of C and the relative concentration of all the recorded elements.

$$C = \sum_r C n_r \tag{5.11}$$

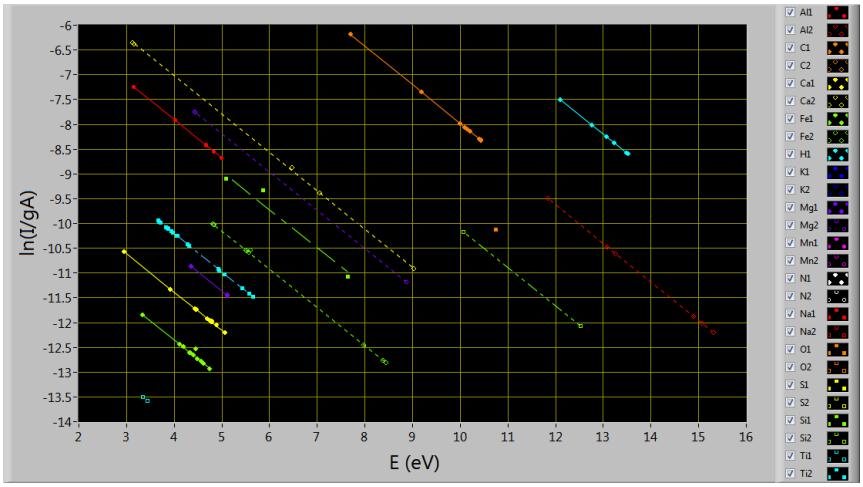

Figure 5.3 – An example of Boltzmann plot, obtained with the developed software, using synthetic spectra.

$$n_r = \frac{U_r(T)\exp(q_r)}{\sum_r U_r(T)\exp(q_r)} \tag{5.12}$$

All the data used for the analysis came from the NIST atomic spectra database. I developed three software pieces to automate the analysis of the spectra. The first one is a variation of the benchmark software described in chapter 3 and it chooses the spectral lines that would be used for the analysis; the second piece of software computes the average of the acquired spectra, subtracts the continuum background, then searches for the selected lines and measures their area. The last piece of software uses the data provided by the first two and builds the Boltzmann plot, computes the temperature and number density of the plasma and then returns the chemical composition of the sample.

The software was originally tested with excellent results using the synthetic spectra provided by the benchmark software (fig. 5.3); however, it completely failed when real spectra were used (fig. 5.4). Most of the time the software returned incorrect concentration values, and sometimes returned inconsistent values, like negative temperatures. After thorough investigations we discovered that the problems weren't in the software alone, but also in the physical model itself.

The equation (3.5), in fact, is a good model for plasma emission only when the plasma is in a state of local thermal equilibrium, otherwise the

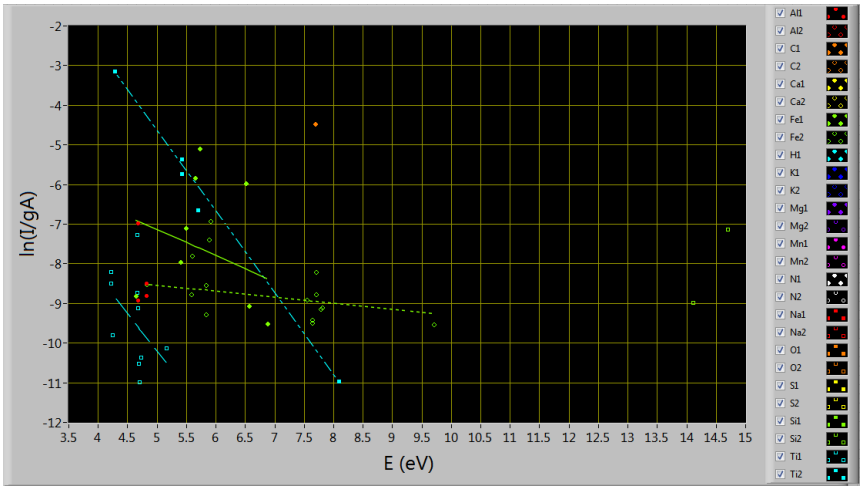

Figure 5.4 – An example of Boltzmann plot, obtained with the developed software, using real LIBS spectra: it is not possible to recover the correct concentrations. In addition, the number of recognized spectral lines is smaller than in the synthetic spectra, due to the noise of the real spectra.

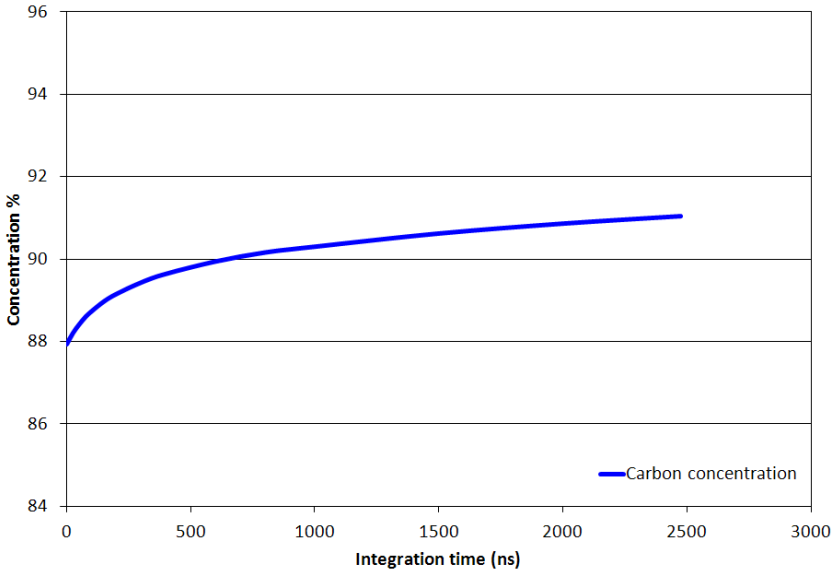

Figure 5.5 – Effect of the integration time on the measured concentration of carbon performed on synthetic spectra.

states' population will not follow a Boltzmann distribution; in addition, the equation doesn't take into account the temporal evolution of the involved quantities. Using the data from [130, 131], which measured the temporal evolution of temperature and electron number density for a coal plasma, we simulated the plasma evolution as a succession of stationary states with the given temperature and number density.

Feeding the obtained spectra to the software for the analysis, we found that the longer the integration time is, the less reliable the calibration free method is: each single spectral line, in fact, has a different temporal evolution, and performing a time average will change the lines ratio, thus changing the obtained temperature. Our measures required the average of 4000 different spectra, further aggravating this problems. In addition, neither plasma temperature nor plasma composition is uniform.

Recent works[136, 137] have performed a spatially resolved spectroscopy of the plasma, using tomography techniques. They showed that the plasma is usually structured as an hotter plasma layer with both an inner and an outer cooler region; the outer region could absorb the light emitted by the inner region, and the rate at which this absorption happens can change greatly depending on the spectral line observed. In fact, the lines that should show the strongest emission are the ones that suffer from the strongest reabsorption, to the point that sometimes they are instead the ones with the lowest intensity; from that comes the negative temperatures obtained with the calibration free method.

All that said, it is still possible to use this system successfully, provided that it is possible to perform time and spatially resolved spectroscopy; Gerhard et al.[138], for example were able to obtain good results, thanks to an accurate control over all the parameters of the plasma. This kind of approach, however, is not feasible on the conveyor belt of a power plant, and for this reason we decided to fall back on the widely used calibration system.

5.2 Calibration system

The simplest and most common way to perform a quantitative analysis using LIBS involves the use of calibration curves. Using samples of known composition similar to the ones that we want to measure, it is usually possible to find a relation between the intensity of a spectral line and the molar concentration of the atom that emits it. Using these calibrations it is then

possible to obtain the composition of unknown samples.

Once again we used an automated software to measure the spectral lines, obtaining for each one its background, amplitude, width and area, along with "global" quantities, like the background shape, area and maximum value. In order to find the best conditions, we repeated the measure on all the coals changing the delay between the laser pulse and the start of the acquisition. We also looked at different parameters to find a way to take into account the unavoidable variations of the plasma due to fluctuation in plasma temperature, plasma density and ablation rate.

Normalization

We tested a lot of different parameters that could provide information on the variation of brightness not related to the elements concentration, like the background intensity at a given wavelength, the area of the whole background emission, the width or the height of a given spectral line. For example the width of the H_α line is sometimes used to obtain information about plasma temperature and density, while the background emission has a shape similar to the black-body emission, so it should provide information on both the plasma temperature and ablation rate.

In the end we found out that only carbon and hydrogen do benefit from a normalization of their spectral lines; for both of them the best normalization parameter was the intensity of the background emission measured near the 248 nm carbon spectral line. For the iron calibration we followed the approach proposed by Romero et al.[120], dividing the intensity of the iron line by the intensity of the 248 nm carbon line, then looking for the relation between this value and the ratio between the iron concentration and the carbon concentration.

Delay

The choice of an optimal delay has been widely discussed in literature, however most of the time the criterion with which this choice is made is the optimization of the ratio between the spectral lines and the background emission. In our work, instead, we chose to use the delay that could provided us with the best results in terms of calibration curves.

During our tests we found out that, not only each element, but each single spectral line has its optimal delay: for example, carbon 248 nm, hydrogen 656 nm and calcium 422 nm provide the best calibration curves if

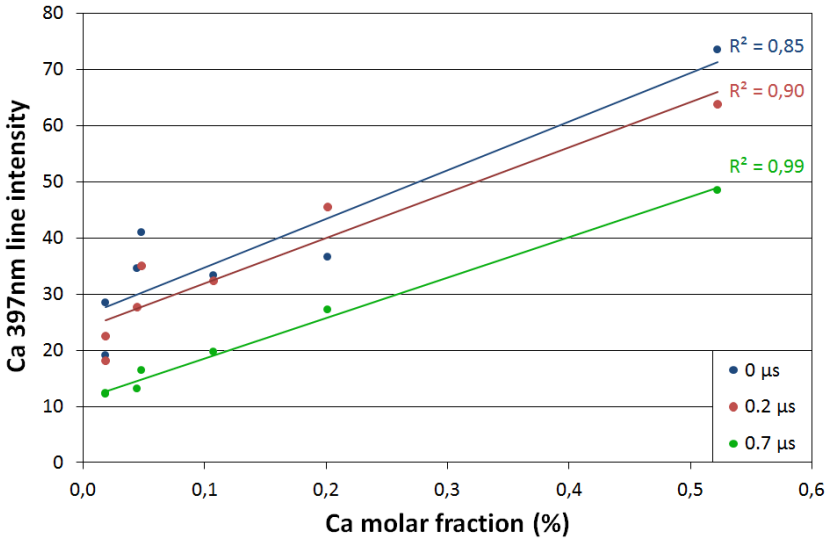

Figure 5.6 – Effect of the delay on the quality of the calibration for the Calcium 397 nm line.

the lines intensity is recorded without a delay between the laser pulse and the start of the measure, calcium 397 nm and silicon 288 nm need a delay of 0.7 μs, while the optimal delay for sodium 589 nm and potassium 766 nm was 2 μs.

We believe that a possible explanation of this behavior can be gained from a simplified analysis of the emission phenomena that occur during plasma evolution, when both the differences in ionization energy of various elements and the differences in the transition energy of their emission lines are taken into account.

We have to consider, in fact, that the lines emitted by neutral atoms are usually the most suitable to perform a calibration and if the plasma temperature is high enough, most of the atomic species are ionized at least once. In this case, the number of neutral atoms of an element is only a fraction of the total amount of atoms of the given element. Since the size of this fraction strongly depends on the plasma temperature and electronic density evolution, the integrated intensity of the emitted lines becomes a function of these parameters too and hence is depending on the acquisition delay time.

5.3 Data analysis

The goal of the work was to provide a system that could replicate the results obtained with standard methods; the most important values are the carbon, hydrogen, sulfur, ash and humidity content. Other important values are the nitrogen and oxygen content, along with the chemical composition of the ashes.

Due to its nature, LIBS measures can not detect the molecular structure of the sample, so it is not possible to separate the fraction of hydrogen and oxygen contained in moisture from the ones coming from hydrocarbons and other compounds.

The ash fraction is measured empirically and its value takes also into account the mass of the oxygen needed to reduce the incombustible elements during the combustion (sec. 1.2); it is however possible to recover this value using the concentration of its components, like aluminum, silicon and calcium.

Oxygen values must be treated with extra care, because the oxygen content value is never measured directly, but is instead inferred from other measures. ASTM standard D3176[139] states that the oxygen content can be obtained by subtracting from 100 the sum of the concentrations of C, H, N, S and ashes. However, as already stated, the ash "concentration" value is not the actual content of incombustible elements, but the weight of what remains after coal combustion: as a results, the oxygen's concentration value thus obtained is purely cosmetic and largely underestimated. For our work we decided to use the sum of the concentration of minor and trace elements, instead of the ash concentration, to obtain the oxygen concentration.

All the concentrations are expressed as weight fraction, while the intensity of a spectral line is proportional to the number of atoms contained in the plasma, so we had to convert all the weight fractions in molar concentrations. In addition, all the elemental concentrations are expressed on the dry basis, so they don't take into account the moisture contribution to oxygen and hydrogen content. The procedure used to convert the concentrations was the following; for simplicity I will call C, H, N, S and O "major elements", A will represent the ash content, M the moisture, while all the other elements will be referred to as "minor elements". A "w" subscript means that the value is a weight fraction, while "m" stands for a molar fraction.

The first step consisted in the calculation of the oxygen content; as already said, the oxygen concentration was estimated as the value needed

so that the sum of major and minor elements concentration is equal to 100%

$$O_w = 100\% - (C_w + H_w + N_w + S_w + [minor]_w) \tag{5.13}$$

All the values are then renormalized to take into account the moisture content: for example

$$C'_w = C_w \frac{100\% - M_w}{100\%} \tag{5.14}$$

The moisture content was also divided into its oxygen and hydrogen contribution

$$H''_w = H'_w + M_w \cdot 0.112 \tag{5.15}$$

$$O''_w = O'_w + M_w \cdot 0.888 \tag{5.16}$$

In this way we obtained the composition of the "wet" coal expressed as weight fraction. To obtain the molar fraction, each concentration was divided by the atomic weight of the relative element, in order to obtain the number of moles of the given element for 100 g of coal; then all the values were renormalized so that the sum of all concentration would give 100%. For example:

$$C_n = \frac{C_w}{12.011} \tag{5.17}$$

$$C_m = C_n \cdot \frac{100\%}{\sum El_n} \tag{5.18}$$

In this way we obtained the molar concentration of all the elements.

For each element we correlated the molar fraction with the area of the corresponding spectral line; we tried out different lines, as well different normalizations and delays, as explained in section 5.2.

For carbon we were able to observe three different lines: two emitted by neutral carbon, at 193.1 nm and 247.9 nm, and one emitted by doubly ionized atoms at 229.7nm. Strangely enough, we weren't able to see the lines emitted by singly ionized carbon, like the ones at 283.7 nm and 426.7 nm. In the end we obtained the best results with the 247.9 nm line, using the background emission between 247 nm and 250 nm as normalization value and without any delay between the laser pulse and the beginning of the acquisition. The calibration curve was obtained performing a linear fit of the data, using the area of the spectral line as the independent variable and the molar fraction as the dependent variable; the same method was used

for all the other elements, with the exception of the iron, that I will discuss later.

For hydrogen the only available line was the one at 656 nm; as for the carbon, the best results were obtained when there was no delay between the laser pulse and the beginning of the acquisition. We also used the same values for the normalization.

For the minor elements (aluminum, silicon, calcium and iron) we didn't use a normalization, although we found out that the best results were obtained when a delay of 0.7 μs was set between the laser pulse and the acquisition.

We studied four different lines for aluminum, each one emitted by neutral atom: 308.2 nm, 309.3 nm, 394.4 nm and 396.2 nm. We tried each one alone and the average of two or more lines: they all provided a good calibration curve, but the one that gave the best results was the 309.3 nm ones.

For silicon we analyzed the 288.2nm line, and a group of six lines between 25 nm and 253 nm; the group of six, however, is mixed with three other lines emitted by iron, so in the end we used the 288.2 nm line.

For calcium we tried two lines emitted by ionized atoms, at 393.4 nm and 396.8 nm, and one emitted by neutral atoms, at 422.7 nm: the one that gave the best results was the one at 396.8 nm.

Iron was one of the most problematic element; first of all, its low concentration, coupled with the low Einstein coefficients makes it so that all its lines have a low intensity, most of the time with the same order of magnitude of the noise. In addition, due to the great number of lines produced by iron and titanium, it is hard to separate each line from the other, and some of them are overlapped by molecular emission.

We selected 9 different lines, the brightest of which were a doublet emitted by ionized atoms at 259.9 nm, and two lines at 302.1 nm and 372 nm emitted by neutral atoms. All of them, however, showed a poor correlation between their intensity and the iron concentration.

We decided then to follow the method proposed by Romero et al.[120], in which they used the carbon 247.9 nm line as a reference: the ratio between iron and carbon molar fraction is correlated with the ratio between 372 nm iron line intensity and the 247.9 nm carbon line intensity. The relation between molar fraction and intensity, however, resulted to be exponential instead of linear, and we didn't manage to figure out why that was so. This kind of behaviour, in fact, is typical of self absorption phenomena, but all the literature points out that the 372 nm iron line begins to be self absorbed for concentrations greater than 20%; in addition, in [120] the same

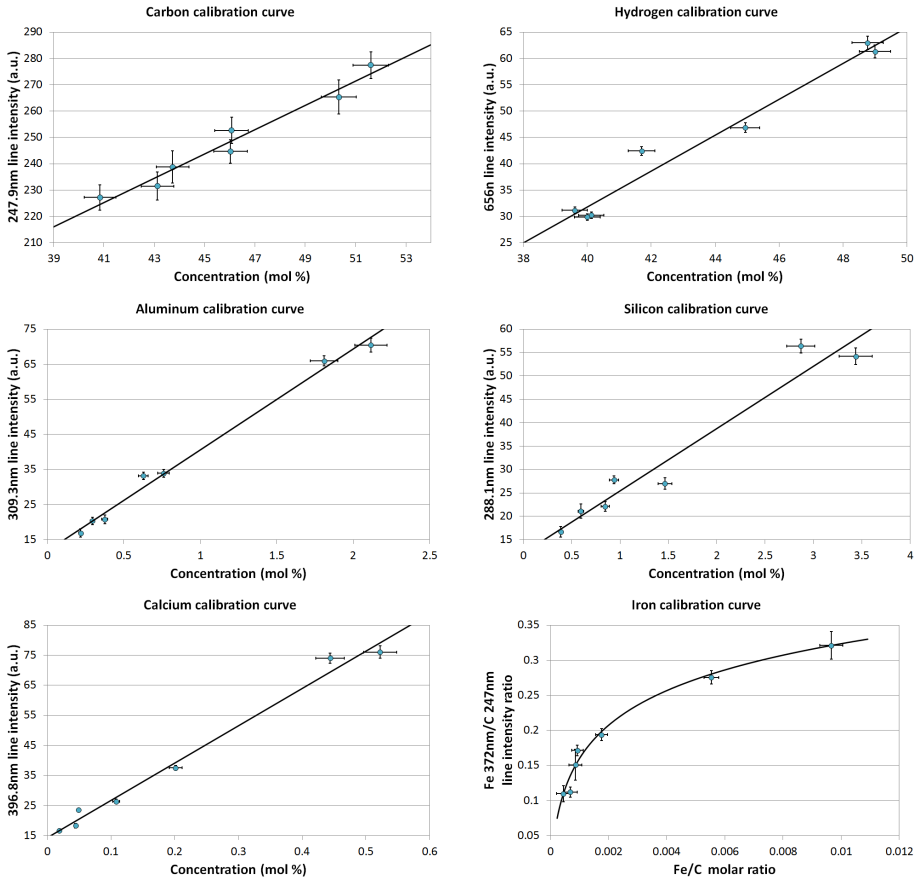

Figure 5.7 – Calibration curves of carbon, hydrogen, aluminum, silicon, calcium and iron.

analysis performed on coals with similar iron concentrations lead to a linear calibration curve.

For different reasons we weren't able to measure the concentration of sulfur, nitrogen and oxygen. In the case of sulfur that was because there wasn't any visible line: all the sulfur lines are extremely weak (an order of magnitude smaller than iron lines) and either in the infrared region (921.3 nm, 922.8 nm, 923.8 nm) or deep UV (180.7 nm, 182 nm, 182.6 nm). Gaft et al. showed in [140] that, due to the air absorption, it is not possible to perform a measure of the sulfur content of coal if the distance that the light has to travel in air is greater than 20 cm.

It was not possible to perform a measure of oxygen and nitrogen, because the air contribution to the mixture was several order of magnitude greater than the amount provided by coal: 0.1 cm^3 of air contain about 97 mg of nitrogen and 30 mg of oxygen, while the ablated coal contain just a few hundreds of picograms of them.

We also had different proofs that we were not measuring the oxygen and nitrogen content of the coal. First of all, there was no correlation between the intensity of the lines and the expected concentration; the other clue was the fact that the ratios between the intensity of oxygen lines and nitrogen lines were constant and independent from the coal.

To be sure we also performed a test, repeating a measure on the same coal under three different atmospheres: air, nitrogen and argon. As expected, the oxygen lines disappeared when the measure was performed in nitrogen and in argon; when performing the measure in argon, the lines of nitrogen and the CN bands also disappeared.

In the end, from the calibration curves we were able to obtain the molar fraction of carbon, hydrogen, aluminum, silicon, calcium and iron: we had however to recover the information about the weight fraction of carbon, hydrogen and ash.

First of all, we recovered the weight fraction of ash. For each element we calculated the molar weight of the oxide it will produce during combustion. For example, aluminum will produce alumina as a combustion byproduct: that means that for every two moles of aluminum in the coal, 3 moles of oxygen will be added to the final amount of ash, and that each mole of aluminum will produce 50.98 g of ash. By multiplying each element's molar fraction by the molar weight of their oxides we obtained the weight of the ashes that we would obtain burning 100 "mole of carbon" (the amount of carbon that contain $6.022 \cdot 10^{25}$ atoms).

We found that there is a linear correlation between this value and the weight fraction of ash in coal.

$$A_M = 50.98 \cdot Al_m + 56.08 \cdot Ca_m + 60.07 \cdot Si_m + 79.84 \cdot Fe_m \tag{5.19}$$

$$A_w = m * A_M + q \tag{5.20}$$

This correction compensates for the small loss of mass due to the neglected elements.

We also found a linear relation between the sum of the molar fraction of all the minor elements, A_m, and the sum of the molar fraction of the four elements we were able to measure.

In order to recover the weight fractions we had to know the molar fraction of every element in the coal: however, nitrogen, oxygen and sulfur concentrations were not known. For this reason we decided to handle all those elements all together as if they were a single one; I will refer to it as "NSO". Its molar fraction was obtained by difference from the other ones

$$NSO_m = 100\% - (C_m + H_m + A_m) \tag{5.21}$$

To find the weight fractions, we had to multiply each element for its atomic weight, obtaining the mass of that elements in 100 moles of carbon, and then we divided those values by the sum of all of them, in order to obtain the concentration.

$$C_w = aC_m \cdot \frac{100\% - A_w}{aC_m + bH_m + cNSO_m} \tag{5.22}$$

$$H_w = bH_m \cdot \frac{100\% - A_w}{aC_m + bH_m + cNSO_m} \tag{5.23}$$

$$NSO_w = cNSO_m \cdot \frac{100\% - A_w}{aC_m + bH_m + cNSO_m} \tag{5.24}$$

However, the exact value for the NSO atomic weight is not known, so we decide instead to use for a, b and c the values that provided the best results for C_w and H_w.

We tested this method using the concentration values of 22 coals obtained from standard measures: we used the molar fractions of C, H, Al, Ca, Fe and Si as if they were the results of a LIBS measure and processed them using the aforementioned method. Using a nonlinear fit we found the values of a, b, c, m and q that provide the best agreement between the value of A_w, C_w and H_w obtained with this method and the ones that came from the standard analysis. The values of a, b, c, m and q thus obtained were used to perform the conversion from molar fraction to mass fraction for the data obtained from LIBS measures on the seven reference coals. As it is visible from the graphs, the libs results are in good agreements with the values from standard analysis.

The results have been accepted for publishing and are actually in press.[141]

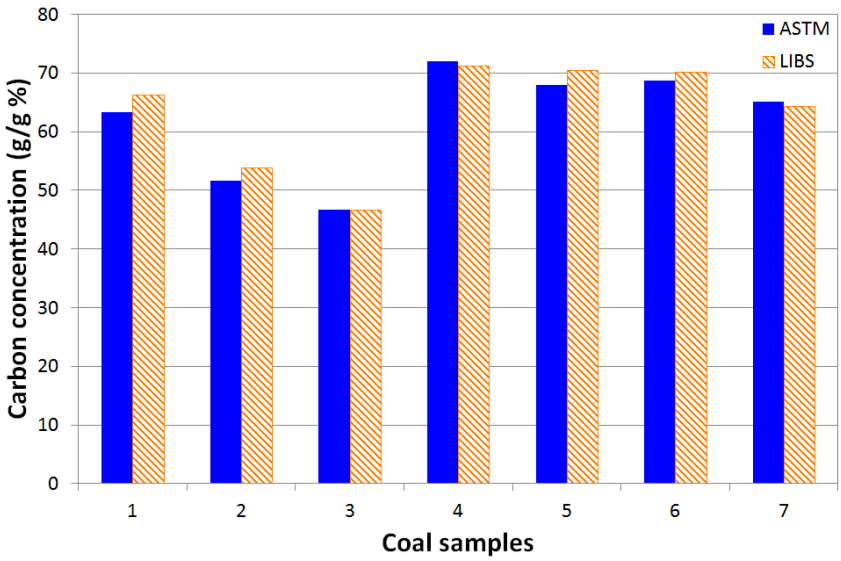

Figure 5.8 – Comparison between the carbon mass fractions obtained with the LIBS analysis and the "true" ones from ASTM standard analysis.

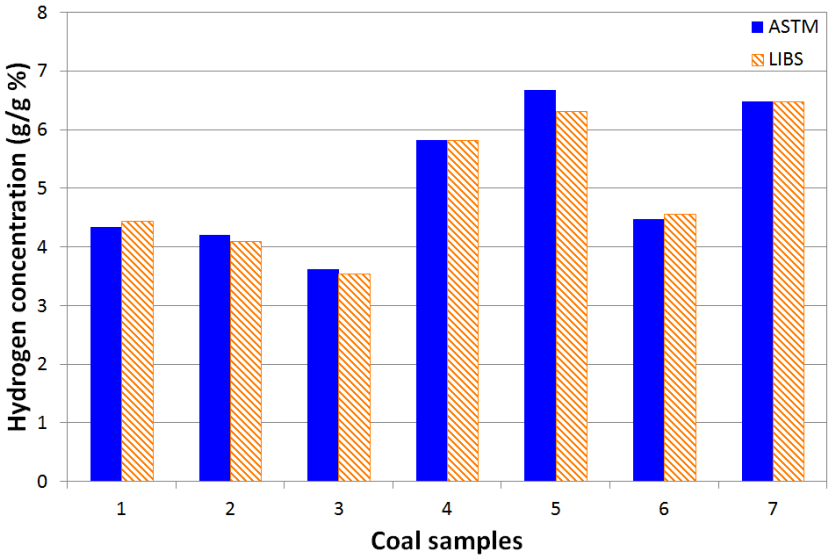

Figure 5.9 – Comparison between the hydrogen mass fractions obtained with the LIBS analysis and the "true" ones from ASTM standard analysis.

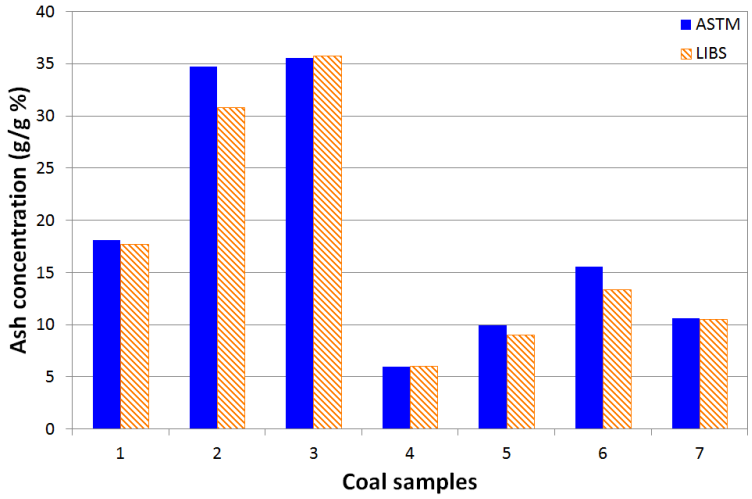

Figure 5.10 – Comparison between the ash mass fractions obtained with the LIBS analysis and the "true" ones from ASTM standard analysis.

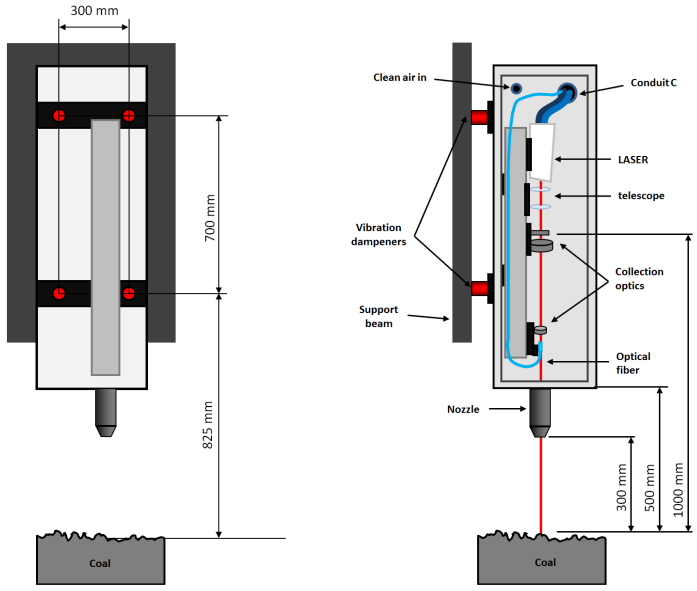

Figure 5.11 – Design of the laser box for the installation on the conveyor belt.

5.4 Power plant test

The original schedule of this work also included a test on the conveyor belt of the ENEL power plant of Torrevaldaliga Nord: the apparatus had to be installed inside one of the conduits that bring the coal from the storage domes to the mills. We performed two preliminary inspections of the designed location, in order to collect the required data, and discussed with the local staff the optimal position for the instrument.

We designed the case for the instrument, taking into account all the problems that could arise when operating in a real power plant. For example, we added vibration dampeners on the support beam, in order to insulate the system from the vibrations inside the conduit. We designed a nozzle and an entry port for compressed air, so that a flow of clean air would keep the pressure inside the case slightly higher than the pressure outside; in this way we would prevent the deposit of dirt on the optics and we would keep the laser path free of dust particles. We decided to put the spectrometers, the laser power supply and control unit and the PC inside a prefab outside the conduit, so they were protected against the dust and vibrations produced by the conveyor belt. We also commissioned an ATEX certification for the device, mandatory to work in potentially explosive environment.

Although the laboratory tests demonstrated the measurement capability of this LIBS instrument, due to the costs involved in the plant installation, and since a spending revue cut the budget for ENEL (in charge for this part of the activity) for on plant experiments, the installation could not be performed in the frame of the existing cooperation agreement.

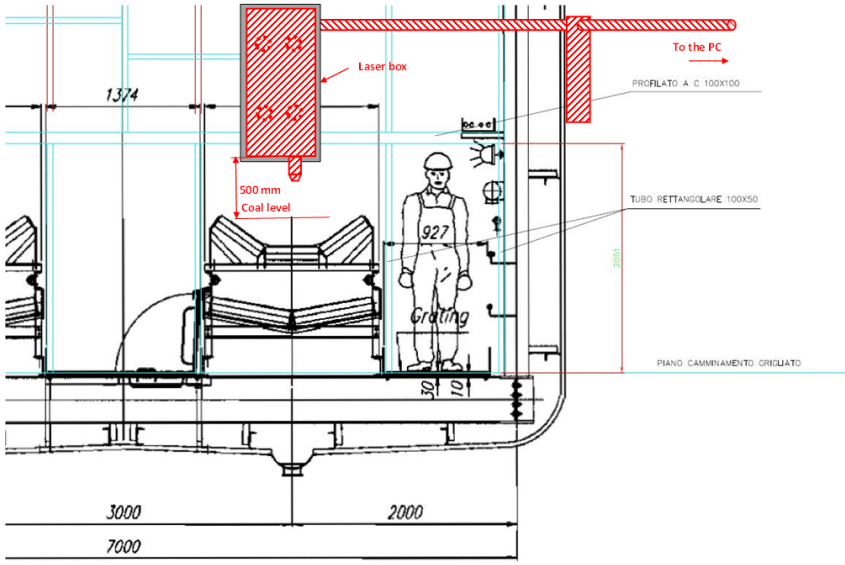

Figure 5.12 – Technical design of the laser box placement over the conveyor belt.

Chapter 6

Conclusions

In my PhD work I have developed, in collaboration with RSE, a LIBS system that could perform a quantitative analysis of coal chemical composition on top of a moving conveyor belt. A working prototype was built and tested, and a version for the test on field was designed as well.

I have followed each step of its development, from the choice of the components to the final test. The main accomplishment was the study, development and optimization of the collection optics, for which we obtained particularly interesting results. The device designed, in fact, provides an extremely cost-effective solution to the problem of a moving sample without resorting to the use of moving parts or deformable optics: that resulted in an increased sturdiness and reliability of the system.

The other greatest accomplishment was the development of softwares for both the data acquisition and the data analysis; the algorithm I have developed for the system provided good results during the tests so far performed. The obtained results have been accepted for publishing and are actually in press.[141]

I was heavily involved in the design, assembling and calibration of the prototypes. The laboratory tests were performed collaborating closely with RSE personal.

Although the device is fully functional, and has already proven itself capable to perform its task, we believe that there is still room for improvement. First of all, an actual test in a real power plant, as was already planned, would provide important feedbacks on the performance of our system. We also believe that a test on a greater number of coals is needed,

in order to provide a better validation of the algorithm used for the data analysis. Last, but not least, the software used for the data analysis could be improved, maybe with the employment of Artificial Neural Network.

Appendix A

Software

A.1 Synthetic spectra generator

This software was one of the most useful that I have developed for my PhD work, because it provides simulated LIBS spectra of a plasma of known composition.

Using a database containing a list of all the known level transitions of the interesting elements, along with their relevant parameters, the software uses the equation (3.5), obtained in section 3.1, to calculate the intensity of each spectral line. It is possible to change the temperature of the plasma, its electron density, the width of the lines and the chemical composition.

With a few changes, the software was used to select the lines used for the Boltzmann plot: for a given line width, the software selects the lines that provide at least 95% of the intensity of the spectrum at their wavelength. The software performs a given number of loops in which the temperature, the density and the chemical composition of the plasma are slightly changed and check if the selected lines still satisfy the requirements; only the lines that pass each check are then used for the Boltzmann plot.

A.2 Ray tracing

The collection optics were designed with the help of different softwares: I used the commercial software WinLens3D and some ray tracing softwares I have developed in LabVIEW. Winlens3D is a versatile optical design software, and it includes a lot of instruments to perform simulations of many different parameters of the designed system. However, the software has a great limitation in the fact that it can only use 800 "rays", disposed in 20 concentric rings, when it performs those simulations; as a result, the simulations provided have a really poor resolution. In addition, the software doesn't allow the employment of automated routines and the record of the results, so the parameters and the results of each simulation have to be entered manually each time. For this reason I have also built some ray tracing softwares, in order to automate the simulations, and obtained much more refined results. In order to optimize the software and reduce the computational time, I wrote a different program for each one of the three main optical configurations: the ideal lens, the off axis parabola and the two spherical mirrors system. At their core the three programs are mostly identical: for each point in the space volume we want to investigate, the software finds the smallest cone with the vertex in that point that completely contains the first element of the system, then produces 109 rays randomly distributed inside the cone. What changes is the part of the software that propagates the rays, simulates their interactions with the system and counts how many of them are correctly collected by the system; keeping into account the size of the cone used for the simulation, the software returns the fraction of light that the system is able to capture. The software automates the whole procedure and saves the results for all the points in the space volume analyzed.

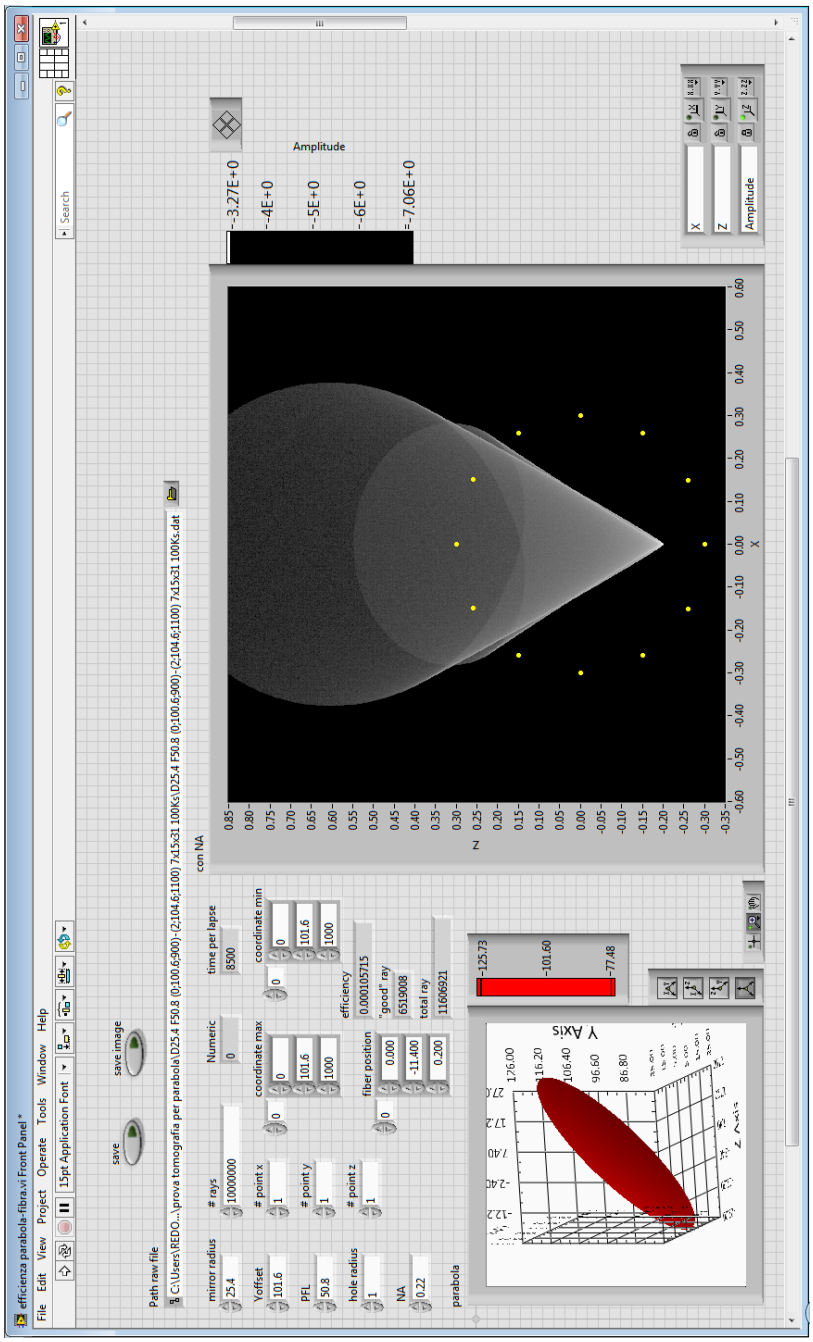

Figure A.1 – Front panel of the ray-tracing software for the parabolic mirror configuration.

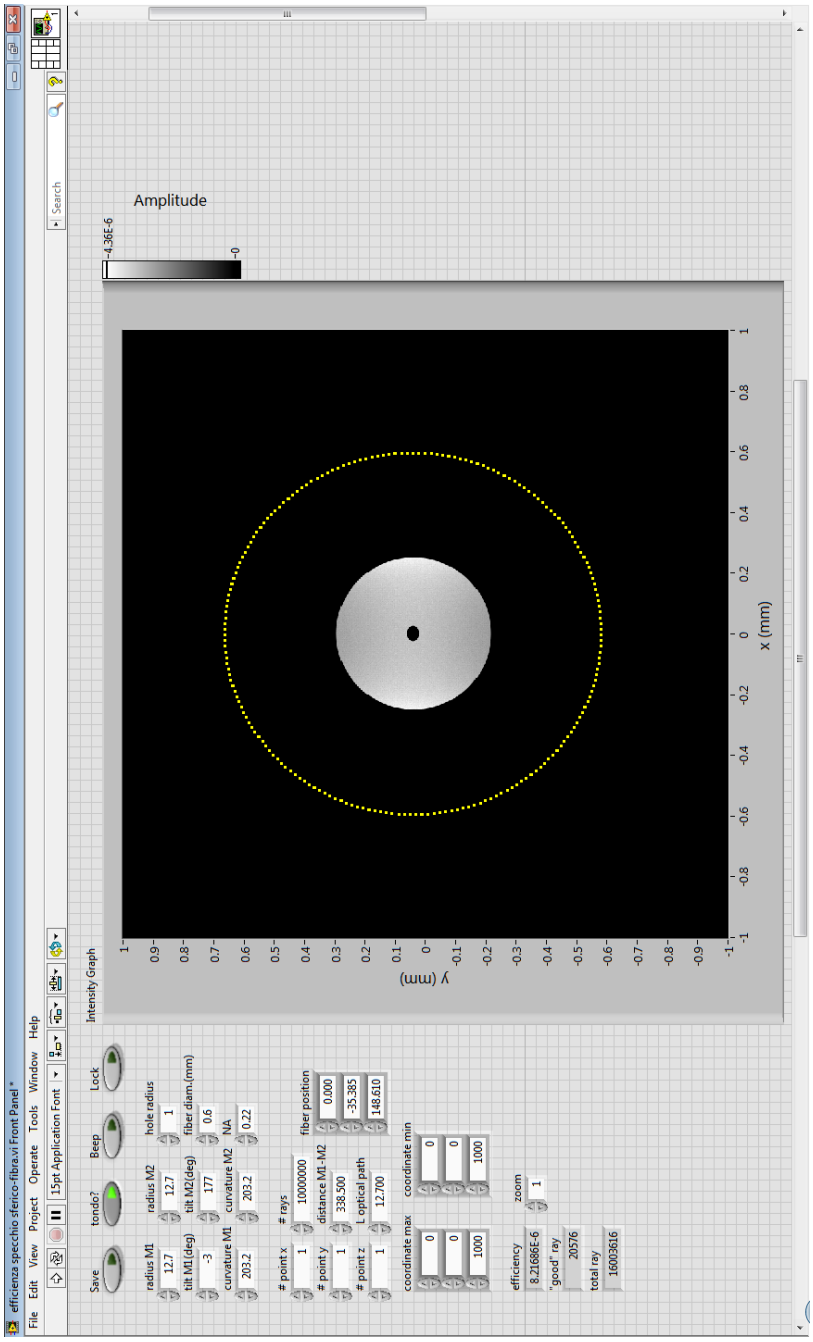

Figure A.2 – Front panel of the ray-tracing software for the spherical mirrors configuration.

A.3 Spectrometers controller

The third most important software I had to develop is the one for the control of the spectrometers and the spectra acquisition. As I have said in section 4.e, the control software for the spectrometers provided by the producer was not suitable for our system, mostly due to the instability and the impossibility to automatically save the spectra in a readable format. The software, in fact, saves the spectra in a proprietary binary file that could be opened only by the software itself. The software I have produced is tailored for our configuration and doesn't have the versatility of the original one; I have also developed only the features that we needed, omitting the other ones.

On the other hand, I have included some features supported by the spectrometer's firmware that weren't included in the original software, e.g. the possibility to trigger each spectrometer with its own delay in relation to an external trigger. I also used this software as an opportunity to improve my LabVIEW programming skills, using advanced features like xControl interfaces, the state machine state structure or the event processing.

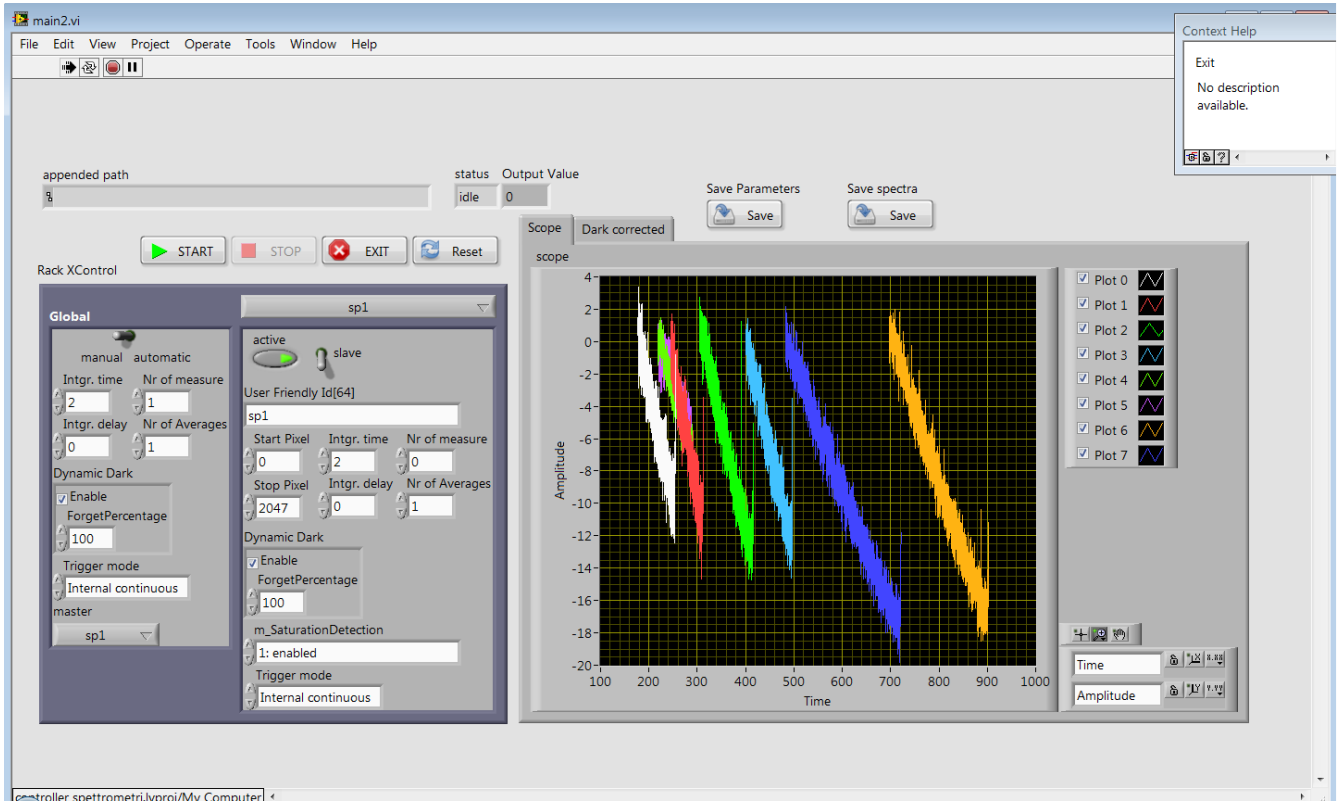

Figure A.3 – Front panel of the software for the control of the spectrometers. The measure parameters can be set for all the spectrometers at the same time using the "Global" frame, or can be set individually using the frame on the right; the spectrometers can be selected from the drop-down menu over the frame.

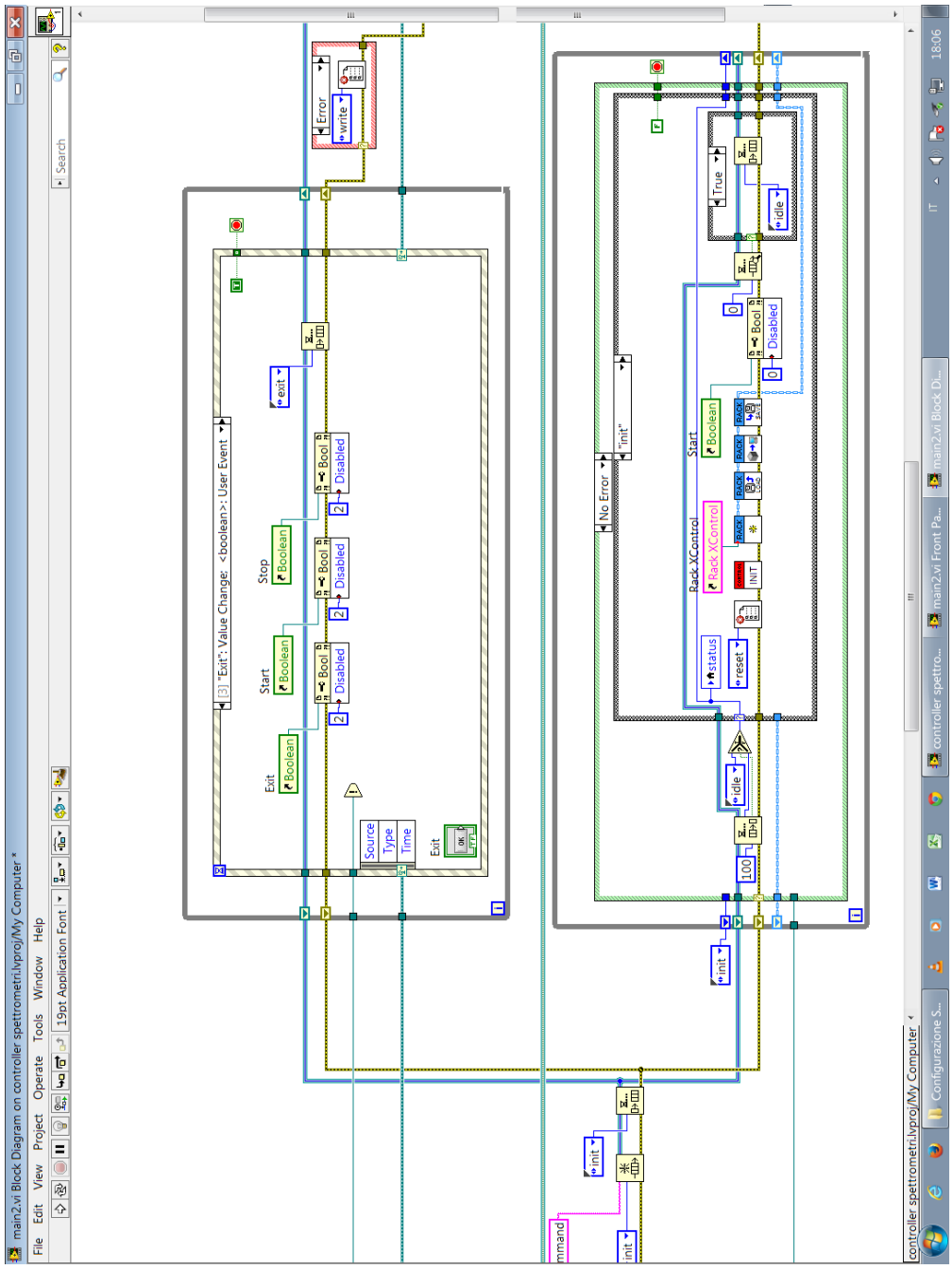

Figure A.4 – Part of the block diagram of the software for the control of the spectrometers.

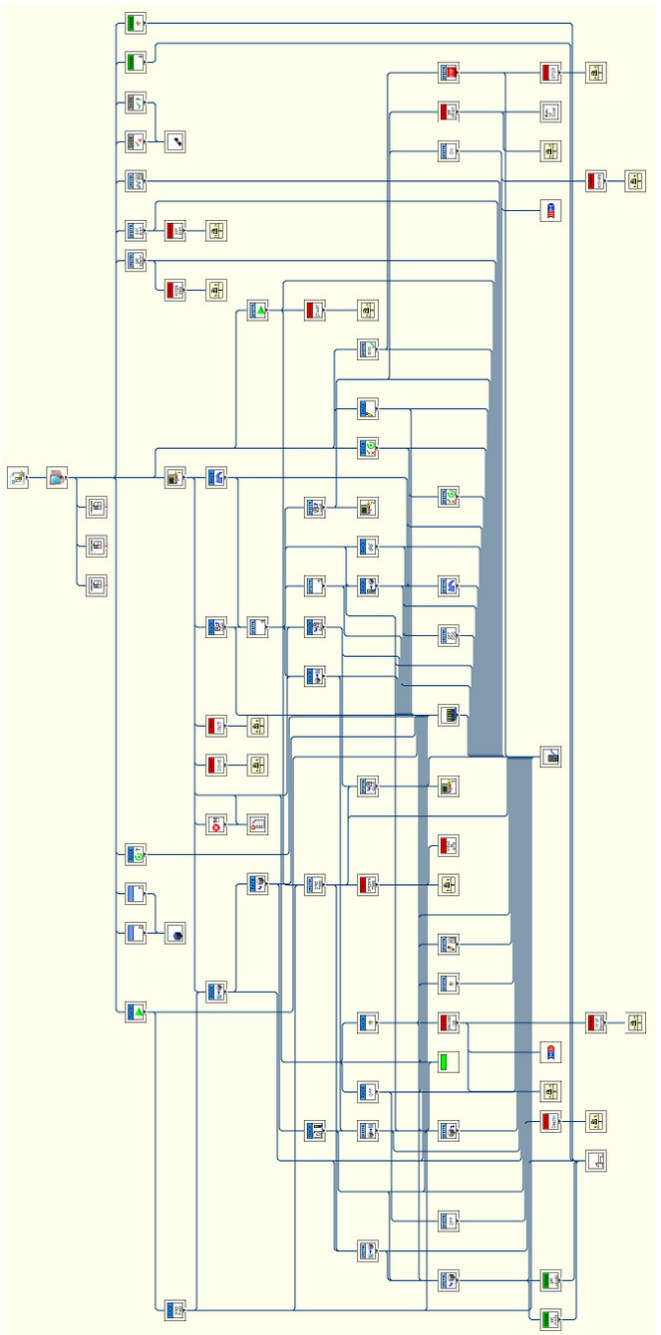

Figure A.5 – VI Hierarchy tree of the software for the control of the spectrometers; only the VI I had written are included.

Appendix B

Pictures

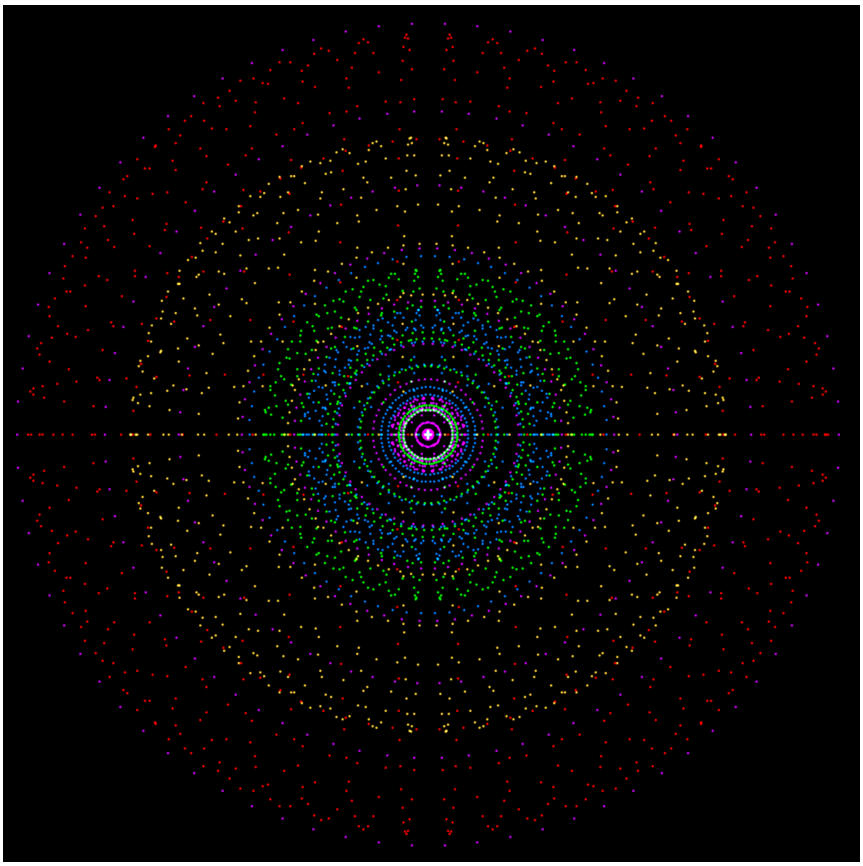

Figure B.1 – Chromatic aberration of a plano-convex silica lens: different wavelengths produce a different spot shape in the focal plane.

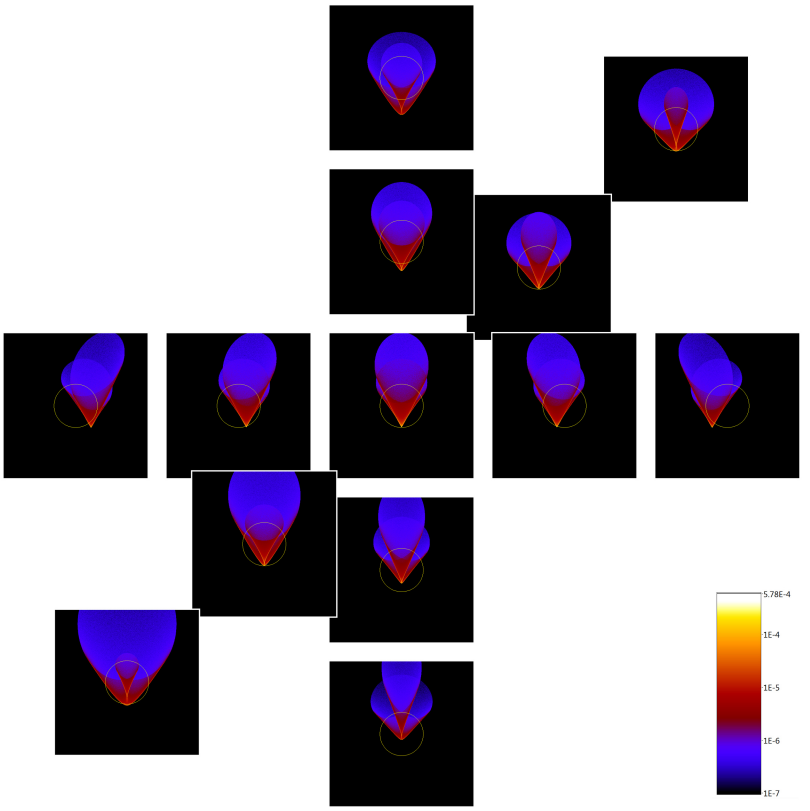

Figure B.2 – Aberrations of the parabolic mirror: variations in shape and size of the light spot on the face of the optical fiber as the position of the light source changes.

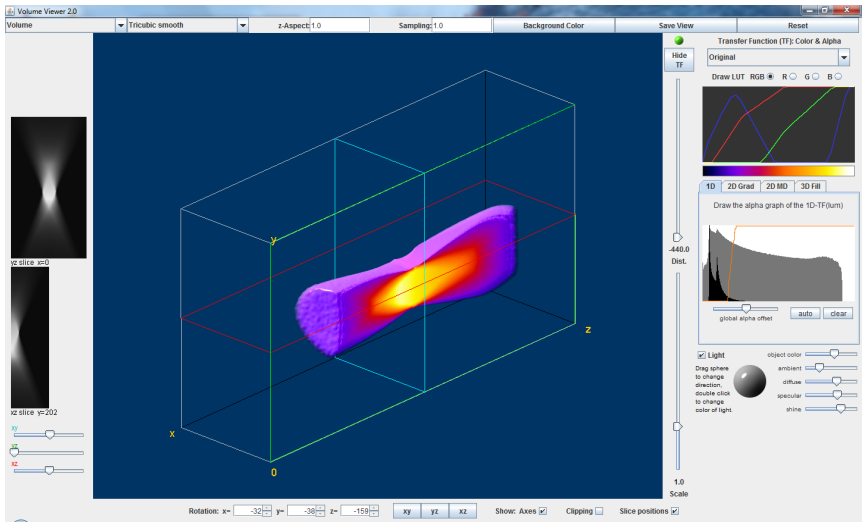

Figure B.3 – 3D graphic representation of the collection efficiency of the spherical mirrors system; the rendered volume is the one in which the collection efficiency is at least half the maximum value.

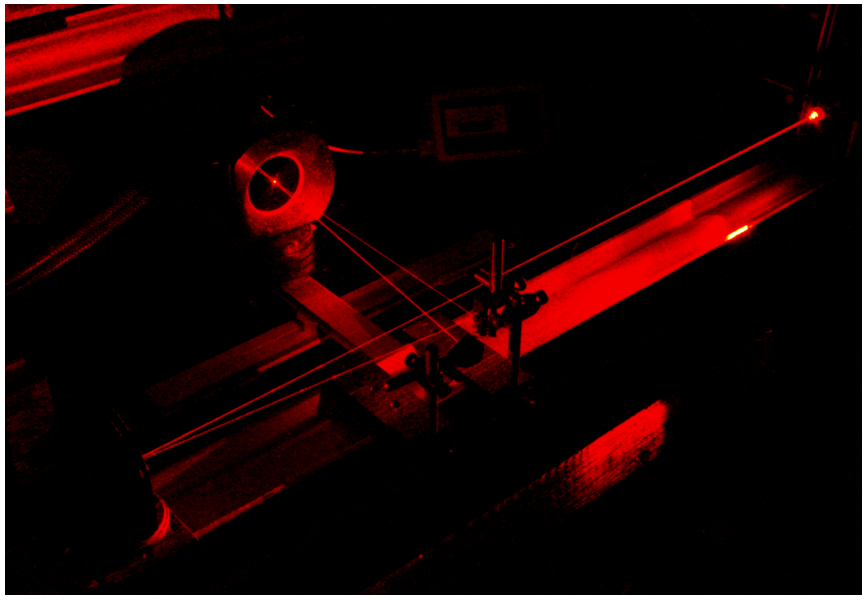

Figure B.4 – An early stage in the realization of the prototype; the laser was used to align the mirrors.

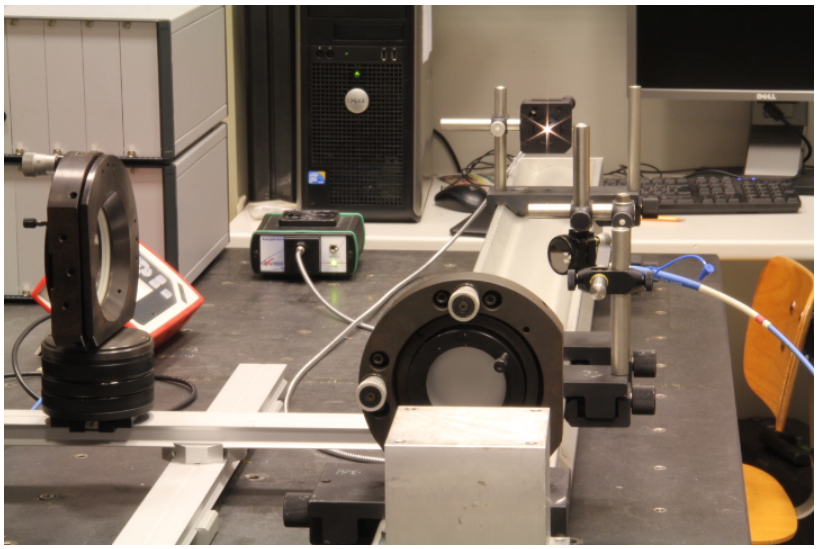

Figure B.5 – A picture of the system employed to measure the collection efficiency of the system; an optical fiber, coupled with a halogen lamp, was used as light source, while the collected light intensity was measured with a power meter.

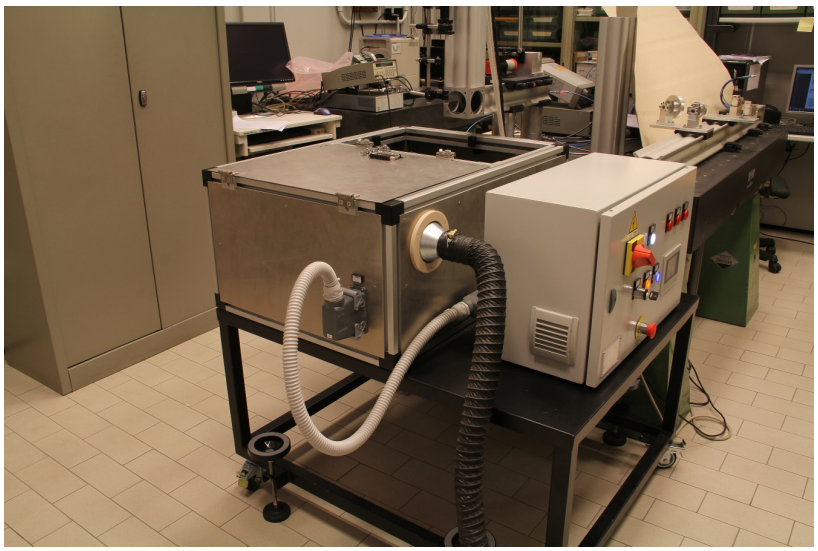

Figure B.6 – Picture of the coal circulator, inside the protective box, and its control unit.

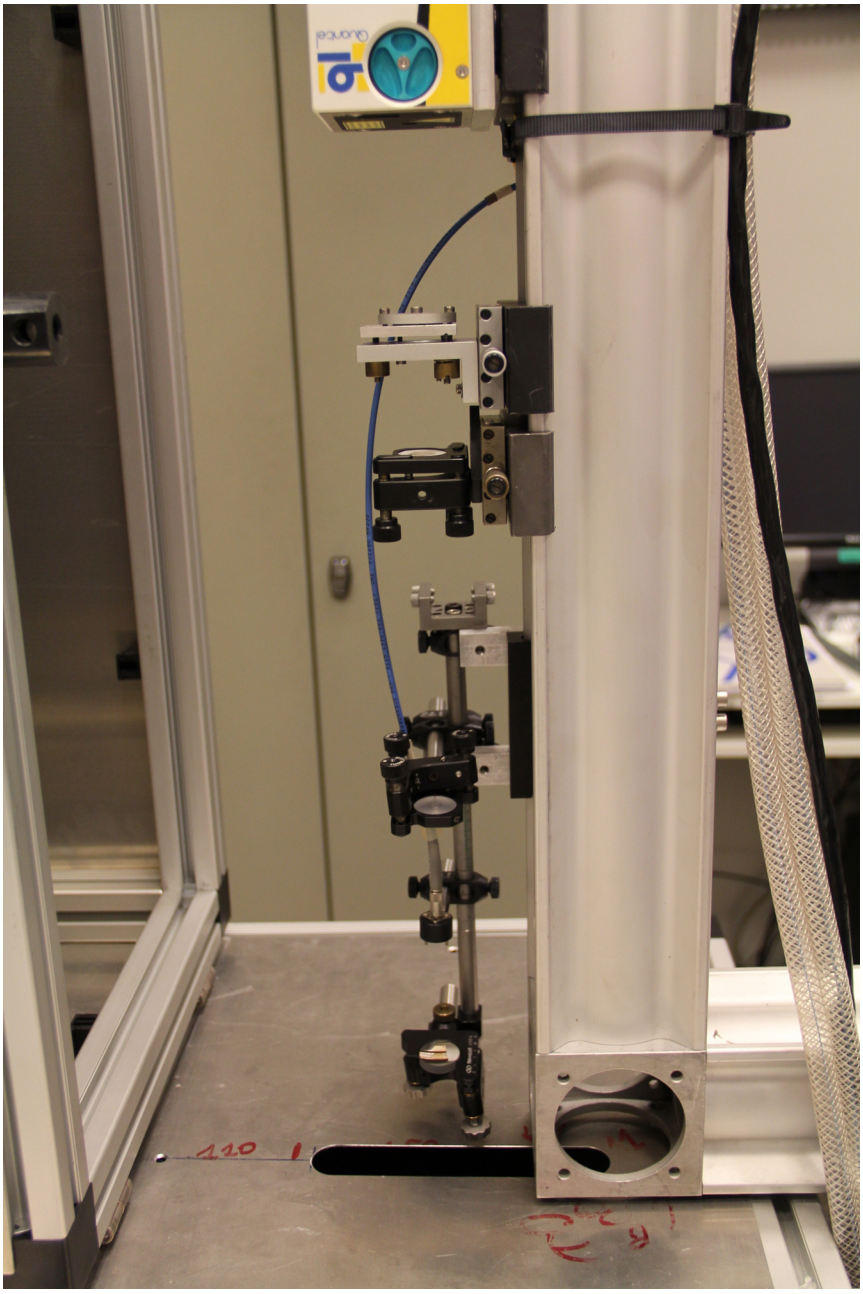

Figure B.7 – Picture of the small scale system used for the tests.

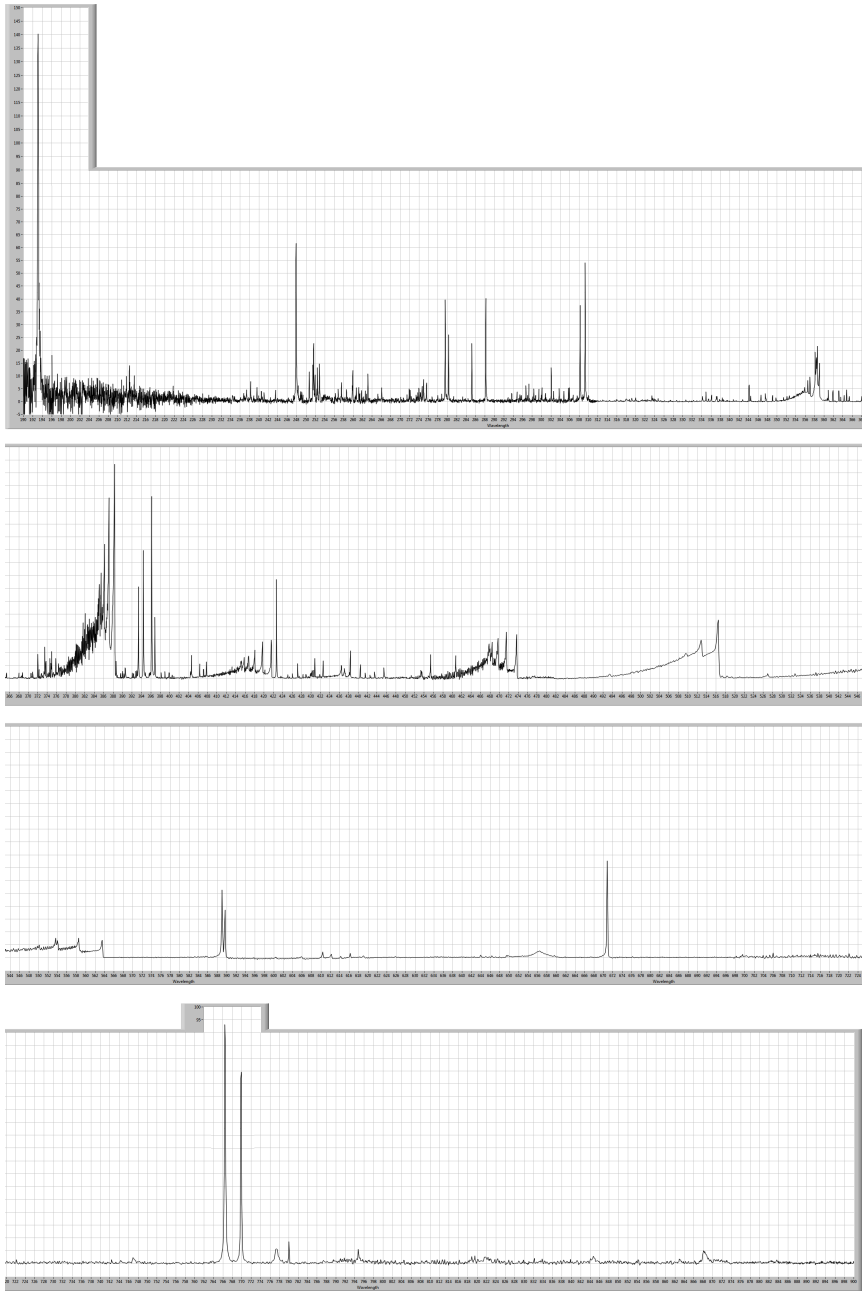

Figure B.8 – One of the collected spectra.

Bibliography

[1] British Petroleum, "BP statistical review of world energy June 2015," Tech. Rep., 2015.

[2] EIA, "Annual energy outlook 2015," Tech. Rep., 2015.

[3] IEA, "2014 key world energy statistics," Tech. Rep., 2014.

[4] IEA, "Energy and climate change," Tech. Rep., 2015.

[5] *IEA online database*. [Online]. Available: `http://www.iea.org/statistics/statisticssearch/`.

[6] ENEA, "Rapporto energia e ambiente - scenari e strategie," Tech. Rep., 2013.

[7] L. L. Sloss, *The importance of $PM_{10/2.5}$ emissions*. IEA Clean Coal Centre, 2004, ISBN: 9290294043.

[8] L. Sloss and I. Smith, *Trace element emissions*. IEA Clean Coal Centre, 2000, ISBN: 9290293446.

[9] T. Pulles and W. Appelman, "Air pollution from electricity-generating large combustion plants," European Environmentl agency, Tech. Rep., 2008.

[10] X. Zhang, *Management of coal combustion wastes*. IEA Clean Coal Centre, 2014, ISBN: 9789290295518.

[11] I. Barnes, *Ash utilisation – Impact of recent changes in power generation practices*. IEA Clean Coal Centre, 2010, ISBN: 9789290294962.

[12] H. Nalbandian, *Trace element emissions from coal*. IEA Clean Coal Centre, 2012, ISBN: 9789290295235.

[13] I. M. Smith, *Cement and concrete – Benefits and barriers in coal fly ash utilisation*. IEA Clean Coal Centre, 2005, ISBN: 9290294094.

[14] R. M. Davidson and S. O. Santos, *Oxyfuel combustion of pulverised coal*. IEA Clean Coal Centre, 2010, ISBN: 9789290294887.

[15] I. Barnes, *Slagging and fouling in coal-fired boilers*. IEA Clean Coal Centre, 2009, ISBN: 9789290294665.

[16] Q. Zhu, *Coal sampling and analysis standards*. IEA Clean Coal Centre, 2010, ISBN: 9789290295556.

[17] R. Gupta, "Advanced coal characterization: a review," *Energy & Fuels*, vol. 21, no. 2, pp. 451–460, Mar. 2007, ISSN: 0887-0624. DOI: 10.1021/ef060411m.

[18] *ASTM D6883 - 04(2012), Standard practice for manual sampling of stationary coal from railroad cars, barges, trucks, or stockpiles*, ASTM International, 2012. DOI: 10.1520/D6883-04R12.

[19] *ISO 13909-(1-8):2001, Hard coal and coke – mechanical sampling (part 1-8)*, 2001.

[20] *ASTM D2234/D2234M, 10 standard practice for collection of a gross sample of coal*, ASTM International, 2010. DOI: 10.1520/D2234_D2234M-10.

[21] *ASTM D7582 - 15, Standard test methods for proximate analysis of coal and coke by macro thermogravimetric analysis*, ASTM International, 2015. DOI: 10.1520/D7582-15.

[22] *ISO 17246:2010, Coal – proximate analysis*, ISO, 2010.

[23] J. G. Speight, "Coal analysis," in *The Chemistry and Technology of Coal*. CRC Press, 2012, pp. 215–250, ISBN: 978-1-4398-3646-0.

[24] *ASTM D5865 - 13, Standard test method for gross calorific value of coal and coke*, ASTM International, 2013. DOI: 10.1520/D5865.

[25] *ASTM D5373 - 14e1, Standard test methods for determination of carbon, hydrogen and nitrogen in analysis samples of coal and carbon in analysis samples of coal and coke*, ASTM International, 2014. DOI: 10.1520/D5373-14E01.

[26] *ISO 29541:2010, Solid mineral fuels – determination of total carbon, hydrogen and nitrogen content – instrumental method*, ISO, 2010.

[27] *ASTM D5016 - 08e1, Standard test method for total sulfur in coal and coke combustion residues using a high-temperature tube furnace combustion method with infrared absorption*, ASTM International, 2008. DOI: 10.1520/D5016-08E01.

[28] *ISO 19579:2006, Solid mineral fuels - Determination of sulfur by IR spectrometry*, ISO, 2011.

[29] *ISO 17247:2013, Coal – ultimate analysis*, ISO, 2013.

[30] *ASTM D3682 - 13, Standard test method for major and minor elements in combustion residues from coal utilization processes*, ASTM International, 2013. DOI: 10.1520/D3682.

[31] *ASTM D6357 - 11, Test methods for determination of trace elements in coal, coke & combustion residues from coal utilization processes by inductively coupled plasma atomic emission, inductively coupled plasma mass & graphite furnace atomic absorption spectrometry*, ASTM International, 2011. DOI: 10.1520/D6357-11.

[32] *ISO 23380:2013, Selection of methods for the determination of trace elements in coal*, ISO, 2013.

[33] C. R. Ward, "Quantitative mineralogical analysis of coal using advanced X-ray diffraction techniques.," in *53rd ICCP Annual Meeting 2001, Copenhagen, Denmark*, 2001.

[34] K. L. Pinetown and R. H. Boer, "WRC Report No. 1264/1/06 - A quantitative evaluation of the modal distribution of minerals in coal deposits in the highveld area and the associated impact on the generation of acid and neutral mine drainage," Water Research Commission (WRC), Tech. Rep., 2006.

[35] S. J. Kelloway, C. R. Ward, C. E. Marjo, I. E. Wainwright, and D. R. Cohen, "Quantitative chemical profiling of coal using core-scanning X-ray fluorescence techniques," *International Journal of Coal Geology*, vol. 128-129, no. 3, pp. 55–67, Aug. 2014, ISSN: 01665162. DOI: 10.1016/j.coal.2014.04.006.

[36] P. Shah, V. Strezov, C. Stevanov, and P. F. Nelson, "Speciation of Arsenic and Selenium in coal combustion products," *Energy & Fuels*, vol. 21, no. 2, pp. 506–512, Mar. 2007, ISSN: 0887-0624. DOI: 10.1021/ef0604083.

[37] H. G. M. Parry, L. Ebdon, J. R. Clinch, P. J. Worsfold, H. Casey, S. M. Smith, T. M. Khong, C. F. Simpson, O. O. Ajayi, D. Littlejohn, C. B. Boss, C. J. Dowle, B. G. Cooksey, W. C. Campbell, S. Greenfield, M. S. Salman, M. Thomsen, and J. F. Tyson, "Coal analysis by analytical atomic spectrometry (ICP-AES and ICP-MS) without sample dissolution," *Analytical Proceedings*, vol. 25, no. 3, p. 69, 1988, ISSN: 0144-557X. DOI: 10.1039/ap9882500069.

[38] A. Saydut, "Microwave acid digestion for the determination of metals in subbitumnious coal bottom ash by ICP-OES," *Energy, Exploration & Exploitation*, vol. 28, no. 2, pp. 105–116, Apr. 2010, ISSN: 0144-5987. DOI: 10.1260/0144-5987.28.2.105.

[39] M. C. Santos and J. A. Nóbrega, "Slurry nebulization in plasmas for analysis of inorganic materials," *Applied Spectroscopy Reviews*, vol. 41, no. 4, pp. 427–448, Aug. 2006, ISSN: 0570-4928. DOI: 10.1080/05704920600726191.

[40] F. G. Antes, F. A. Duarte, M. F. Mesko, M. A. Nunes, V. A. Pereira, E. I. Müller, V. L. Dressler, and E. M. Flores, "Determination of toxic elements in coal by ICP-MS after digestion using microwave-induced combustion," *Talanta*, vol. 83, no. 2, pp. 364–369, Dec. 2010, ISSN: 00399140. DOI: 10.1016/j.talanta.2010.09.030.

[41] S. Fadda, A. Rivoldini, and I. Cau, "ICP-MS determination of 45 trace elements in whole coal using microwave oven acid digestion for sample preparation," *Geostandards and Geoanalytical Research*, vol. 19, no. 1, pp. 41–54, Apr. 1995, ISSN: 16394488. DOI: 10.1111/j.1751-908X.1995.tb00151.x.

[42] M. A. López-Antón, M. Díaz-Somoano, R. Ochoa-González, and M. R. Martínez-Tarazona, "Analytical methods for mercury analysis in coal and coal combustion by-products," *International Journal of Coal Geology*, vol. 94, pp. 44–53, May 2012, ISSN: 01665162. DOI: 10.1016/j.coal.2012.01.010.

[43] M. Borsaru and Z. Jecny, "Application of PGNAA for bulk coal samples in a 4π geometry.," *Applied radiation and isotopes*, vol. 54, no. 3, pp. 519–26, Mar. 2001, ISSN: 0969-8043.

[44] M. Borsaru, M. Berry, M. Biggs, and A. Rojc, "In situ determination of sulphur in coal seams and overburden rock by PGNAA," *Nuclear Instruments and Methods in Physics Research Section B:*

Beam Interactions with Materials and Atoms, vol. 213, pp. 530–534, Jan. 2004, ISSN: 0168583X. DOI: 10.1016/S0168-583X(03)01623-9.

[45] H.-f. Sang, F.-l. Wang, L.-m. Liu, and H.-j. Sang, "Detection of element content in coal by pulsed neutron method based on an optimized back-propagation neural network," *Nuclear Instruments and Methods in Physics Research Section B: Beam Interactions with Materials and Atoms*, vol. 239, no. 3, pp. 202–208, Sep. 2005, ISSN: 0168583X. DOI: 10.1016/j.nimb.2005.04.071.

[46] S. Potgieter-Vermaak, N. Maledi, N. Wagner, J. H. P. Van Heerden, R. Van Grieken, and J. H. Potgieter, "Raman spectroscopy for the analysis of coal: a review," *Journal of Raman Spectroscopy*, vol. 42, no. 2, pp. 123–129, Feb. 2011, ISSN: 03770486. DOI: 10.1002/jrs.2636.

[47] Y. Yao, D. Liu, J. Liu, and S. Xie, "Assessing the water migration and permeability of large intact bituminous and anthracite coals using NMR relaxation spectrometry," *Transport in Porous Media*, vol. 107, no. 2, pp. 527–542, Mar. 2015, ISSN: 0169-3913. DOI: 10.1007/s11242-014-0452-y.

[48] S. De, "A method of rapid determination of moisture in coal by microwave absorption," *Fuel*, vol. 67, no. 7, pp. 1020–1023, Jul. 1988, ISSN: 00162361. DOI: 10.1016/0016-2361(88)90106-8.

[49] J. MacPhee, L. Giroux, J. P. Charland, J. Gransden, and J. Price, "Detection of natural oxidation of coking coal by TG-FTIR — mechanistic implications," *Fuel*, vol. 83, no. 13, pp. 1855–1860, Sep. 2004, ISSN: 00162361. DOI: 10.1016/j.fuel.2004.02.017.

[50] L. J. Radziemski and D. A. Cremers, "A brief history of laser-induced breakdown spectroscopy: From the concept of atoms to LIBS 2012," *Spectrochimica Acta - Part B Atomic Spectroscopy*, vol. 87, pp. 3–10, 2013, ISSN: 05848547. DOI: 10.1016/j.sab.2013.05.013.

[51] L. J. Radziemski, "From LASER to LIBS, the path of technology development," *Spectrochimica Acta - Part B Atomic Spectroscopy*, vol. 57, no. 7, pp. 1109–1113, 2002, ISSN: 05848547. DOI: 10.1016/S0584-8547(02)00052-6.

[52] R. Noll, C. Fricke-Begemann, M. Brunk, S. Connemann, C. Meinhardt, M. Scharun, V. Sturm, J. Makowe, and C. Gehlen, "Laser-induced breakdown spectroscopy expands into industrial applications," *Spectrochimica Acta Part B: Atomic Spectroscopy*, vol. 93, pp. 41–51, 2014, ISSN: 05848547. DOI: 10.1016/j.sab.2014.02.001.

[53] S. Merk, C. Scholz, S. Florek, and D. Mory, "Increased identification rate of scrap metal using laser induced breakdown spectroscopy Echelle spectra," *Spectrochimica Acta Part B: Atomic Spectroscopy*, vol. 112, pp. 10–15, Oct. 2015, ISSN: 05848547. DOI: 10.1016/j.sab.2015.07.009.

[54] P. Werheit, C. Fricke-Begemann, M. Gesing, and R. Noll, "Fast single piece identification with a 3D scanning LIBS for aluminium cast and wrought alloys recycling," *Journal of Analytical Atomic Spectrometry*, vol. 26, no. 11, p. 2166, 2011, ISSN: 0267-9477. DOI: 10.1039/c1ja10096c.

[55] G. Asimellis, N. Michos, I. Fasaki, and M. Kompitsas, "Platinum group metals bulk analysis in automobile catalyst recycling material by laser-induced breakdown spectroscopy," *Spectrochimica Acta Part B: Atomic Spectroscopy*, vol. 63, no. 11, pp. 1338–1343, Nov. 2008, ISSN: 05848547. DOI: 10.1016/j.sab.2008.09.016.

[56] A. M. Matiaske, I. B. Gornushkin, and U. Panne, "Double-pulse laser-induced breakdown spectroscopy for analysis of molten glass," *Analytical and Bioanalytical Chemistry*, vol. 402, no. 8, pp. 2597–2606, Mar. 2012, ISSN: 1618-2642. DOI: 10.1007/s00216-011-5165-2.

[57] J. Anzano, B. Bonilla, B. Montull-Ibor, and J. Casas-González, "Plastic identification and comparison by multivariate techniques with laser-induced breakdown spectroscopy," *Journal of Applied Polymer Science*, vol. 121, no. 5, pp. 2710–2716, Sep. 2011, ISSN: 00218995. DOI: 10.1002/app.33801.

[58] L. Sun, H. Yu, Z. Cong, Y. Xin, Y. Li, and L. Qi, "In situ analysis of steel melt by double-pulse laser-induced breakdown spectroscopy with a Cassegrain telescope," *Spectrochimica Acta Part B: Atomic Spectroscopy*, vol. 112, pp. 40–48, Oct. 2015, ISSN: 05848547. DOI: 10.1016/j.sab.2015.08.008.

[59] G. Lorenzetti, S. Legnaioli, E. Grifoni, S. Pagnotta, and V. Palleschi, "Laser-based continuous monitoring and resolution of steel grades in sequence casting machines," *Spectrochimica Acta Part B: Atomic Spectroscopy*, vol. 112, pp. 1–5, Oct. 2015, ISSN: 05848547. DOI: 10.1016/j.sab.2015.07.006.

[60] H. Xia and M. C. M. Bakker, "Reliable classification of moving waste materials with LIBS in concrete recycling," *Talanta*, vol. 120, pp. 239–247, Mar. 2014, ISSN: 00399140. DOI: 10.1016/j.talanta.2013.11.082.

[61] V. Spizzichino and R. Fantoni, "Laser induced breakdown spectroscopy in archeometry: a review of its application and future perspectives," *Spectrochimica Acta Part B: Atomic Spectroscopy*, vol. 99, pp. 201–209, Sep. 2014, ISSN: 05848547. DOI: 10.1016/j.sab.2014.07.003.

[62] D. Anglos and V. Detalle, "Cultural heritage applications of LIBS," in *Laser-Induced Breakdown Spectroscopy*, S. Musazzi and U. Perini, Eds., Springer Berlin Heidelberg, 2014, ch. 20, pp. 531–554, ISBN: 978-364245084-6. DOI: 10.1007/978-3-642-45085-3_20.

[63] I. Gaona, P. Lucena, J. Moros, F. J. Fortes, S. Guirado, J. Serrano, and J. J. Laserna, "Evaluating the use of standoff LIBS in architectural heritage: Surveying the Cathedral of Málaga," *Journal of Analytical Atomic Spectrometry*, no. 6, p. 810, ISSN: 0267-9477. DOI: 10.1039/c3ja50069a.

[64] S. Guirado, F. Fortes, V. Lazic, and J. Laserna, "Chemical analysis of archeological materials in submarine environments using laser-induced breakdown spectroscopy. On-site trials in the Mediterranean Sea," *Spectrochimica Acta Part B: Atomic Spectroscopy*, vol. 74–75, pp. 137 –143, 2012, 6th Euro-Mediterranean Symposium on Laser Induced Breakdown Spectroscopy (EMSLIBS 2011). DOI: http://dx.doi.org/10.1016/j.sab.2012.06.032.

[65] M. A. Kasem, R. E. Russo, and M. A. Harith, "Influence of biological degradation and environmental effects on the interpretation of archeological bone samples with laser-induced breakdown spectroscopy," *Journal of Analytical Atomic Spectrometry*, vol. 26, no. 9, p. 1733, 2011, ISSN: 0267-9477. DOI: 10.1039/c1ja10057b.

[66] P. Lucena, I. Gaona, J. Moros, and J. J. Laserna, "Location and detection of explosive-contaminated human fingerprints on distant targets using standoff laser-induced breakdown spectroscopy," *Spectrochimica Acta - Part B Atomic Spectroscopy*, vol. 85, pp. 71–77, 2013, ISSN: 05848547. DOI: 10.1016/j.sab.2013.04.003.

[67] J. Serrano, J. Moros, C. Sánchez, J. Macías, and J. J. Laserna, "Advanced recognition of explosives in traces on polymer surfaces using LIBS and supervised learning classifiers," *Analytica Chimica Acta*, vol. 806, pp. 107–116, Jan. 2014, ISSN: 00032670. DOI: 10.1016/j.aca.2013.11.035.

[68] I. Gaona, J. Serrano, J. Moros, and J. J. Laserna, "Evaluation of laser-induced breakdown spectroscopy analysis potential for addressing radiological threats from a distance," *Spectrochimica Acta Part B: Atomic Spectroscopy*, vol. 96, pp. 12–20, Jun. 2014, ISSN: 05848547. DOI: 10.1016/j.sab.2014.04.003.

[69] E. J. Judge, J. E. Barefield, J. M. Berg, S. M. Clegg, G. J. Havrilla, V. M. Montoya, L. A. Le, and L. N. Lopez, "Laser-induced breakdown spectroscopy measurements of uranium and thorium powders and uranium ore," *Spectrochimica Acta Part B: Atomic Spectroscopy*, vol. 83-84, pp. 28–36, May 2013, ISSN: 05848547. DOI: 10.1016/j.sab.2013.03.002.

[70] F. R. Doucet, G. Lithgow, R. Kosierb, P. Bouchard, and M. Sabsabi, "Determination of isotope ratios using laser-induced breakdown spectroscopy in ambient air at atmospheric pressure for nuclear forensics," *Journal of Analytical Atomic Spectrometry*, vol. 26, no. 3, p. 536, 2011, ISSN: 0267-9477. DOI: 10.1039/c0ja00199f.

[71] M. Gaft, L. Nagli, Y. Groisman, and A. Barishnikov, "Industrial online raw materials analyzer based on laser-induced breakdown spectroscopy," *Applied Spectroscopy*, vol. 68, no. 9, pp. 1004–1015, Sep. 2014, ISSN: 00037028. DOI: 10.1366/13-07382.

[72] J.-h. Kwak, C. Lenth, C. Salb, E.-J. Ko, K.-W. Kim, and K. Park, "Quantitative analysis of arsenic in mine tailing soils using double pulse-laser induced breakdown spectroscopy," *Spectrochimica Acta Part B: Atomic Spectroscopy*, vol. 64, no. 10, pp. 1105–1110, Oct. 2009, ISSN: 05848547. DOI: 10.1016/j.sab.2009.07.008.

[73] D. L. Death, A. P. Cunningham, and L. J. Pollard, "Multi-element and mineralogical analysis of mineral ores using laser induced breakdown spectroscopy and chemometric analysis," *Spectrochimica Acta Part B: Atomic Spectroscopy*, vol. 64, no. 10, pp. 1048–1058, Oct. 2009, ISSN: 05848547. DOI: 10.1016/j.sab.2009.07.017.

[74] D. Pokrajac, A. Lazarevic, V. Kecman, A. Marcano, Y. Markushin, T. Vance, N. Reljin, S. McDaniel, and N. Melikechi, "Automatic classification of laser-induced breakdown spectroscopy (LIBS) data of protein biomarker solutions," *Applied Spectroscopy*, vol. 68, no. 9, pp. 1067–1075, Sep. 2014, ISSN: 00037028. DOI: 10.1366/14-07488.

[75] P. Sivakumar, A. Fernández-Bravo, L. Taleh, J. F. Biddle, and N. Melikechi, "Detection and classification of live and dead Escherichia Coli by laser-induced breakdown spectroscopy," *Astrobiology*, vol. 15, no. 2, pp. 144–153, Feb. 2015, ISSN: 1531-1074. DOI: 10.1089/ast.2014.1181.

[76] S. Manzoor, S. Moncayo, F. Navarro-Villoslada, J. A. Ayala, R. Izquierdo-Hornillos, F. J. M. de Villena, and J. O. Caceres, "Rapid identification and discrimination of bacterial strains by laser induced breakdown spectroscopy and neural networks," *Talanta*, vol. 121, no. 2, pp. 65–70, Apr. 2014, ISSN: 00399140. DOI: 10.1016/j.talanta.2013.12.057.

[77] W. Lei, V. Motto-Ros, M. Boueri, Q. Ma, D. Zhang, L. Zheng, H. Zeng, and J. Yu, "Time-resolved characterization of laser-induced plasma from fresh potatoes," *Spectrochimica Acta Part B: Atomic Spectroscopy*, vol. 64, no. 9, pp. 891–898, Sep. 2009, ISSN: 05848547. DOI: 10.1016/j.sab.2009.07.015.

[78] K. Devey, M. Mucalo, G. Rajendram, and J. Lane, "Pasture vegetation elemental analysis by laser-induced breakdown spectroscopy," *Communications in Soil Science and Plant Analysis*, vol. 46, no. sup1, pp. 72–80, Feb. 2015, ISSN: 0010-3624. DOI: 10.1080/00103624.2014.988578.

[79] O. T. Butler, W. R. L. Cairns, J. M. Cook, and C. M. Davidson, "2014 atomic spectrometry update – a review of advances in environmental analysis," *J. Anal. At. Spectrom.*, vol. 30, no. 1, pp. 21–63, 2015, ISSN: 0267-9477. DOI: 10.1039/C4JA90062F.

[80] G. Kim, J.-h. Kwak, K.-R. Kim, H. Lee, K.-W. Kim, H. Yang, and K. Park, "Rapid detection of soils contaminated with heavy metals and oils by laser induced breakdown spectroscopy (LIBS)," *Journal of Hazardous Materials*, vol. 263, pp. 754–760, Dec. 2013, ISSN: 03043894. DOI: 10.1016/j.jhazmat.2013.10.041.

[81] A. Tarifa and J. R. Almirall, "Fast detection and characterization of organic and inorganic gunshot residues on the hands of suspects by CMV-GC–MS and LIBS," *Science & Justice*, vol. 55, no. 3, pp. 168–175, May 2015, ISSN: 13550306. DOI: 10.1016/j.scijus.2015.02.003.

[82] M. E. Sigman, "Application of laser-induced breakdown spectroscopy to forensic science: analysis of paint and glass samples," Tech. Rep., 2010.

[83] M. Tofanelli, L. Pardini, M. Borrini, F. Bartoli, A. Bacci, A. D'Ulivo, E. Pitzalis, M. C. Mascherpa, S. Legnaioli, G. Lorenzetti, S. Pagnotta, G. de Holanda Cavalcanti, M. Lezzerini, and V. Palleschi, "Spectroscopic analysis of bones for forensic studies," *Spectrochimica Acta Part B: Atomic Spectroscopy*, vol. 99, pp. 70–75, Sep. 2014, ISSN: 05848547. DOI: 10.1016/j.sab.2014.06.006.

[84] X. Wang, V. Motto-Ros, G. Panczer, D. De Ligny, J. Yu, J. M. Benoit, J. L. Dussossoy, and S. Peuget, "Mapping of rare earth elements in nuclear waste glass–ceramic using micro laser-induced breakdown spectroscopy," *Spectrochimica Acta Part B: Atomic Spectroscopy*, vol. 87, pp. 139–146, Sep. 2013, ISSN: 05848547. DOI: 10.1016/j.sab.2013.05.022.

[85] J. K. Antony, N. J. Vasa, V. L. N. S. Raja, and A. S. Laxmiprasad, "Laser induced breakdown spectroscopy analysis of lunar simulants under high vacuum conditions," in *TENCON 2010 - 2010 IEEE Region 10 Conference*, IEEE, Nov. 2010, pp. 449–453, ISBN: 978-1-4244-6889-8. DOI: 10.1109/TENCON.2010.5686698.

[86] A. De Giacomo, M. Dell'Aglio, R. Gaudiuso, S. Amoruso, and O. De Pascale, "Effects of the background environment on formation, evolution and emission spectra of laser-induced plasmas," *Spectrochimica Acta Part B: Atomic Spectroscopy*, vol. 78, pp. 1–19, Dec. 2012, ISSN: 05848547. DOI: 10.1016/j.sab.2012.10.003.

[87] X. Bai, F. Cao, V. Motto-Ros, Q. Ma, Y. Chen, and J. Yu, "Morphology and characteristics of laser-induced aluminum plasma in argon and in air: a comparative study," *Spectrochimica Acta Part B: Atomic Spectroscopy*, vol. 113, pp. 158–166, Nov. 2015, ISSN: 05848547. DOI: 10.1016/j.sab.2015.09.023.

[88] S. M. Clegg, R. Wiens, A. K. Misra, S. K. Sharma, J. Lambert, S. Bender, R. Newell, K. Nowak-Lovato, S. Smrekar, M. D. Dyar, and S. Maurice, "Planetary geochemical investigations using raman and laser-induced breakdown spectroscopy," *Applied Spectroscopy*, vol. 68, no. 9, pp. 925–936, Sep. 2014, ISSN: 00037028. DOI: 10.1366/13-07386.

[89] J. A. Aguilera, J. Bengoechea, and C. Aragón, "Curves of growth of spectral lines emitted by a laser-induced plasma: influence of the temporal evolution and spatial inhomogeneity of the plasma," *Spectrochimica Acta Part B: Atomic Spectroscopy*, vol. 58, no. 2, pp. 221–237, Feb. 2003, ISSN: 05848547. DOI: 10.1016/S0584-8547(02)00258-6.

[90] G. Colonna, L. D. Pietanza, and M. Capitelli, "Coupled solution of a time-dependent collisional-radiative model and boltzmann equation for atomic hydrogen plasmas:implications with LIBS plasmas," *Spectrochimica Acta Part B: Atomic Spectroscopy*, vol. 56, no. 6, pp. 587–598, Jun. 2001, ISSN: 05848547. DOI: 10.1016/S0584-8547(01)00223-3.

[91] G. Cristoforetti, A. De Giacomo, M. Dell'Aglio, S. Legnaioli, E. Tognoni, V. Palleschi, and N. Omenetto, "Local thermodynamic equilibrium in laser-induced breakdown spectroscopy: Beyond the McWhirter criterion," *Spectrochimica Acta Part B: Atomic Spectroscopy*, vol. 65, no. 1, pp. 86–95, Jan. 2010, ISSN: 05848547. DOI: 10.1016/j.sab.2009.11.005.

[92] T. A. Labutin, A. M. Popov, V. N. Lednev, and N. B. Zorov, "Correlation between properties of a solid sample and laser-induced plasma parameters," *Spectrochimica Acta Part B: Atomic Spectroscopy*, vol. 64, no. 10, pp. 938–949, Oct. 2009, ISSN: 05848547. DOI: 10.1016/j.sab.2009.07.033.

[93] D. W. Hahn and N. Omenetto, "Laser-induced breakdown spectroscopy (LIBS), part I: Review of basic diagnostics and plasma-particle

interactions: still-challenging issues within the analytical plasma community," *Applied Spectroscopy*, vol. 64, pp. 335–366, 2010, ISSN: 00037028. DOI: 10.1366/000370210793561691.

[94] ——, "Laser-induced breakdown spectroscopy (LIBS), Part II: Review of instrumental and methodological approaches to material analysis and applications to different fields," *Applied Spectroscopy*, vol. 66, no. 4, pp. 347–419, Apr. 2012, ISSN: 00037028. DOI: 10.1366/11-06574.

[95] A. De Giacomo, M. Dell'Aglio, O. De Pascale, R. Gaudiuso, V. Palleschi, C. G. Parigger, and A. C. Woods, "Plasma processes and emission spectra in laser induced plasmas: a point of view," *Spectrochimica Acta Part B: Atomic Spectroscopy*, vol. 100, pp. 180–188, Oct. 2014, ISSN: 05848547. DOI: 10.1016/j.sab.2014.08.013.

[96] D. A. Cremers and L. J. Radziemski, *Handbook of Laser-Induced Breakdown Spectroscopy*. Oxford, UK: John Wiley & Sons Ltd, Mar. 2013, ISBN: 9781118567371. DOI: 10.1002/9781118567371.

[97] S. Musazzi and U. Perini, Eds., *Laser-Induced Breakdown Spectroscopy*, ser. Springer Series in Optical Sciences. Berlin, Heidelberg: Springer Berlin Heidelberg, 2014, vol. 182, ISBN: 978-3-642-45084-6. DOI: 10.1007/978-3-642-45085-3.

[98] V. Lazic, J. J. Laserna, and S. Jovićević, "Insights in the laser-induced breakdown spectroscopy signal generation underwater using dual pulse excitation — Part I: Vapor bubble, shockwaves and plasma," *Spectrochimica Acta Part B: Atomic Spectroscopy*, vol. 82, pp. 42–49, Apr. 2013, ISSN: 05848547. DOI: 10.1016/j.sab.2013.01.012.

[99] ——, "Insights in the laser induced breakdown spectroscopy signal generation underwater using dual pulse excitation — Part II: Plasma emission intensity as a function of interpulse delay," *Spectrochimica Acta Part B: Atomic Spectroscopy*, vol. 82, pp. 50–59, Apr. 2013, ISSN: 05848547. DOI: 10.1016/j.sab.2013.01.009.

[100] A. J. Effenberger and J. R. Scott, "Effect of atmospheric conditions on LIBS spectra," *Sensors*, vol. 10, no. 5, pp. 4907–4925, May 2010, ISSN: 1424-8220. DOI: 10.3390/s100504907.

[101] Y. G. Mbesse Kongbonga, H. Ghalila, M. B. Onana, and Z. Ben Lakhdar, "Classification of vegetable oils based on their concentration of saturated fatty acids using laser induced breakdown spectroscopy (LIBS)," *Food Chemistry*, vol. 147, pp. 327–331, Mar. 2014, ISSN: 03088146. DOI: 10.1016/j.foodchem.2013.09.145.

[102] U. Panne, R. Neuhauser, C. Haisch, H. Fink, and R. Niessner, "Remote analysis of a mineral melt by laser-induced plasma spectroscopy," *Applied Spectroscopy*, vol. 56, no. 3, pp. 375–380, Mar. 2002, ISSN: 00037028. DOI: 10.1366/0003702021954755.

[103] M. Abdelhamid, S. Grassini, E. Angelini, G. M. Ingo, and M. A. Harith, "Depth profiling of coated metallic artifacts adopting laser-induced breakdown spectrometry," *Spectrochimica Acta Part B: Atomic Spectroscopy*, vol. 65, no. 8, pp. 695–701, Aug. 2010, ISSN: 05848547. DOI: 10.1016/j.sab.2010.03.017.

[104] J. A. Varela, J. M. Amado, M. J. Tobar, M. P. Mateo, A. Yañez, and G. Nicolas, "Characterization of hard coatings produced by laser cladding using laser-induced breakdown spectroscopy technique," *Applied Surface Science*, vol. 336, pp. 396–400, May 2015, ISSN: 01694332. DOI: 10.1016/j.apsusc.2015.01.037.

[105] B. L. Chadwick and D. Body, "Development and commercial evaluation of laser-induced breakdown spectroscopy chemical analysis technology in the coal power generation industry," *Applied Spectroscopy*, vol. 56, no. 1, pp. 70–74, 2002.

[106] X.-W. Li, Z. Wang, Y. Fu, Z. Li, and W. Ni, "A model combining spectrum standardization and dominant factor based partial least square method for carbon analysis in coal using laser-induced breakdown spectroscopy," *Spectrochimica Acta Part B: Atomic Spectroscopy*, vol. 99, pp. 82–86, 2014. DOI: 10.1016/j.sab.2014.06.017.

[107] T. B. Yuan, Z. Wang, Z. Li, W. Ni, and J. Liu, "A partial least squares and wavelet-transform hybrid model to analyze carbon content in coal using laser-induced breakdown spectroscopy," *Analytica Chimica Acta*, vol. 807, pp. 29–35, 2014. DOI: 10.1016/j.aca.2013.11.027.

[108] M. Dong, J. Lu, S. Yao, J. Li, J. Li, Z. Zhong, and W. Lu, "Application of LIBS for direct determination of volatile matter content in coal," *Journal of Analytical Atomic Spectrometry*, vol. 26, p. 2183, 2011. DOI: 10.1039/c1ja10109a.

[109] M. P. Mateo, G. Nicolas, and A. Yañez, "Characterization of inorganic species in coal by laser-induced breakdown spectroscopy using UV and IR radiations," *Applied Surface Science*, vol. 254, pp. 868–872, 2007. DOI: 10.1016/j.apsusc.2007.08.043.

[110] Y. Liangying, L. Jidong, C. Wen, W. Ge, S. Kai, and F. Wei, "Analysis of pulverized coal by laser-induced breakdown spectroscopy," *Plasma Science and Technology*, vol. 7, no. 5, pp. 3041–3044, 2006. DOI: 10.1088/1009-0630/7/5/015.

[111] J. Feng, Z. Wang, L. West, Z. Li, and W. Ni, "A PLS model based on dominant factor for coal analysis using laser-induced breakdown spectroscopy," *Analytical and Bioanalytical Chemistry*, vol. 400, pp. 3261–3271, 2011. DOI: 10.1007/s00216-011-4865-y.

[112] S. Yao, J. Lu, M. Dong, K. Chen, J. Li, and J. Li, "Extracting coal ash content from laser-induced breakdown spectroscopy (LIBS) spectra by multivariate analysis," *Applied Spectroscopy*, vol. 65, no. 10, pp. 1197–1201, 2011. DOI: 10.1366/10-06190.

[113] T. Ctvrtnickova, M. P. Mateo, A. Yañez, and G. Nicolas, "Application of LIBS and TMA for the determination of combustion predictive indices of coals and coal blends," *Applied Surface Science*, vol. 257, pp. 5447–5451, 2011. DOI: 10.1016/j.apsusc.2010.12.025.

[114] A. F. M. Y. Haider, M. A. Rony, R. S. Lubna, and K. M. Abedin, "Detection of multiple elements in coal samples from Bangladesh by laser-induced breakdown spectroscopy," *Optics & Laser Technology*, vol. 43, no. 8, pp. 1405–1410, 2011. DOI: 10.1016/j.optlastec.2011.04.009.

[115] A. F. M. Y. Haider, M. A. Rony, and K. M. Abedin, "Determination of the ash content of coal without ashing: A simple technique using laser-induced breakdown spectroscopy," *Energy & Fuels*, vol. 27, 2013. DOI: 10.1021/ef400566u.

[116] Z. Wang, T. B. Yuan, S.-L. Lui, Z. Y. Hou, X.-W. Li, Z. Li, and W. Ni, "Major elements analysis in bituminous coals under different ambient gases by laser-induced breakdown spectroscopy with PLS modeling," *Frontiers of Physics*, vol. 7, no. 6, pp. 708–713, 2012. DOI: 10.1007/s11467-012-0262-z.

[117] J. Li, J. Lu, Z. Lin, S. Gong, C. Xie, L. Chang, L. Yang, and P. Li, "Effects of experimental parameters on elemental analysis of coal by laser-induced breakdown spectroscopy," *Optics & Laser Technology*, vol. 41, pp. 907–913, 2009. DOI: 10.1016/j.optlastec.2009.03.003.

[118] N. Idris, M. Ramli, M. Mahidin, R. Hedwig, Z. S. Lie, and K. H. Kurniawan, "Examination of the capability of the laser-induced breakdown spectroscopy (LIBS) technique as the emerging laser-based analytical tool for analyzing trace elements in coal," in *AIP Proceedings*, N. Mufti, M. Diantoro, and M. Djamal, Eds., vol. 1617, Malang, East Java; Indonesia: AIP Publishing, 2014, pp. 175–178, ISBN: 9780735412545. DOI: 10.1063/1.4897131.

[119] D. Body and B. L. Chadwick, "Simultaneous elemental analysis system using laser induced breakdown spectroscopy," *Review of Scientific Instruments*, vol. 72, no. 2001, pp. 1625–1629, 2001. DOI: 10.1063/1.1338486.

[120] C. E. Romero, R. D. Saro, J. Craparo, A. Weisberg, R. Moreno, and Z. Yao, "Laser-induced breakdown spectroscopy for coal characterization and assessing slagging propensity," *Energy and Fuels*, vol. 24, pp. 510–517, 2010. DOI: 10.1021/ef900873w.

[121] L. Zhang, Z.-Y. Hu, W.-B. Yin, D. Huang, W.-G. Ma, L. Dong, H.-P. Wu, Z.-X. Li, L.-T. Xiao, and S.-T. Jia, "Recent progress on laser-induced breakdown spectroscopy for the monitoring of coal quality and unburned carbon in fly ash," *Frontiers of Physics*, vol. 7, no. 6, pp. 690–700, Sep. 2012. DOI: 10.1007/s11467-012-0259-7.

[122] W. Yin, L. Zhang, L. Dong, W. Ma, and S. Jia, "Design of a laser-induced breakdown spectroscopy system for on-line quality analysis of pulverized coal in power plants," *Applied Spectroscopy*, vol. 63, no. 8, pp. 865–872, 2009. DOI: 10.1366/000370209788964458.

[123] J. Zheng, J. Lu, B. Zhang, M. Dong, S. Yao, W. Lu, and X. Dong, "Experimental study of laser-induced breakdown spectroscopy (LIBS) for direct analysis of coal particle flow.," *Applied spectroscopy*, vol. 68, no. 6, pp. 672–9, Jan. 2014. DOI: 10.1366/13-07278.

[124] M. Gaft, E. Dvir, H. Modiano, and U. Schone, "Laser induced breakdown spectroscopy machine for online ash analyses in coal," *Spectrochimica Acta Part B: Atomic Spectroscopy*, vol. 63, no. 10, pp. 1177–1182, 2008. DOI: 10.1016/j.sab.2008.06.007.

[125] C. E. Romero, Z. Yao, R. De Saro, J. Craparo, S. Lam, R. Silfies, R. Plangemann, F. Lyter, and K. Quinty, "Development and demonstration of laser induced breakdown spectroscopy for in-situ on-line coal analysis," 2011 International Pittsburgh Coal Conference, http://www.lehigh.edu/energy/research/PDF/.

[126] M. Capitelli, F. Capitelli, and A. Eletskii, "Non-equilibrium and equilibrium problems in laser-induced plasmas," *Spectrochimica Acta Part B: Atomic Spectroscopy*, vol. 55, no. 6, pp. 559–574, Jun. 2000. DOI: 10.1016/S0584-8547(00)00168-3.

[127] E. Tognoni, G. Cristoforetti, S. Legnaioli, V. Palleschi, A. Salvetti, M. Mueller, U. Panne, and I. Gornushkin, "A numerical study of expected accuracy and precision in calibration-free laser-induced breakdown spectroscopy in the assumption of ideal analytical plasma," *Spectrochimica Acta Part B: Atomic Spectroscopy*, vol. 62, no. 12, pp. 1287–1302, Dec. 2007. DOI: 10.1016/j.sab.2007.10.005.

[128] J. Aguilera and C. Aragón, "Characterization of a laser-induced plasma by spatially resolved spectroscopy of neutral atom and ion emissions.," *Spectrochimica Acta Part B: Atomic Spectroscopy*, vol. 59, no. 12, pp. 1861–1876, Dec. 2004. DOI: 10.1016/j.sab.2004.08.003.

[129] M. N. Saha, "On a physical theory of stellar spectra," *Proceedings of the Royal Society of London A: Mathematical, Physical and Engineering Sciences*, vol. 99, no. 697, pp. 135–153, 1921, ISSN: 0950-1207. DOI: 10.1098/rspa.1921.0029.

[130] M. Dong, X. Mao, J. J. Gonzalez, J. Lu, and R. E. Russo, "Time-resolved LIBS of atomic and molecular carbon from coal in air, argon and helium," *Journal of Analytical Atomic Spectrometry*, vol. 27, no. 12, 2012. DOI: 10.1039/c2ja30222e.

[131] P. Rebolledo, P. Pacheco, R. Sarmiento, R. Cabanzo, and E. Mejía-Ospino, "Temporary spectral analysis of a laser plasma of mineral coal," *Journal of Physics: Conference Series*, vol. 466, pp. 1–4, 2013. DOI: 10.1088/1742-6596/466/1/012015.

[132] V. Lazic, R. Barbini, F. Colao, R. Fantoni, and A. Palucci, "Self-absorption model in quantitative laser induced breakdown spectroscopy measurements on soils and sediments," *Spectrochimica Acta Part B: Atomic Spectroscopy*, vol. 56, no. 6, pp. 807–820, Jun. 2001. DOI: 10.1016/S0584-8547(01)00211-7.

[133] A. El Sherbini, T. El Sherbini, H. Hegazy, G. Cristoforetti, S. Legnaioli, V. Palleschi, L. Pardini, A. Salvetti, and E. Tognoni, "Evaluation of self-absorption coefficients of aluminum emission lines in laser-induced breakdown spectroscopy measurements," *Spectrochimica Acta Part B: Atomic Spectroscopy*, vol. 60, no. 12, pp. 1573–1579, Dec. 2005. DOI: 10.1016/j.sab.2005.10.011.

[134] S. S. Harilal, J. R. Freeman, P. K. Diwakar, and A. Hassanein, "Femtosecond laser ablation: fundamentals and applications," in *Laser-Induced Breakdown Spectroscopy*, S. Musazzi and U. Perini, Eds., Springer Berlin Heidelberg, 2014, ch. 6, pp. 143–166, ISBN: 978-3-642-45085-3. DOI: 10.1007/978-3-642-45085-3_6.

[135] A. Ciucci, M. Corsi, V. Palleschi, S. Rastelli, A. Salvetti, and E. Tognoni, "New procedure for quantitative elemental analysis by laser-induced plasma spectroscopy," *Applied Spectroscopy*, vol. 53,

[136] I. Gornushkin, S. Merk, A. Demidov, U. Panne, S. Shabanov, B. Smith, and N. Omenetto, "Tomography of single and double pulse laser-induced plasma using Radon transform technique," *Spectrochimica Acta Part B: Atomic Spectroscopy*, vol. 76, pp. 203–213, Oct. 2012. DOI: 10.1016/j.sab.2012.06.033.

[137] L. Mercadier, J. Hermann, C. Grisolia, and A. Semerok, "Diagnostics of nonuniform plasmas for elemental analysis via laser-induced breakdown spectroscopy: demonstration on carbon-based materials," *Journal of Analytical Atomic Spectrometry*, vol. 28, p. 1446, 2013. DOI: 10.1039/c3ja50127b.

[138] C. Gerhard, J. Hermann, L. Mercadier, L. Loewenthal, E. Axente, C. R. Luculescu, T. Sarnet, M. Sentis, and W. Viöl, "Quantitative analyses of glass via laser-induced breakdown spectroscopy in argon," *Spectrochimica Acta Part B: Atomic Spectroscopy*, vol. 101, pp. 32–45, 2014. DOI: 10.1016/j.sab.2014.07.014.

[139] *ASTM D3176-15, Standard practice for ultimate analysis of coal and coke*, ASTM International, 2010. DOI: 10.1520/D3176-15.

[140] M. Gaft, L. Nagli, I. Fasaki, M. Kompitsas, and G. Wilsch, "Laser-induced breakdown spectroscopy for on-line sulfur analyses of minerals in ambient conditions," *Spectrochimica Acta Part B: Atomic Spectroscopy*, vol. 64, no. 10, pp. 1098–1104, 2009. DOI: 10.1016/j.sab.2009.07.010.

[141] D. A. Redoglio, E. Golinelli, S. Musazzi, U. Perini, and F. Barberis, "A large depth of field LIBS measuring system for elemental analysis of moving samples of raw coal," *Spectrochimica Acta Part B: Atomic Spectroscopy*, DOI: 10.1016/j.sab.2015.11.005.